A STUDY OF DEFORMED LIGHT NUCLEI USING THE SPRUNG-BANERJEE INTERACTION

By

Paul Douglas Curry, B.Sc.

Submitted to the School of Graduate Studies
in Partial Fulfilment of the Requirements
for a M.Sc. Degree

McMaster University

April, 1973

MASTER OF SCIENCE (1973) McMASTER UNIVERSITY
(Physics) Hamilton, Ontario

TITLE: A Study of Deformed Light Nuclei Using the Sprung-Banerjee Interaction

AUTHOR: Paul Douglas Curry
B.Sc. (McMaster University)

SUPERVISOR: Professor D.W.L. Sprung

NUMBER OF PAGES: xi, 224

ABSTRACT:

The light even-even nuclei have been studied using the density dependent effective interaction of Sprung and Banerjee. The nuclei were studied initially, using a harmonic variational procedure, to determine the most appropriate parameters of the force for the Hartree Fock study.

This chosen force was then used in a comparative study of spherical nuclei to determine the inadequacies of our Hartree Fock approach, as opposed to the spherical basis calculations of Campi. Some deformed nuclei were then examined and our results were compared with those of K. Lassey and A. B. Volkov, and of J. Zofka and G. Ripka.

ACKNOWLEDGEMENTS

I would like to express my most sincere gratitude to my supervisor, Professor D.W.L. Sprung with whom it has been my privilege to study. He has consistently been a willing and available consellor, whether explaining the subtleties of nuclear physics or the "vagueries" of an income tax form. His dry wit, candor and numerous contests and picnics have made what could be a dry association, great fun. Were it not for his sympathy, gently prodding and biennial apologetics to the Graduate Studies Office, this work would not yet be completed.

I would also like to thank Professor A.B. Volkov, Keith Lassey, Paul Dunmore and Dr. X. Campi for many useful and enlightening discussions. Appreciation should also be expressed to both Professor A.B. Volkov and Professor R.F.W. Bader who initially interested me in different aspects of this problem.

I am also indebted to the director, Dr. Keech, the staff of the McMaster Computer Centre, and the CDC 6400 computer, for the contribution they made to this research.

I would like to thank Jan Coleman for her patient help typing this long and at times difficult thesis.

It would be improper of me to omit mention of the debt I owe to my mother, the late Mrs. Velma Margaret Curry who for twenty years was to me both mother and father. Without her dedication, sacrifice and encouragement my education would never have been possible.

Finally, I would like to thank my wife, Mary Jane, who has patiently endured the disruptions which accompany the writing of a thesis. Without her loving help and encouragement this thesis would never have been completed at this time.

TABLE OF CONTENTS

		Page
INTRODUCTION		1
CHAPTER 1	Hartree Fock Theory	5
CHAPTER 2	Nuclear Matter	13
CHAPTER 3	The Potential	20
	3.1 The Hamiltonian	20
	3.2 Types of Potentials	21
	3.3 Density Dependence	26
	3.4 Rearrangement Term	27
	3.5 The Coulomb Potential	35
	3.6 The Spin Orbit Interaction	37
CHAPTER 4	Variational Calculations	39
	4.1 Choice of Force	39
	4.2 Comparison of Forces, G-0, G-1, G-3	47
	4.3 Symmetry Energy of Nuclear Matter	66
CHAPTER 5	Hartree Fock Results	74
	5.1 Introduction	74
	5.2 The Program	75
	5.3 Spherical Nuclei	86
	5.3.1 Oxygen 16	89
	5.3.2 Calcium 40	102
	5.3.3 Helium 4	117
	5.3.4 Conclusions	124
	5.4 Deformed Nuclei	126
	5.4.1 Neon 20	129
	5.4.2 Magnesium 24	142

		Page
5.4.3	Silicon 28	150
5.4.4	Sulphur 32	162
5.4.5	Argon 36	177
5.5	Conclusions	192
5.5.1	Systematics	192
5.5.2	Clustering	202
5.5.3	Discussion of Zofka and Ripka's Paper	216
5.5.4	Suggestions	218
5.5.5	Epilogue	218
APPENDIX 1		219
BIBLIOGRAPHY		222

LIST OF TABLES

		Page
Table 3.1	Parameters of Coulomb Approximation	36
Table 4.1	Binding Energies and Radii of ^{16}O with and without the Coulomb Force	41
Table 4.2	Binding Energy and Radius of ^{40}Ca	43
Table 4.3	Calculated and Experimental Observables for all the 4A nuclei to ^{40}Ca	44
Table 4.4	Binding Energies and Radii of ^{16}O for forces G-1 and G-3	48
Table 4.5	Binding Energies and Radii of ^{40}Ca for forces G-1 and G-3	49
Table 4.6	Binding Energies and Radii for force G-3 k_s=1.30 fm^{-1} for ^{16}O and ^{40}Ca	51
Table 4.7	Properties of ^{16}O calculated for different values of the Symmetry Energy in Nuclear Matter	70
Table 4.8	Binding Energy and Radii of Deformed nuclei for various Symmetry Energy values	
Table 5.1	Calculated Properties of ^{16}O	95
Table 5.2	Calculated Properties of ^{40}Ca	106
Table 5.3	Calculated Properties of ^{4}He	121
Table 5.4	Properties of ^{20}Ne vs λ	134
Table 5.5	Calculated Properties of ^{20}Ne	135
Table 5.6	Calculated Properties of ^{24}Mg	146
Table 5.7	Calculated Properties of Prolate ^{28}Si	152
Table 5.8	Calculated Properties of Oblate ^{28}Si	158
Table 5.9	Calculated Properties of Triaxial ^{32}S	169
Table 5.10	Properties of various configurations of ^{32}S	174

		Page
Table 5.11	Calculated Properties of ^{36}Ar	187
Table 5.12	Properties of the 4A nuclei	199
Table 5.13	Binding energy differences for 4A, 4A-1 and 4A+1 nuclei	203
Table 5.14	Bond energies of the 4A nuclei	210

LIST OF FIGURES

		Page
Figure 4.1	The BE/A in MeV for the 4A nuclei for force G-0	46
Figure 4.2	Binding energy of ^{16}O vs E_S in MeV for G-0, G-1, G-3	52
Figure 4.3	Radius in fm of ^{16}O vs E_S for G-0, G-1, G-3	54
Figure 4.4	Binding energy of ^{40}Ca vs E_S for G-0, G-1, and G-3	56
Figure 4.5	Radius in fm of ^{40}Ca vs E_S for G-0, G-1 and G-3	58
Figure 4.6	Binding energy of ^{16}O vs E_S for k_S=1.35 and 1.30 fm^{-1}	60
Figure 4.7	Radius of ^{16}O vs E_S for k_S=1.35 and 1.30 fm^{-1}	62
Figure 4.8	Binding energy of ^{40}Ca vs E_S k_S=1.35 and 1.30 fm^{-1}	64
Figure 4.9	Radius of ^{40}Ca vs E_S k_S=1.35 and 1.30 fm^{-1}	67
Figure 5.1	Rearrangement Factor λ vs Atomic Number A	76
Figure 5.2	Single particle energy levels of ^{16}O vs λ	79
Figure 5.3	Gaussian fit to ^{16}O density profile	82
Figure 5.4	Proton Single Particle levels for ^{40}Ca vs λ	84
Figure 5.5	Radii and binding energy vs λ of ^{16}O and ^{40}Ca	87
Figure 5.6	Density distribution of ^{16}O	90
Figure 5.7	Density profile of ^{16}O	92
Figure 5.8	Proton Single Particle levels of ^{16}O	97
Figure 5.9	Neutron single particle levels for ^{16}O	99

		Page
Figure 5.10	Density distribution of ^{40}Ca	103
Figure 5.11	Density profile of ^{40}Ca	104
Figure 5.12	Proton single particle levels of ^{40}Ca	110
Figure 5.13	Neutron single particle levels of ^{40}Ca	112
Figure 5.14	Density distribution of ^{4}He	118
Figure 5.15	Density profile of ^{4}He	119
Figure 5.16	Proton and Neutron single particle levels of ^{4}He	122
Figure 5.17	Density distribution of ^{20}Ne	130
Figure 5.18	Density distribution of ^{20}Ne with ^{4}He superimposed	132
Figure 5.19	Proton single particle energy levels of ^{20}Ne	138
Figure 5.20	Neutron single particle energy levels of ^{20}Ne	140
Figure 5.21	Density distribution of ^{24}Mg	
	(a) in the x-z plane	143
	(b) in the y-z plane	144
Figure 5.22	Proton single particle energy levels of ^{24}Mg	148
Figure 5.23	Density distribution of Prolate ^{28}Si	151
Figure 5.24	Proton single particle energy levels of Prolate ^{28}Si	154
Figure 5.25	Density distribution of Oblate ^{28}Si	157
Figure 5.26	Proton single particle energy levels of Oblate ^{28}Si	160
Figure 5.27	Density distribution of Prolate ^{32}S	163
Figure 5.28	Density distribution of Oblate ^{32}S	164
Figure 5.29	Density distribution of Triaxial ^{32}S	
	(a) in the x-z plane	165
	(b) in the y-z plane	166

		Page
Figure 5.30	Composite of Triaxial ^{32}S	167
Figure 5.31	Proton single particle energy levels of Triaxial ^{32}S	172
Figure 5.32	Proton single particle energy levels of the configurations of ^{32}S	175
Figure 5.33	Density distribution of ^{36}Ar	178
Figure 5.34	Density profile of ^{36}Ar and (^{40}Ca-^{4}He)	179
Figure 5.35	Proton single particle energy levels of ^{36}Ar and ^{40}Ca	181
Figure 5.36	Density profile of ^{36}Ar	183
Figure 5.37	Proton single particle energy levels of ^{36}Ar	190
Figure 5.38	Binding Energy vs A.	193
Figure 5.39	Mass Radius vs A	195
Figure 5.40	HFC single particle energy levels vs A	197
Figure 5.41	Neutron absorption cross section vs neutron number	204
Figure 5.42	Neutron scattering cross section in barns vs neutron number	206
Figure 5.43	Bond energy vs Atomic number	211
Figure 5.44	Alpha cluster energy difference vs Atomic number	213

THERE'S NO HEAVIER BURDEN THAN A GREAT POTENTIAL!

INTRODUCTION

This thesis is a study of light nuclei using a Hartree Fock approach which employs effective potentials deduced from a realistic nucleon-nucleon force.

The structure of the nucleus is generally accepted to be consistent with the Nuclear Shell Model. The A particles of a given nucleus are confined to single particle orbitals and move in a central field. This immediately suggests a form of Hartree Fock calculation in which it is assumed that a given particle moves in a potential created by the other A-1 nucleons.

Realistic nucleon-nucleon forces, such as those of Reid, Lassila et al. of Yale, and Hamada-Johnson, have been deduced from scattering data. However these tend to have very strong repulsive cores and relatively weak attractive parts. These are unsuitable for Hartree Fock calculations since the short range parts are so strong that the matrix elements produced are unworkably large. In addition, strong second order contributions from the potential can be produced that are not handled by Hartree Fock which is a first order approximation. These difficulties have lead to the adoption of Brueckner theory in which the effect of the two body force acting to all orders of perturbation theory is taken into account. The two body force V is replaced by a reaction

matrix or G-matrix, which is in general a non local, density dependent operator. The net result of this theory is that Hartree Fock calculations must be done using "effective forces" deduced from a realistic nucleon-nucleon force. The effective force must reproduce the G-matrix elements. Even if the original force had a hard core, the effective force has a relatively weak repulsive core and is thus suitable for use in Hartree Fock.

At this point we can distinguish three main types of nuclear structure theories. At one extreme are those who seek to apply the Brueckner theory without approximation using the G-matrix. This approach is possible for spherical nuclei but not for ones we would like to study. At the other extreme are those who accept the general basis of the Brueckner Hartree Fock approach but make little or no attempt to calculate the G-matrix. They replace it by a purely phenomenological effective interaction. The phenomenological force is a mathematical function which may or may not resemble the realistic nucleon-nucleon force. It is created in a rather ad hoc fashion and adjusted to reproduce certain gross features of the nucleus such as binding energy, radius, and s-wave phase shifts. These forces may be static or density dependent such as the forces of Hughes and Volkov (1970).

Finally there is the group of theories exemplified by this study which use an effective force deduced by some more or less well founded argument from a nuclear matter

calculation based on a realistic potential. Such forces have been developed from the Reid potential recently by both Negele and Sprung, independently. An effective nucleon-nucleon force was constructed which reproduced the G-matrix in Nuclear Matter at each constant density. However in our applications we retreat somewhat from this ideal situation by allowing two adjustable parameters in the force. These are the binding energy per nucleon and the saturation density of nuclear matter.

In this thesis there will be an examination of only light nuclei up to ^{40}Ca. This is basically due to the limitations of the computer programs which are restricted to a four shell basis. A larger basis would lead to unmanageably large matrices and dragonalizations, unless our methods of calculation were considerably reorganized.

The general structure of the thesis is as follows:

In Chapter I, Hartree Fock theory will be discussed briefly without derivation, with emphasis on the Volkov approach.

In Chapter II, the highlights of Nuclear Matter theory will be enumerated with a discussion of the G-matrix.

In Chapter III, the forces examined in this thesis will be elaborated on, with respect to their physical meaning and their treatment in the computer program.

In Chapter IV, there will be detailed results of an examination of the Sprung forces G-0, G-1 and G-3 using the

General Oscillator Model or "Poor Man's Hartree Fock"

Chapter V will list the results of a study of the 4A nuclei using a full Hartree Fock calculation.

CHAPTER I

1.1 Hartree Fock Theory

Historically, Hartree Theory (1928) was a direct application of the Variational principle in atomic physics. A particle or electron was said to move in a field provided by the central stationary nucleus and each of the other remaining electrons. The practical solution of this scheme proceeded as follows. Each electron was treated in turn with modifications being made to both the potential and wave functions recursively until the change between successive steps was less than a given tolerance. Although somewhat successful, the method had two fundamental problems:

(a) the wave functions were not orthogonal, and

(b) the wave functions were not antisymmetrized,

as they ought to be when dealing with fermions. The Pauli principle could be taken into account only incidentally. These problems were overcome by the development of Hartree Fock Theory, largely owing to the efforts of Fock and J.C. Slater (1930). The complete wave function of the system was treated as a determinant of single particle wave functions

$$\psi = \frac{1}{\sqrt{A!}} \begin{vmatrix} \psi_{n_1}(r_1) & \psi_{n_1}(r_2) & \cdots & \psi_{n_1}(r_A) \\ \psi_{n_2}(r_1) & \psi_{n_2}(r_2) & \cdots & \psi_{n_2}(r_A) \\ \vdots & & & \\ \psi_{n_A}(r_1) & \psi_{n_A}(r_2) & & \psi_{n_A}(r_A) \end{vmatrix}$$

This wave function obeys the Pauli principle in that two identical rows would cause the determinate to vanish as it is antisymmetric and the exchange of any two rows or columns would result in a change of sign In addition it can be demonstrated that the wave functions are orthogonal since all orbitals move in the same potential. Practically,however, it is similar to Hartree theory and the solution can also be carried out recursively.

Recently, Nuclear Physics has been able to comfortably adopt Hartree Fock Theory. Although there is no dominating force centre to attract or repel nucleons, each does exist in a field created by the mutual interaction with its neighbours. One difficulty, however, was that Hartree Fock is a first order process. This created no problem in atomic physics which dealt with the relatively weak coulomb force; however special care is required in nuclear physics to keep the second order component of the force as small as possible if one wishes to apply Hartree Fock theory directly to the nucleon-nucleon force.

No attempt is made here to develop Hartree Fock theory. This has been done numerous times and is well known. However there are various practical approaches from which to choose.

The coordinate space approach developed by Veneroni and Vautherin (1967) has recently been adapted by X. Campi (1972) to the study of the Sprung type effective force.

The problem is solved iteratively in r-space on a grid of 0.1 fm. steps. The approach is very good for spherical nuclei and can be used for large nuclei. There is no problem with truncation of the basis set and the computer code is very fast. It cannot be used for deformed nuclei unless one assumes sphericity, in which case the results are not too meaningful.

In order to study deformed nuclei one must use a matrix dragonalization approach similar to that developed by Dr. Volkov and his students.

Hartree Fock is an application of the Variational principle

$$\delta E = \delta \langle \psi | H - \lambda | \psi \rangle = 0$$

The variational principle can be shown to be equivalent to matrix diagonalization. This will be the justification of our approach.

An arbitrary function ψ can be written in terms of a complete set of functions

$$\psi = \sum_{i}^{\infty} c_i \phi_i$$

where

$$c_i = \int \phi_i^* \psi \, d\tau$$

However one cannot in practice sum to infinity, so we truncate the basis to N functions which we believe will adequately represent ψ

$$\psi_{app} = \sum_{i=1}^{N} a_i \phi_i$$

To find the ground state we now take

$$\langle \delta\psi_{app} | H-\lambda | \psi_{app} \rangle = 0$$

The variation itself is not general but is limited to the above mentioned subset. Thus we may write

$$\delta\psi_{app} = \sum_{i=1}^{N} d_i \phi_i$$

The integral

$$\int \delta\psi_{app}^{*} (H-\lambda) \psi_{app} \, d\tau = 0$$

becomes

$$\sum_{ij} \int (d_i^{*}\phi_i [H-\lambda] a_j \phi_j) d\tau = 0$$

or

$$\sum_{i} \left(\sum_{j} \langle \phi_i | H-\lambda | \phi_j \rangle a_j\right) d_i = 0$$

The bracket must be zero for any arbitrary d_i or d_i^{*}

$$\sum_{j} \langle \phi_i | H-\lambda | \phi_j \rangle a_j = 0$$

$$\sum_{j=1}^{N} (H_{ij}-\lambda\delta_{ij}) a_j = 0$$

This is the matrix expression for N equations in N unknowns. The determinant of the coefficients is zero if the solution exists. This is equivalent to the diagonalization of the matrix H. The eigenvalues determined by

$$|H_{ij}-\lambda\delta_{ij}| = 0$$

This will give N values of λ the lowest being the ground state.

However, the justification of our approach is more by analogy than by rigour. The variation above was

of the wave function only. For a density dependent force the potential should also be varied. This as we shall later see leads to the rearrangement term. Thus the above derivation is somewhat less than rigorous.

Dr. Volkov and his collaborators (Manning 1967, Hughes 1970, Lassey 1972) used single particle wave functions which were the product of a space, spin, and isospin part.

$$\psi_n(r,\sigma,\tau) = \phi_n(r)\ \chi_n(\sigma)\ \tau_n(\tau)$$

This is only an approximation owing to the inclusion of spin orbit and Coulomb terms in the Hamiltonian. However, it is assumed to be a good approximation since the contributions of these other forces are small. Thus the wave functions are considered separable.

The space part of the single particle wave functions are expanded as the sum of cylindrically symmetric harmonic oscillator basis functions

$$\phi_n = \sum_i^N c_i\ \psi_i \quad i \equiv n,m,n_z$$

These are of the form

$$\psi_{n,m,n_z}(\sqrt{\alpha}\rho,\phi,\sqrt{\beta}z) = P_{n,m}(\sqrt{\alpha}\rho)\,\Phi_m(\phi)\,Z_{n_z}(\sqrt{\beta}z)$$

and are the solutions of the equation

$$\frac{\hbar^2}{2m}\,[-\nabla^2+\alpha^2\rho^2+\beta^2z^2]\psi_i = E_i\ \psi_i$$

where $E_i = \frac{\hbar^2}{m}(2n_i+|m_i|+1)\,\alpha_i+(n_{z_i}+\frac{1}{2})\,\beta_i$

A more detailed description of the cylindrical harmonic oscillator functions is given in Appendix 1 or Copley and Volkov (1966).

The Hartree Fock calculations were restricted to a basis of the first four shells; 1s, 1p, 2s-1d and 2p-1f All quantum numbers must be consistent with $N=2n+|m|+n_z$ where N is the principle quantum number having the values N=0,1,2,3,... A list of these is also given in Appendix 1.

Each deformed cylindrical harmonic oscillator basis state which has been used requires oscillator constants α and β. This gives us a formidable number of parameters to be fitted. For any calculation of the properties of a particular nucleus with a given force we adopt a two step procedure. The first step is to obtain a set of optimum oscillator constants consistent with the orthogonality constraints also indicated in Appendix 1. The program which accomplishes this has gone by the name MINDET in the past. Our version is called MDNM5G.

To optimize the α_i and β_i values, the procedure which Lassey (1972) called the General Oscillator Model (G.O.M.) or poor man's Hartree Fock, treats each state as a single harmonic oscillator state. Unlike Hartree Fock, there is no mixing. However each state is allowed to have different values of α and β subject to the orthonogality and time reversibility constraints. The oscillator constants refer only to the space part are not

different for different spin and isospin states. Each state may thus have up to four particles in it.

A suitable configuration of states is chosen for a given nucleus and the energy is minimized as a function of α and β's.

In addition to the set of oscillator constants to be used in the Hartree Fock calculations the binding energy for the nucleus, its radius, and such properties as $\langle \rho^2 \rangle$, $\langle z^2 \rangle$, quadrupole moment and crude single particle energy levels are calculated.

This procedure was used to examine Sprung's family of forces before choosing one for further study using the Hartree Fock program.

Given the set of oscillator constants for a particular force and nucleus, Hartree Fock calculations were performed. Besides the properties mentioned above, we calculate the nuclear asymmetry and improved single particle levels for both the protons and neutrons separately. In addition density maps were obtained for some cases.

The choice of the cylindrical harmonic oscillator basis was a matter of utility. This basis has the advantage that deformed nuclei may be handled with a reasonably small basis, and the calculation of matrix elements can procede rapidly. However, the wave functions do not have good angular momentum and are only moderately successful with

triaxially symmetric nuclei such as ^{24}Mg or ^{32}S. To do these properly a much larger basis would be necessary or the use of a cartesian harmonic oscillator basis would be advisable. In the cartesian basis,

$$\psi(x,y,z) = X(x)\ Y(y)\ Z(z)$$

However, these have neither good angular momentum j or its z-component m.

In order to have good angular momentum and a good z-component a spherical basis is necessary.

$$\psi(r,\theta,\phi) = R(r)\ \Theta(\theta)\ \Phi(\phi)$$

The spherical basis would require an inordinately large basis set to properly deal with deformed axially symmetric nuclei, let alone triaxial nuclei.

Thus a compromise must be made and the choice was the deformed cylindrically symmetric basis.

CHAPTER II

From the study of nuclei over the last four decades certain facts have been established. Nuclei saturate. This means the volume of the nucleus is proportional to the number of particles

$$R \propto r_o A^{1/3}$$

where r_o is a proportionality constant of about 1.2 fm.

From electron scattering, the central density of all but the lightest nuclei, is found to be about 0.17 nuclei per fm^3. The binding energy per particle is found to be quite constant also, about 8 MeV per particle. The semi-emperical mass formula, based on a liquid drop picture of the nucleus, gives quite a good fit to nuclear binding energies.

$$E/A = a_1 + a_2/A^{1/3} + (a_3 + a_4/A^{1/3})\left(\frac{N-Z}{A}\right)^2$$

$$+ E_{coul} + E_{shell} + E_{pair} + E_{deformation} + \cdots$$

Here the terms on the second line represent particular small effects which do not vary smoothly from nucleus to nucleus. They must be estimated from theory or removed simply by smoothing the data. The parameters $a_1 \ldots a_4$ can then be adjusted to give a best fit to nuclear binding energies.

From these facts, the idealized system of nuclear matter has been invented. It is an infinitely large nucleus, with the density ρ equal to a constant. Since it is a

homogeneous system the single particle orbitals will be plane waves and the occupied states will fill a sphere of radius k_F in momentum space. Here

$$\rho = \left(2/3\pi^2\right) k_F^{\,3}$$

The value ρ=0.17 particles per cubic fermi corresponds to $k_F = 1.36\ fm^{-1}$. To avoid an infinite coulomb energy we suppose the coulomb force to be turned off. Then, because nuclear matter forces are charge symmetric we expect N=Z and the binding energy of the system will be the coefficient a_1 in the semi-empirical mass formula, since $A\to\infty$. This has the value -16 MeV per particle.

Nuclear matter is popular with theorists because there are no surface effects and the single particle orbitals are represented by plane waves. Thus nuclear matter has become a testing ground for models of the nucleon-nucleon force.

As the theory is generally accepted it is non-relativistic and includes the two-body force only. The forces used must provide reasonable fits to the nucleon-nucleon scattering data. (Some authors such as Nogami, Ross and Bhaduri, (1970) and Loiseau (1971) believe the three-body force may contribute a small amount to the net energy per particle, about 1 MeV).

The Brueckner theory of nuclear matter requires that one evaluate the G-matrix, which is defined in analogy to the Lipmann-Schwinger equation for the reaction matrix T:

$$T = V - V \frac{1}{e} T$$

This is derived from two-body scattering theory

$$\langle r|\psi\rangle = e^{ik\cdot r} - \int\langle r|\underset{\sim}{q}\rangle \frac{d^3q}{q^2-k^2-i\varepsilon} \langle \underset{\sim}{q}|V|\psi\rangle$$

The $-i\varepsilon$ is equivalent to the usual asymptotic boundary condition

$$\langle r|\psi\rangle \sim e^{ik\cdot r} + \frac{e^{ik\cdot r}}{r} f(\theta)$$

By studying the integral term of the Lippmann-Schwinger equation one may identify

$$\langle \underset{\sim}{k}'|V|\psi\rangle \sim f(\theta)$$

where $f(\theta)$ is the usual scattering amplitude; $\underset{\sim}{k}\cdot\underset{\sim}{k}' = kk'\cos\theta$

We can iterate the equation for $|\psi\rangle$:

$$|\psi\rangle = |\underset{\sim}{k}\rangle - \frac{1}{e} V|\underset{\sim}{k}\rangle + \frac{1}{e} V \frac{1}{e} V|\underset{\sim}{k}\rangle$$

$$- \frac{1}{e} V \frac{1}{e} V \frac{1}{e} V|\underset{\sim}{k}\rangle$$

from which:

$$\langle \underset{\sim}{k}'|V|\psi\rangle = \langle \underset{\sim}{k}'|V|\underset{\sim}{k}\rangle - \langle \underset{\sim}{k}|V \frac{1}{e} V|\underset{\sim}{k}\rangle$$

$$+ \langle \underset{\sim}{k}|V \frac{1}{e} V \frac{1}{e} V|\underset{\sim}{k}\rangle - \ldots\ldots$$

Finally we can define

$$\langle \underset{\sim}{k}'|V|\psi\rangle \equiv \langle \underset{\sim}{k}'|T|\underset{\sim}{k}\rangle \sim f(\theta)$$

with

$$T = V - V \frac{1}{e} T$$

which is the Lipmann-Schwinger equation for the T operator. Thus T is defined as the operator whose matrix element is the scattering amplitude. In the above we have identified

$$\frac{1}{e} \sim \frac{1}{q^2-k^2-i\varepsilon}$$

The $(+i\varepsilon)$ prescription for treating the singularity at the pole $(q=k)$ effectively forbids scattering into state k, which is already occupied.

Similarly in nuclear matter theory where there are more than two particles, the analogous equation, called the Brueckner Goldstone equation is

$$G = V - V \frac{Q}{e} G$$

Q prevents scattering into occupied states below the fermi surface,

$$|k| < k_F$$

The denominator e becomes

$$e = T_1 + T_2 + U_1 + U_2 - W$$

U is the single particle potential and W is the starting energy.

$$W = \frac{\hbar^2}{2m} (k_\alpha^2 + k_\beta^2) + U(k_\alpha) + U(k_\beta)$$

of the two interacting particles in their initial states α and β.

With Brueckner theory the two body problem is solved exactly, allowing for the presence of other particles in an average way. Two particles are considered to be in a potential created by all the other particles and they are subject to

the Pauli principle. This is in contrast to Hartree Fock theory which considers each single particle as in a field created by all the other particles. Thus it is a solution of the one body problem allowing for the presence of other particles in an average way.

In the Brueckner theory

$$E/A = \langle T \rangle + \frac{1}{2\rho} \sum_{mn} \langle mn|G|mn \rangle$$

+ higher cluster contributions

If we compare this to the semi empirical mass formula value for binding energy per nucleon of -16 MeV per particle we may identify

$\langle T \rangle$	$\sim$	+23 MeV
$\frac{1}{2\rho} \sum_{mn} \langle mn\|G\|mn \rangle$	$\sim$	-35 MeV
others	$\sim$	-4 MeV
Total	$\sim$	-16 MeV

This, if we recall, is all in aid of treating the true potential which has an infinite core in a workable fashion. We now see that

$$\langle mn|G|mn \rangle = \langle mn|V_{True}|\psi_{mn} \rangle$$

where ψ_{mn} is a correlated two body wave function.

To apply the Brueckner theory to finite nuclei is more difficult. The single particle orbitals, which were simply plane waves, are replaced by some suitable basis which represents as closely as possible finite nuclear

single particle orbitals. Q limits excitation to unoccupied states and the denominator e will refer to the energies of the particles under consideration in the finite nucleus.

Hartree Fock states are then computed using the appropriate G-matrix for finite nuclei as the net two-body interaction. However, Brueckner Hartree Fock is difficult because of the double self consistency; the Hartree Fock self consistency, and the Brueckner self consistency of the G matrix which involves the single particle energies and orbitals but which also determines them.

Instead of the above complicated procedure, Brueckner, Gammel and Weitzner (1958) proposed to split the calculation into two separate parts. They proposed to calculate G in nuclear matter as a function of density and then use it to do Hartree Fock calculations. The Local Density Approximation is employed, in which one uses the G matrix appropriate to the density $\rho(R)$ at the point where the particles interact. Such an approximation would be justified if the density $\rho(\underset{\sim}{R})$ varied slowly over a distance equal to the range of the nucleon-nucleon force.

In later work the further approximation was made of replacing G (which is now local) by a "local effective interaction." This was done since one has more intuition as to how a local force should look and behave. The criterion for the local effective force is that

$$\langle mn|V_{eff}|mn\rangle = \langle mn|G|mn\rangle$$

as closely as possible ($\sim$ 3-5% in practice at worst)

Because V_{eff} is local, it turns out that the best one can hope to do is fit to the diagonal matrix elements of G. This is probably sufficient since these are the most important matrix elements in nuclear matter.

Sprung has constructed a density dependent effective force which reproduces the G matrix elements for a reasonable range of densities. This was done by fitting his function to the true G matrix values in nuclear matter at several densities. The value of the density used with such a force is determined by the Local Density Approximation. This, however is not an unambiguous function. It may take the form of the centre of mass density, the geometric or the arithmetic mean density of the two particles being considered.

The particular form which Sprung and Campi found best, and which is used in this study is the arithmetic mean. This will be discussed briefly in the next chapter. It is hoped however that keeping track of the density dependence of the G matrix in this way that one will more or less be using the correct G matrix for finite nuclei

$$\langle mn|G_{N.M.}(\rho)|mn\rangle$$

$$\sim \langle mn|G_{F.N.}|mn\rangle$$

CHAPTER III

THE POTENTIAL

(a) The Hamiltonian

The Hamiltonian used by Dr. Volkov, his collaborators (Manning 1967, Hughes 1970) and this author is

$$H = \sum_{i=1}^{A} T_i + \frac{1}{2} \sum_{ij=1}^{A} V_{ij}(\underset{\sim}{r}_1, \underset{\sim}{r}_2) - T_{c.m.}$$

$$+ \sum_{i<j}^{A} \frac{e^2}{|\underset{\sim}{r}_i - \underset{\sim}{r}_j|} + c \sum_{i=1}^{A} \underset{\sim}{\ell}_i \cdot \underset{\sim}{s}_i$$

where T_i is the one body kinetic energy operator, V_{ij} is a two body potential, $T_{c.m.}$ is the centre of mass kinetic energy operator which is subtracted out of the total Hamiltonian leaving an intrinsic Hamiltonian. The last two terms are the Coulomb and the spin orbit terms respectively.

The Hamiltonian used by X. Campi and Dr. Sprung (1972) in the coordinate space representation includes, in addition an energy dependent term (X. Campi 1972)

$$(W-W_o)A\ \delta(r)$$

where $W_o(k_F)$ is twice the average energy of a particle in nuclear matter at fermi momentum k_F and W is the corresponding energy for the two interacting particles in the finite nucleus. The energy dependent force acts only on S states.

The effect of the energy dependent term is found

to be about 0.6 MeV per particle. Also Campi's (1972) calculations for E/A are about 300 keV low for light nuclei. Since it would be awkward to amend our programme to include the W-dependent force, we have allowed for both these effects by renormalizing the Sprung Banerjee force so as to saturate nuclear matter with a binding energy of 17.5 MeV per particle, (unless otherwise indicated). This compares to X. Campi, who used 16.5 MeV per particle. The adjustment of the binding energy per particle E/A or the saturation density k_F is carried out according to the prescription given by Sprung and Banergee (1971).

(b) Types of Potentials

In recent years several "realistic" forces have been developed (Reid (1968), Hamada Johnston (1962), etc.). These however are difficult to handle owing to their strong repulsive core. Thus two classes of approximation have been evolved:

(a) the phenomenological force

(b) the effective force derived from a realistic force.

Dr. Volkov's approach was that of the phenomenological interaction. As we have already indicated the phenomenological force is a rather ad hoc mathematical function which may or may not bear any relation to the realistic force. However, it is constrained by the following conditions (Hughes (1970)):

1) That the interaction reproduce the correct, experimentally determined S-wave phase shifts for free nucleon-nucleon scattering at various relative energies, especially those which are important for nucleons interacting within a finite nucleus.

2) That the interaction have roughly the same long range behaviour as "realistic" potentials.

3) That the interaction saturates nuclear matter at the "correct" saturation density,

$$k_F = 1.36 \text{ fm}^{-1}$$

and binding energy per particle,

$$E/A = -16 \text{ MeV}$$

4) That the interactions have small second order correction terms in nuclear matter.

5) That the matrix elements for the interaction be easily evaluated.

In the second "realistic force" case, one wishes to approximate the G-matrix elements as closely as possible with some well behaved effective interaction potential.

In both types of forces developed at McMaster, gaussians have been used to facilitate the calculations of matrix elements.

(i) The Volkov Potential

Initially Volkov used a double gaussian two body interaction (Volkov 1965, Hughes 1970) of the form

$$V(r) = \{V_a \exp\left(-\frac{r^2}{\lambda_a^2}\right) + V_r \exp\left(-\frac{r^2}{\lambda_r^2}\right)\}$$

$$(W + MP_x + BP_\sigma + HP_\tau)$$

where P_x, P_σ and P_τ are the Majarana or space exchange operator, Bartlett or spin and Heisenberg or isospin exchange operators.respectively. V_a and V_r are the attractive and repulsive strengths of the force respectively.

However these forces did not saturate nuclear matter and only crudely fitted the S-wave scattering data.

An improvement in the S-wave scattering fit was accomplished by making λ_r velocity dependent. (Hughes, 1970)

$$\lambda_r(k) = \lambda_r{}^o[1 + c_1(k-c_2)^2]$$

where k is the relative wave number. These forces did then saturate nuclear matter but at an unrealistically high density, corresponding to

$$k_F = 2.5 \text{ fm}^{-1}$$

Thus, in order to get a realistic saturation density of nuclear matter, density dependence was incorporated (Volkov 1969, Hughes 1970, Manning 1967, Manning and Volkov 1967, Lassey 1972)

$$V(r) = \{V_a(1 + c_3 k_F{}^{n_1})e^{-(\frac{r}{\lambda_a})^2}$$

$$+ V_r(1 + c_4 k_F{}^{n_2})\, e^{-(\frac{r}{\lambda_r(k)})^2}\}$$

$$x(W + MP_x + BP_\sigma + HP_\tau)$$

where $k_F^{\,n} = (\frac{3\pi}{2}\rho)^{n/3}$

and $\lambda_r(k) = \lambda_r^{\,o}[1 + c_1(k-c_2)^2]$

The Volkov forces specifically mentioned in this thesis will have saturation density $k_F = 1.36$ fm^{-1} and B.E./A = -16 MeV.

The development of these forces and the choice and determination of the various parameters is elaborated on at great length by Hughes (1970).

(ii) The Sprung-Banerjee Potential

Dr.Sprung's force is an effective interaction derived from the realistic Reid potential. It is a local, effective interaction which reproduces the G matrix for reasonable densities of infinite nuclear matter. It has been shown that the non-local nature of the realistic force can be simplified to a local momentum dependent force by Brandow (1966). However further simplification to a purely local force in each partial wave is possible by averaging the momentum dependence over the Fermi sea at a given density (Donnelly 1968, Bhaduri and Warke 1968, Negele 1970, and Seimens 1970). A purely central force was created by averaging over the angular momentum states as well. Thus due to averaging, the force has no explicit momentum dependence, nor dependence on L and J. It still has an exchange character which we now discuss.

The force is expressed as a sum of Gaussians with a simple parameterization of the density dependence

$$V(r) = \sum_{i}^{5} [V_i^{o}(WMBH)_i + V_i' k_F^{n_i} (WMBH)_i'] e^{-(\frac{r}{\lambda_i})^2}$$

Three families of forces were produced: G-0, G-1 and G-3 with the index of the density dependence

$$n_i = n = 0.5,\ 1.0 \text{ and } 3.0$$

respectively,

The force can be alternatively expressed by stating the force which acts in each (S,T) subspace; triplet even, singlet even, singlet odd and triplet odd. These were converted to the more convenient (for our program anyway) Wigner, Majorana, Bartlett and Heisenberg exchange parameters by the transformations

$$^3S = W + M + B + H$$

$$^1S = W + M - B - H$$

$$^1P = W - M - B + H$$

$$^3P = W - M + B - H$$

where W + M is normalized to 1 following the Volkov convention

In Chapter four the various families of forces are studied: density approximation G-0, G-1, G-3; saturation density, k_F; and symmetry energy. The prescription for each of these is given by Sprung and Banerjee (1971).

The problem is to use a force equivalent to that of Campi for the Hartree Fock calculations of chapter five so that a meaningful comparison can be made. This is because Campi found his force to give good results for nuclei up to ^{208}Pb, while in the present work we study only light nuclei. The force used was G-0, with $k_F = 1.35\ fm^{-1}$, BE/A = 17.5 MeV and symmetry energy prescription.

(c) Density Dependence

As mentioned above, density dependence was found necessary by Volkov and Hughes in their study of phenomenological forces to produce a more realistic saturation density in nuclear matter and to prevent the collapse of nuclei with A>16. (Hughes 1970)

In nuclear matter, density is a constant

$$\rho = \frac{2}{3\pi^2} k_F^3$$

However for finite nuclei where the density varies with r, the Local Density Approximation is used. The symbol ρ is often interpreted as the density at the centre of mass.

$$\underset{\sim}{R} \quad \underset{\sim}{r}_1 + \underset{\sim}{r}_2$$

However this would give too high a density for two particles at opposite sides of the nucleus since the density at the centre of the nucleus is invariably quite high, while the particles would actually be in a low density region.

Volkov and Hughes (1970) have considered as alternatives both the geometric and the arithmetic means of the densities

$$\rho(R) = \sqrt{\rho(|r_1|)\rho(|r_2|)}$$

$$\rho(R) = \frac{1}{2}[\rho(r_1) + \rho(r_2)]$$

and have concluded that the arithmetic mean is superior. Sprung and Campi (1972) have also come to this conclusion. The arithmetic mean gives the correct symmetry energy in nuclear matter, as compared to proper G-matrix calculations.

In order to quickly determine the density at a point, the density is first calculated properly as the sum of squared orbitals, but then is fitted to a single gaussian. This approximation is used since it allows us to use Volkov's matrix element program even for the density dependent force. The fitting is done by constraining the gaussian to have the same $\langle\rho^2\rangle$, $\langle z^2\rangle$ and normalization as the nuclear density.

This approach was sufficient for the Volkov type force which had a weak density dependence. For forces with strong density dependence, however, we may require a more accurate approximation. We could expand the ρ^λ as a sum of several gaussians. This would be especially critical in the case of strong deformation or asymmetry (Hughes 1970).

(d) Rearrangement Term

As had already been indicated, the use of density dependent forces requires the variation of the density dependent force, as well as the wave functions. This not

only alters the variational nature of the matrix diagonalization approach, but also adds an extra complicating term to the Hartree Fock equations. This term is called the rearrangement term. The density dependence is a way of including in an approximate way the presence of other nucleons in the nucleus. The importance of the density dependent force and the rearrangement term has been indicated by Ripka (1969):

"It may be thought at first sight, that the density dependent forces are just one more of the effective interactions already used, and that the density dependence just adds a few extra parameters to the force so that it will obviously give a better fit to nuclear spectra. This point of view is wrong. The reason is that the density dependence of the force changes the dynamics of the system. Indeed, each time the density of a nucleus is changing--either because nucleons are captured or lost, or because the nucleus is vibrating or still because the nucleus makes a transition into a deformed shape--the interaction between all the nucleons is altered and this may result in a collective motion which is given the unimaginative name of rearrangement effects."

The following discussion also follows Ripka closely. The Hartree Fock Hamiltonian

$$E = \langle\Phi|H(\rho)|\Phi\rangle$$

$$= \sum_{\alpha}\langle\alpha|\tau|\alpha\rangle + \frac{1}{2}\sum_{\alpha\beta}\langle\alpha\beta|v(\rho)|\alpha\beta-\beta\alpha\rangle$$

becomes

$$\delta E = \langle \delta\alpha | t | \alpha \rangle + \frac{1}{2} \sum_{\beta} \langle \delta\alpha\beta | v(\rho) | \alpha\beta - \beta\alpha \rangle + \frac{1}{2} \sum_{\gamma\beta}^{A} \langle \gamma\beta | \delta v(\rho) | \gamma\beta - \beta\gamma \rangle$$

for each variation of α.

Now each single particle orbital can be expanded:

$$\psi_\alpha = \sum_i C_i^\alpha \psi_i(r)$$

where $\psi_i(r)$ is an harmonic oscillator orbital.

The variation becomes

$$\frac{\delta}{\delta C_i^{\alpha*}} [E - e_\alpha \sum_i C_i^{\alpha*} C_i^\alpha] = 0$$

Now the density becomes

$$\rho(\underset{\sim}{r}) = \sum_\alpha |\psi_\alpha(r)|^2 = \sum_\alpha \sum_{ij} C_i^{\alpha*} C_j^\alpha \phi_i^*(r) \phi_j(r)$$

If the density dependent potential is of the form

$$v(\rho) = v_o(r) + v_1(r) f(\rho_1, \rho_2)$$

where $r = |\underset{\sim}{r}_1 - \underset{\sim}{r}_2|$

and if the density dependence is of the form $f \simeq (\sqrt{\rho(r_1)\rho(r_2)})^\nu$ as in Lassey's case, then the derivative of the potential

$$\frac{\partial v}{\partial C_i^{\alpha*}} \sim v_1(r) \left\{ \frac{\partial}{\gamma\rho_1} f(\rho_1, \rho_2) \frac{\partial}{\gamma C_i^{\alpha*}} + \frac{\partial}{\partial\rho_2} f(\rho_1, \rho_2) \frac{\partial \rho_2}{\partial C_i^{\alpha*}} \right\}$$

$$\approx v_1(r)\left\{ \frac{\nu}{2} \frac{(\sqrt{\rho_1\rho_2})^{\nu}}{\rho_1} \frac{\partial\rho_1}{\partial C_i^{\alpha*}} + \frac{\nu}{2} \frac{(\rho_1\rho_2)^{\nu/2}}{\rho_2} \frac{\partial\rho_2}{\partial C_i^{\alpha*}} \right\}$$

where

$$\frac{\partial\rho(r_1)}{\partial C_i^{\alpha*}} = \sum_j C_j^{\alpha} \phi_i^*(r_1)\, \phi_j(r_1)$$

This allows us to evaluate the "rearrangement term"

$$\frac{1}{2} \sum_{\lambda\mu} \langle\lambda\mu| \frac{\partial v}{\partial C_i^{\alpha*}} |\lambda\mu\rangle$$

The derivative of the potential becomes:

$$\frac{\partial v}{\partial C_i^{\alpha*}} = v_1(r) f(\rho_1\rho_2) \frac{\nu}{2}$$

$$\left\{ \frac{1}{\rho_1} \sum_j C_j^{\alpha} \phi_i^*(r_1) \phi_j(r_1) + \frac{1}{\rho_2} \sum_j C_j^{\alpha} \phi_i(r_2) \phi_j(r_2) \right\}$$

$$= v_1(r) f(\rho_1\rho_2) \left\{ \frac{\nu}{\rho(R)} \sum_j C_j^{\alpha} \phi_i^*(R) \phi_j(R) \right\} \text{ "1+2"}$$

This simply means the average of values at $R=r_1$ and $R=r_2$. In Ripka's paper (1969) this is the term:

$$\phi_i^*(R) \phi_j(R) \frac{dv}{d\rho}$$

Ripka finds the Hartree Fock equations

$$\sum_j \langle i|h|j\rangle C_j^{\alpha} = e_{\alpha} C_i^{\alpha}$$

where h is the Hartree Fock field whose matrix elements are

$$\langle i|h|j\rangle = \langle i|t|j\rangle + \sum_{\alpha} \langle i\alpha|v|j\alpha\rangle$$

$$+ \frac{1}{2} \sum_{\alpha\beta} \langle\alpha\beta| \phi_i(R) \phi_j(R) \frac{dv}{d\rho} |\alpha\beta\rangle$$

This last term is the rearrangement term. It then follows that:

$$\frac{\delta T}{\delta C_i^{\alpha*}} = \frac{\delta}{\delta C_i^{\alpha*}} \left\{ \sum_{ij} C_i^{\alpha*} C_j^{\alpha} \langle i|t|j\rangle \right\}$$

$$= \sum_j C_j^{\alpha} \langle i|t|j\rangle$$

and

$$\frac{\delta V}{\delta C_i^{\bar{\alpha}*}} = \frac{1}{2} \frac{\delta}{\delta C_i^{\bar{\alpha}*}} \left\{ \sum_{\alpha\beta} \sum_{jk\ell m} C_j^{\alpha*} C_k^{\beta*} C_\ell^{\alpha} C_m^{\beta} \langle jk|v|\ell m\rangle \right\}$$

The indices $i=j$ and $\bar{\alpha}=\alpha$ or $i=k$ and $\bar{\alpha}=\beta$ give 2 equivalent terms, and so they drop out when differentiated, giving

$$\frac{2}{2} \sum_{\beta} \sum_{k\ell m} C_k^{\beta} C_\ell^{\bar{\alpha}} C_m^{\beta} \langle ik|v|\ell m\rangle$$

The summation can further be reduced since $\phi_\beta = \sum_k C_k^{\beta} \phi_k$ giving

$$\sum_{\beta} \sum_{\ell} \langle i\beta|v|\ell\beta\rangle C_\ell^{\alpha}$$

Or if we change the dummy index ℓ to j

$$\sum_{\beta} \sum_{j} \langle i\beta|v|j\beta\rangle C_j^{\alpha}$$

where $\beta \equiv$ sum over Hartree Fock orbitals.

Thus in detail the rearrangement field is obtained from

$$\langle i|h_R|j\rangle = \frac{1}{2} \sum_{\alpha\beta} \langle \alpha\beta|v_1(r)(\sqrt{\rho_1\rho_2})^{\nu} \frac{\nu}{2} \{ \frac{1}{\rho(r_1)} \sum_j C_j^{\alpha} \phi_i^*(r_1) \phi_j(r_1)$$

$$+ \frac{1}{\rho(r_2)} \sum_j C_j^{\alpha} \phi_i^*(r_2) \phi_j(r_2) \} | \alpha\beta\rangle$$

Thus:

$$\langle i|h_R|j\rangle = \frac{1}{2}\sum_{\alpha\beta}\langle\alpha\beta|v_1(r)(\sqrt{\rho_1\rho_2})^{\nu}\frac{\nu}{2}\{\frac{1}{\rho(r_1)}\phi_i^*(r_1)\phi_j(r) + \frac{1}{\rho(r_2)}\phi_i^*(r_2)\phi_j(r_2)\}|\alpha\beta\rangle$$

For a zero range force $v_1(r)\rightarrow\delta(r_1-r_2)$ and $\rho(r_1) = \rho(r_2) = \rho(R)$

$$\langle i|h_R|j\rangle = \frac{1}{2}\sum_{\alpha\beta}\langle\alpha\beta|(\frac{dv}{d\rho})_R\phi_i^*(R)\phi_j(R)|\alpha\beta\rangle$$

If we allow $\langle\alpha| = \phi_\alpha^*$ to switch places with $\phi_i^*(R)$ and similarly $\phi_j(R)$ with $|\alpha\rangle$ we get

$$\langle i|h_R|j\rangle = \frac{1}{2}\sum_{\alpha\beta}\langle i\beta|(\frac{dv}{d\rho})_R\phi_\alpha^*(R)\phi_\alpha(R)|j\beta\rangle$$

But $\sum_\alpha \phi_\alpha^*(R)\phi_\alpha(R) \equiv \rho(R)$

Thus for the delta function force

$$\langle i|h_R|j\rangle = \frac{1}{2}\sum_\beta\langle i\beta|\rho(R)(\frac{dv}{d\rho})_R|j\beta\rangle$$

In general one must deal with more complicated forces including exchange terms

$$\langle i|h_R|j\rangle = \frac{1}{2}\sum_{\alpha\beta}\langle i\beta|v(r)(\sqrt{\rho_1\rho_2})^{\nu}\frac{\nu}{2}\frac{\phi_\alpha^*(r_1)\phi_\alpha(r_1)}{\rho(r_1)}|j\beta\rangle + \frac{1}{2}\sum_{\alpha\beta}\langle\alpha i|v(r)(\sqrt{\rho_1\rho_2})^{\nu}\frac{\nu}{2}\frac{\phi_\beta^*(r_2)\phi_\beta^*(r_2)}{\rho(r_2)}|\alpha j\rangle + \text{exchange}$$

By interchanging the dummy indices α and β we get

$$\langle i|h_R|j\rangle = \frac{1}{2}\sum_\beta\langle i\beta|v_1(r)\nu(\sqrt{\rho_1\rho_2})^{\nu}|j\beta\rangle + \text{exchange}$$

Thus the direct rearrangement terms are simply the previously calculated matrix elements of $v_1(r)(\sqrt{\rho_1\rho_2})^\nu$ multiplied by ν where $\nu(\sqrt{\rho_1\rho_2})^\nu$ is $\rho\frac{df}{d\rho}$

The exchange part is not so simple. This is

$$\frac{1}{2}\sum_{\alpha\beta}\langle i\beta|\, v_1(r)(\sqrt{\rho_1\rho_2})^\nu\,\frac{\nu}{2}\,\frac{\phi_\alpha^*(r_1)\phi_\beta(r_1)}{\rho(r_1)}\,|\alpha j\rangle$$

$$+\frac{1}{2}\sum_{\alpha\beta}\langle \alpha i|v_1(r)(\sqrt{\rho_1\rho_2})^\nu\,\frac{\nu}{2}\,\frac{\phi_\beta^*(r_2)\phi_\alpha(r_2)}{\rho(r_2)}\,|j\beta\rangle$$

The factor $\frac{1}{2}$ can be removed from each term if the dummy indices are changed, $\alpha\to\beta$, $\beta\to\alpha$, $1\to2$, and $2\to1$ in the second term. This gives

$$\frac{1}{2}\sum_{\alpha\beta}\langle i\beta|v_1(r)(\sqrt{\rho_1\rho_2})^\nu\,\nu\,\frac{\phi_\alpha^*(r_1)\phi_\beta(r_1)}{\rho(r_1)}\,|\alpha j\rangle$$

This can be restated as in Lassey's Thesis (1972)

$$\frac{1}{2}\sum_{\beta}\langle i\beta|(\rho\,\frac{dv}{d\rho})\sum_{\alpha}\frac{\phi_\alpha^*(r_1)\phi_\alpha(r_2)\phi_\beta(r_1)}{\rho(r_1)\phi_\beta(r_2)}\,|\beta j\rangle$$

where $\rho\,\frac{dv}{d\rho}$ is $v_1(r)(\sqrt{\rho_1\rho_2})^\nu$

and $|\alpha\rangle$ has been replaced by $|\beta\rangle$ by multiplication and division by $\phi_\beta(r_2)$. This is approximated by Lassey to

$$\lambda\sum_{\beta}\langle i\beta|\rho\,\frac{dv}{d\rho}\,|\beta j\rangle$$

where $2\lambda \equiv \xi_\beta(r_1r_2) \equiv \sum_{\alpha}\frac{\phi_\alpha^*(r_1)\phi_\alpha(r_2)\phi_\beta(r_1)}{\rho(r_1)\phi_\beta(r_2)}$

It was also shown that for a zero range force $\lambda = 0.5$. Using the Slater approximation, which treats the wave functions as plane waves in calculating the mixed density, λ can be argued

to be close to 0.5, again for short range interactions. The approximation λ = constant is probably not a good one, but we have so far been unable to improve on this aspect of the calculation. (See below)

From a study of single particle levels in ^{40}Ca as a function of λ we find agreement with the single particle energies of Campi for both neutrons and protons as follows:

Level	λ
s	-0.5
p	0.0
d	+0.5

This is not understood at all. Total binding energy does not depend much on λ. There is either no minimum or an inconsequentially shallow one. The radius decreases linearly as λ decreases for both neutrons and protons. The S levels are not bound enough and the $2S_{1/2}$ level is quite above the $d_{3/2}$ level.

In addition there seems no justification for varying the value λ to obtain the lowest binding energy as was done by Lassey. His choice of λ would appear to be arbitrary. We have chosen λ = 0.4 since it is close to 0.5, and because the single particle energies are not totally unreasonable at that value. However a λ of 0.3 could position the p and d levels slightly better, within 3 MeV of the Campi levels. A little more spin orbit force might help by separating the p levels a bit more. However we may be paying the price of not having the W-dependent

force in the Hamiltonian.

It is believed that the approach may be improved by approximating $\xi_\beta(r_1 r_2)$ to a gaussian instead of a constant. The estimate of Lassey from the Slater approximation was:

$$\xi_\beta(r_1,r_2) \sim 3 \frac{j_1(k_F r)}{(k_F r)} \quad j_o(k_o r)$$

where $r = \underset{\sim}{r}_1 - \underset{\sim}{r}_2$.

If $k_F r \equiv x$ and $k_o r \equiv y$.

$$\xi_\beta(r_1,r_2) \sim (1 - \frac{x^2}{10} \ldots)(1 - \frac{y^2}{6} \ldots)$$

$$\sim e^{-x^2/10} \; e^{-y^2/6}$$

If we estimate $k_o^2 \sim \frac{3}{5} k_F^2$ we find

$$\xi_\beta(r_1,r_2) \sim e^{-\frac{x^2}{5}} = e^{-k_F^2 \, r^2/5}$$

Since we can approximate $k_F \sim 1 \text{ fm}^{-1}$ we get

$$\xi_\beta(r_1 r_2) \sim e^{-r^2/5}$$

It is from this type of estimate that we obtain the approximation

$$\frac{1}{2} \bar{\xi} \equiv \lambda \sim 0.4$$

The problem is that, since the entire Volkov approach is gaussian oriented, the programme requires that $\xi(r_1,r_2)$ be either a gaussian or a constant.

(e) The Coulomb Potential

Owing to the use of axially symmetric wave functions the two body matrix elements of the Coulomb potential cannot

easily be calculated as they can for a spherically symmetric basis. There is a closed form in terms of hypergeometric functions, however the expression is so complicated that the computer code would be time consuming. If we are to use the standard Volkov matrix element code, then the Coulomb potential

$$V_c(r) = \frac{e^2}{r}$$

must be expressed as a sum of gaussians:

$$V_c^{app}(r) = e^2 \sum_{n=1}^{N_c} C_n \exp\{-(r/B_n)^2\}$$

The fitting procedure used to determine the C_n and B_n coefficients is described in the Appendix of Lassey's thesis (1972). The matrix elements of $V_c(r)$ can be quite reasonably reproduced with $N_c=6$. The strengths C_n and ranges B_n are tabulated below in Table 3.1, as computed by Lassey.

Table 3.1

n	C_n (fm^{-1})	B_n (fm)
1	315.060	0.014972
2	10.3501	0.21660
3	1.23224	0.78641
4	0.47666	1.6841
5	0.26451	3.5436
6	0.19582	11.822

The matrix elements are accurate within 0.5%. Errors greater than 0.1% are for matrix elements of small magnitude (Lassey, 1972). High accuracy is not required at small r owing to an r^2 weighting factor in the matrix element. On the other hand the finite radius of the nucleus excuses a poor fit at large r. For these reasons the results are accurate.

(f) The Spin Orbit Interaction

The Shell model demonstrated the importance of the spin-orbit interaction. This force split the degenerate p,d, ... levels and divided the energy levels up into shells corresponding to the observed magic numbers.

The two body spin orbit interaction can be approximated by the one body operator

$$V_{SO}(r) = U_{LS} \frac{1}{r} \frac{do}{dr} \underset{\sim}{\ell} \cdot \underset{\sim}{s}$$

for spherical nuclei, but for deformed nuclei the one body operator becomes

$$V_{SO}(\underset{\sim}{r}) = U_{LS} \underset{\sim}{s} \cdot (\nabla \rho (\underset{\sim}{r}) \times \underset{\sim}{k})$$

$\underset{\sim}{k}$ is the momentum operator $i\underset{\sim}{\nabla}$ and $\rho(\underset{\sim}{r})$ is the density distribution (Blin Stoyle 1955).

The matrix elements of this operator can be readily calculated if we assume a gaussian density distribution. This procedure is explained in Appendix 3 of Lassey's thesis (1972).

The spin orbit strength U_{LS} used in this work was 130.0 MeV - fm^5 which is the same as that used by X. Campi.

References to forces A and B of Volkov , in Lassey's thesis use a spin orbit strength of 150.8 MeV - fm^5 which was derived by Negele for a similar effective interaction.

CHAPTER 4

Variational Calculations

In this chapter Sprung's effective nucleon nucleon forces are studied using a simplified Hartree Fock procedure. This is a variational calculation in which each orbital is represented by a single oscillator function. The variation is done with respect to the oscillator α_i and β_i of each single particle orbital ϕ_i. The even even nuclei up to ^{40}Ca were studied. Even though this is a simpler program than Hartree Fock, it is believed that the results will be reasonably good. The forces were studied to determine which would be most suitable for the Hartree Fock calculations, and in the process to determine the general trends and properties of the forces with respect to binding energy per nucleon (E_s), saturation density (k_s), and symmetry energy value.

4.1 Choice of Force

In order to determine which form of Sprung's forces to use, one must consider the behavior of these forces, G-0, G-1 and G-3 with respect to saturation density k_F, binding energy per nucleon in nuclear matter, and symmetry energy value. This behavior is measured with respect to total binding energy, radius, and sometimes single particle

energies and quadrupole moments.

The first nucleus used for this study was ^{16}O. Since it is a spherical closed shell nucleus the effect of no mixing of basis orbitals should be minimal. Oxygen is not so large, as is ^{40}Ca, that the calculation would be time consuming. On the other hand it is not so small, as is ^{4}He, that our treatment of the density dependence might be inadequate.

The saturation density we selected at the outset was $k_s = 1.35$ fm^{-1} since Campi had found that it had worked well over the whole range of spherical nuclei. Since we can only examine nuclei up to A = 40, we cannot establish a preferred value for k_s in a reliable way.

Using this saturation density several variational calculations were done for ^{16}O using force G-0 each having a different binding energy in nuclear matter. The calculations were done with and without the Coulomb contribution in order to determine its effect on the total binding energy.

The results are tabulated in Tabel 4.1. It is found that the effect of the Coulomb potential in ^{16}O is to reduce the binding about 13 MeV and increase the radius about 0.025 fm.

The favoured force would seem to be one with E_s of 17.5 MeV per particle in nuclear matter. The radius is essentially

TABLE 4.1

	With Coulomb		Without Coulomb	
BE/A	Total Binding Energy	Radius	Total Binding Energy	Radius
14.5	- 86.6	2.815	- 99.32	2.787
16.0	-103.6	2.772	-116.53	2.747
16.5	-109.06	2.758	-122.02	2.734
17.0	-114.85	2.746	-127.87	2.723
17.5	-120.86	2.731	-133.95	2.708
18.0	-126.32	2.723	-	-
EXPT	-127.62	2.73		

the same as the experimental value, and the total binding energy is only 7 MeV low. This it is believed would be improved by the Hartree Fock procedure which allows mixing and should gain a few MeV binding energy. (See Ch. 5). In addition the value 17.5 MeV per particle seems reasonable compared to Campi's value of 16.5 MeV per particle. We do not have the"starting energy" dependent term in our Hamiltonian which Campi found to contribute about 0.5 MeV per particle. Further Campi found his ^{16}O calculation to be about 300 keV per particle underbound.

As a further check on the reliability of this force a calculation was done for ^{40}Ca. The results were very good. The radius again was almost identical to the experimental value and the total binding energy was still about 0.4 MeV low per particle. (See Table 4.2)

Using the same force, and the simplified Hartree Fock programme, the A=4n nuclei from ^{4}He to ^{40}Ca were studied. The results are tabulated in Table 4.3.

As can be seen from Fig.4.1 the binding energy per nucleon is lower in gereral than the experimental values with the exception of ^{4}He which is over bound. In all but the ^{16}O and ^{40}Ca nuclei the radii are too great by 0.2 or 0.3 fm. It can be speculated that this discrepancy for the deformed nuclei is due to the lack of mixing of

TABLE 4.2

E_s	Total Binding Energy	Per Particle	Radius
17.5	326.25	8.16	3.51
EXPT	342	8.55	3.50

TABLE 4.3

		CALCULATED					EXPERIMENTAL		
Nuclei	A	BE	BE/A	$\langle r^2 \rangle^{1/2}$	Q	Q/R	BE	BE/A	$\langle r^2 \rangle^{1/2}$
He	4	29.72	7.43	1.866	0.0	0.0	28.3	7.075	1.67
Be	8	52.3	6.54	2.63	6.75	0.977	56.5	7.06	-
C	12	81.04	6.75	2.71	-3.76	-0.511	92.2	7.68	2.42
O	16	120.86	7.55	2.73	0.00	0.00	127.6	7.975	2.73
Ne	20	147.41	7.37	3.14	6.62	0.670	150.6	8.03	
Mg	24	171.5	7.16	3.24	6.44	0.612	198.3	8.26	2.98
Si(prolate)	28	218.7	7.79	3.355	6.88	0.611	236.5	8.45	3.04
Si(oblate)	28	208.5	7.45	3.39	-5.78	-0.504	236.5	8.45	3.04
S(prolate)	32	246.6	7.71	3.37	3.90	0.343	271	8.47	3.12-3.33
S(oblate)	32	239.6	7.49	3.42	-4.41	-0.377	271	8.47	3.12-3.33
Ar	36	289.5	8.04	3.455	-3.16	-0.264	306	8.5	
Ca	40	326.3	8.16	3.51	0.0	0.0	342	8.55	3.50

Figure 4.1

B.E./A in MeV for the 4 A nuclei for force G-O ; k_s = 135 fm^{-1}, E_s = 17.5 MeV

(a) Solid line is the variational procedure

(b) Broken line is experiment

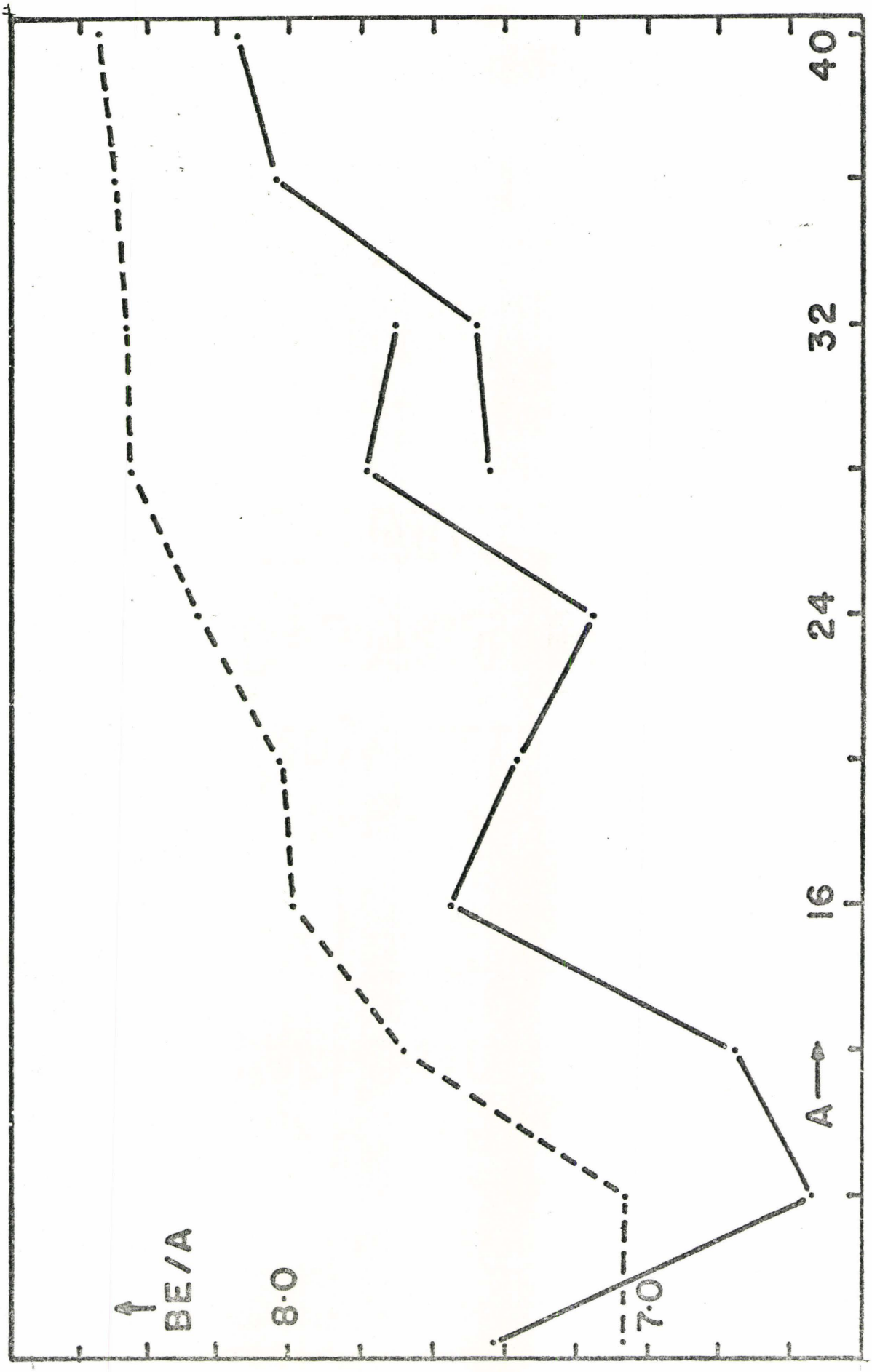

Figure 4.1

basis orbitals; and the fact that we have not projected out the ground state with J=0. The ^{4}He discrepancy is not understood. In Campi's work there is seen a trend for ^{4}He to be less underbound. In Table 4.3, the quadrupole moments of the nuclei are also quite reasonable. These will be compared with other calculations later.

4.2 Comparison of Forces G-0, G-1, G-3

Having obtained a G-0 force which gives such good results we then attempted to get a similar G-1 and G-3 force and to compare them. The forces were normalized to a saturation density of k_s=1.35 fm^{-1} and calculations were performed for three or four values of binding energy per nucleon for both ^{16}O and ^{40}Ca. In Table 4.4a and 4.4b are listed the binding energy and radii of ^{16}O for the various binding energies per nucleon in nuclear matter using forces G-1 and G-3 respectively. Similarly Table 4.5a and 4.5b show results for ^{40}Ca. These results are displayed graphically for ^{16}O and ^{40}Ca in Figs. 4.2 to 4.5.

From Fig.4.2 we see that the binding energy of ^{16}O will be lower for the G-1 and G-3 forces at a given binding energy per nucleon in nuclear matter, than for G-0; and that the G-1 and particularly the G-3 force will approach the G-0 result only at abnormally large values of E_s

From Fig.4.3 we see that the radii of ^{16}O for the

TABLE 4.4a

Force G-1 $k_s = 1.35$ fm^{-1} for ^{16}O

E_s	B.E.	BE/A	Radius
16.5	106.158	6.635	2.727
17.0	111.746	6.984	2.715
17.5	117.425	2.339	2.704
EXPT	127.6	7.98	2.73

TABLE 4.4b

Force G-3 $k_s = 1.35$ fm^{-1} for ^{16}O

E_s	B.E.	BE/A	Radius
16.5	91.097	5.694	2.681
17.0	96.464	6.029	2.671
17.5	101.764	6.360	2.661
18.0	107.121	6.695	2.652

TABLE 4.5a

Force G-1 $k_s = 1.35\ fm^{-1}$ for ^{40}Ca

E_s	BE	BE/A	Radius
16.5	285.24	7.131	3.5183
17.0	300.07	7.502	3.5065
17.5	315.10	7.878	3.4950
EXPT	342.	8.55	3.50

Force G-3 $k_s = 1.35\ fm^{-1}$ for Ca^{40}

E_s	BE	BE/A	Radius
16.5	245.50	6.138	3.4978
17.0	259.45	6.486	3.4886
17.5	273.21	6.830	3.4799
18.0	287.08	7.177	3.4718

G-1 and G-3 forces are progressively lower than G-0. At E_s=17.5 the G-1 is about 4% lower and the G-3 is about 10% lower than the G-0 force. The G-1 and G-3 radii would equal the G-0 (17.5 MeV/A) result at about E_s=16.4 and 14.0 MeV/A respectively.

Figures 4.4 and 4.5 show similar results for ^{40}Ca. Both binding energy per nucleon and the radius are lower for the G-1 and G-3 forces.

The conclusion of this study was that the G-1 and G-3 forces do not give results as reasonable as the G-0 force does at a saturation density of 1.35 fm^{-1}. Thus the G-0 force seems at this stage to be more reliable.

It was then believed that if force G-3 did not give reasonable results at k_s=1.35 fm^{-1} perhaps another value of the saturation density could be found which would give better results. The G-3 force was then normalized to k_s=1.30 fm^{-1} and calculations of BE and radius were performed at various BE/A in nuclear matter.

Table 4.6a and 4.6b give the results for ^{16}O and ^{40}Ca respectively calculated with k_s=1.30 fm^{-1}. These results are displayed in Figs. 4.6-4.9.

In Fig.4.6 the binding energy of ^{16}O is plotted as a function of BE/A in nuclear matter for both k_s=1.30 fm^{-1} and 1.35 fm^{-1}. The new k_s=1.30 fm^{-1} binding energies are

TABLE 4.6a

Force G-3 $k_s = 1.30\ fm^{-1}$ for ^{16}O

E_s	BE	BE/A	Radius
16.5	99.85	6.24	2.743
17.0	105.18	6.57	2.734
17.5	110.62	6.91	2.726
18.0	116.08	7.26	2.718
EXP	127.		2.73

TABLE 4.6b

Force G-3 $k_s = 1.30\ fm^{-1}$ for ^{40}Ca

E_s	BE	BE/A	Radius
16.5	263.83	6.60	3.594
17.0	277.60	6.94	3.586
17.5	291.61	7.29	3.578
18.0	305.64	7.64	3.572
EXP	342		3.50

Figure 4.2

Binding energy of ^{16}O vs. E_s, both in MeV

(a) Solid line is force G-O.

(b) Broken line is force G-1.

(c) Alternating dashes and dots is force G-3.

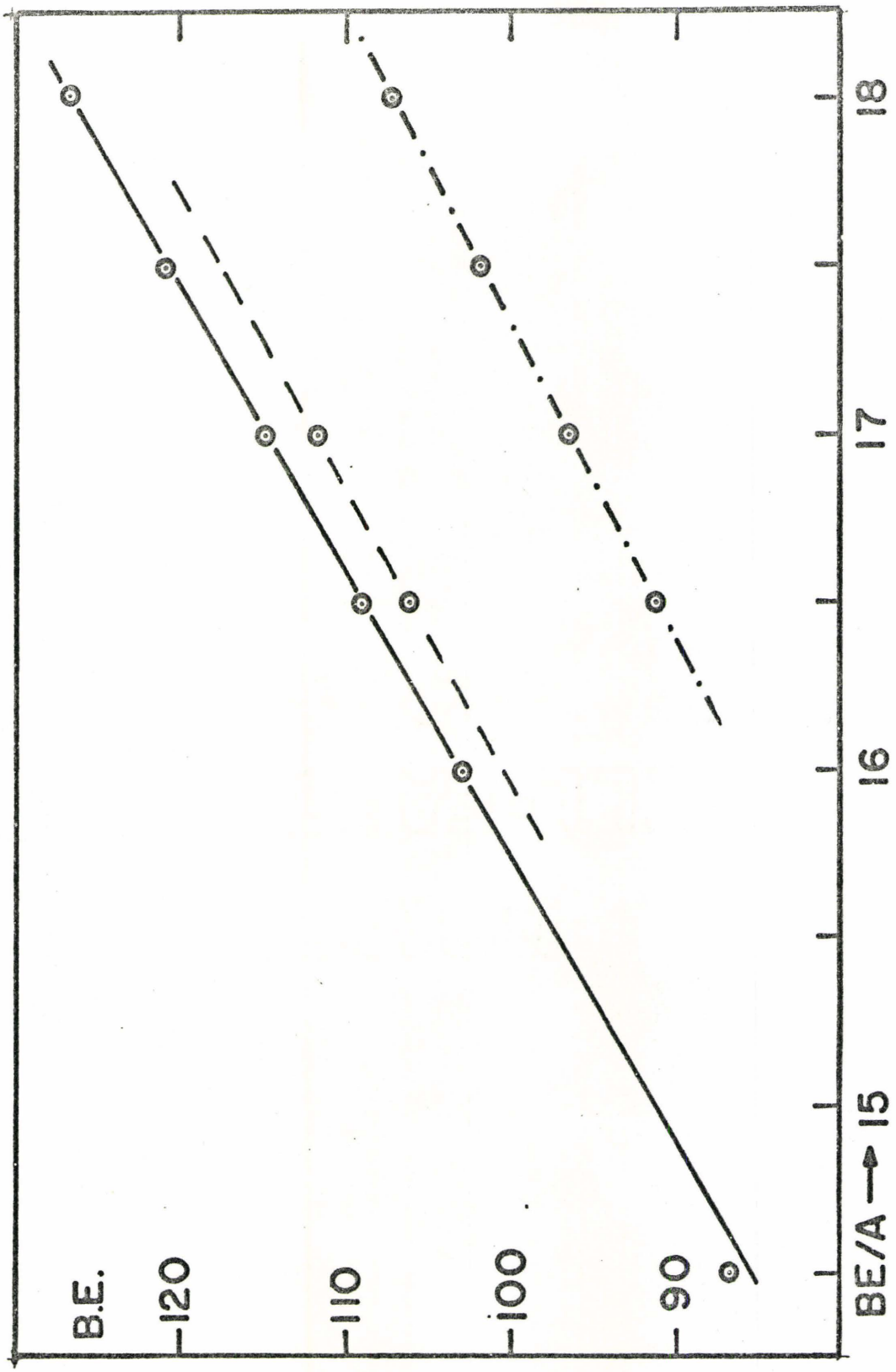

Figure 4.2

Figure 4.3

Radius in fm of ^{16}O vs. E_s in MeV

(a) Solid line is force G-O.

(b) Broken line is force G-1.

(c) Alternation dashes and dots is for force G-3.

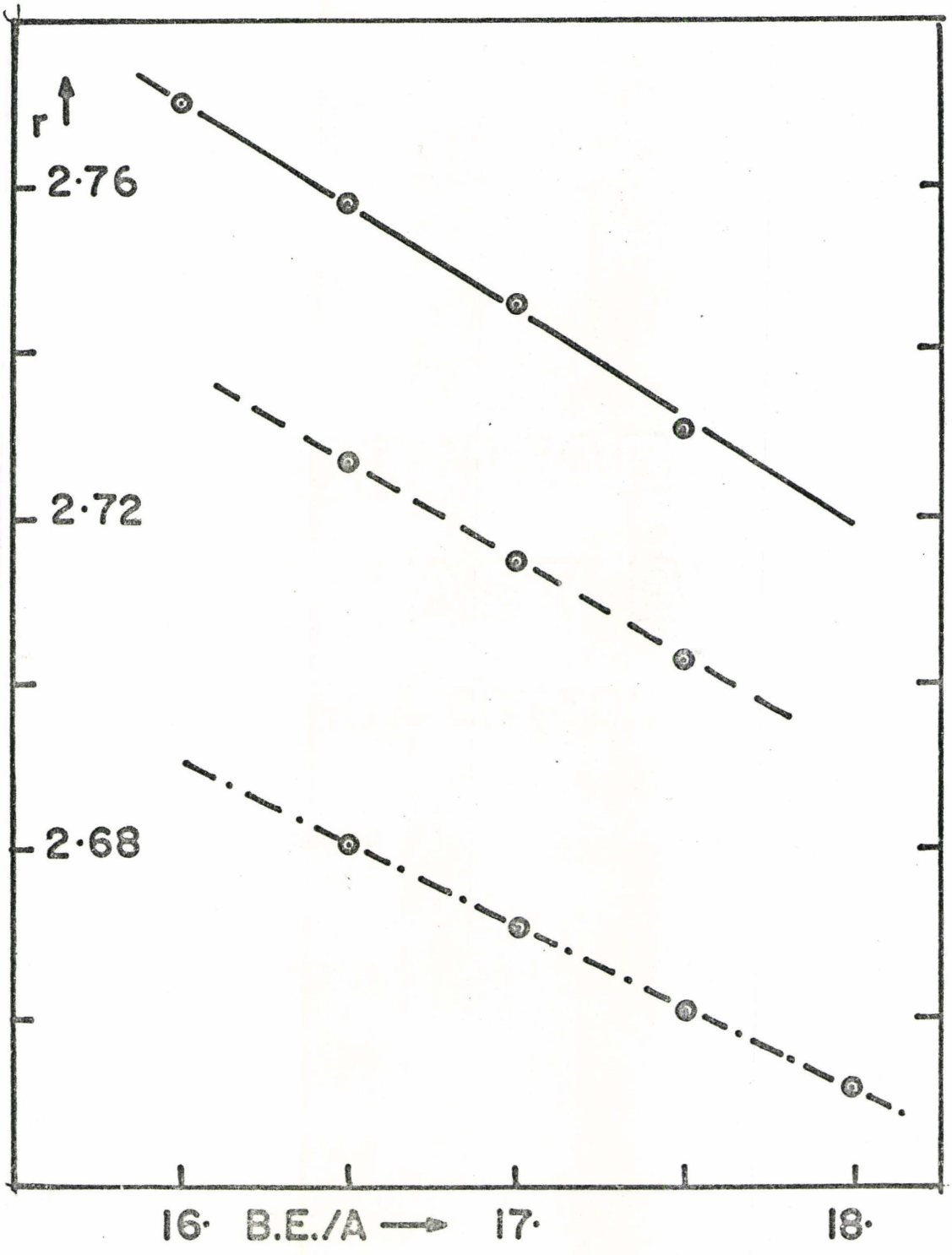

Figure 4.3

Figure 4.4

Binding energy of ^{40}Ca vs. E_s, both in MeV

(a) Solid line is force G-O.

(b) Broken line is force G-1.

(c) Alternating dots and dashes is for force G-3.

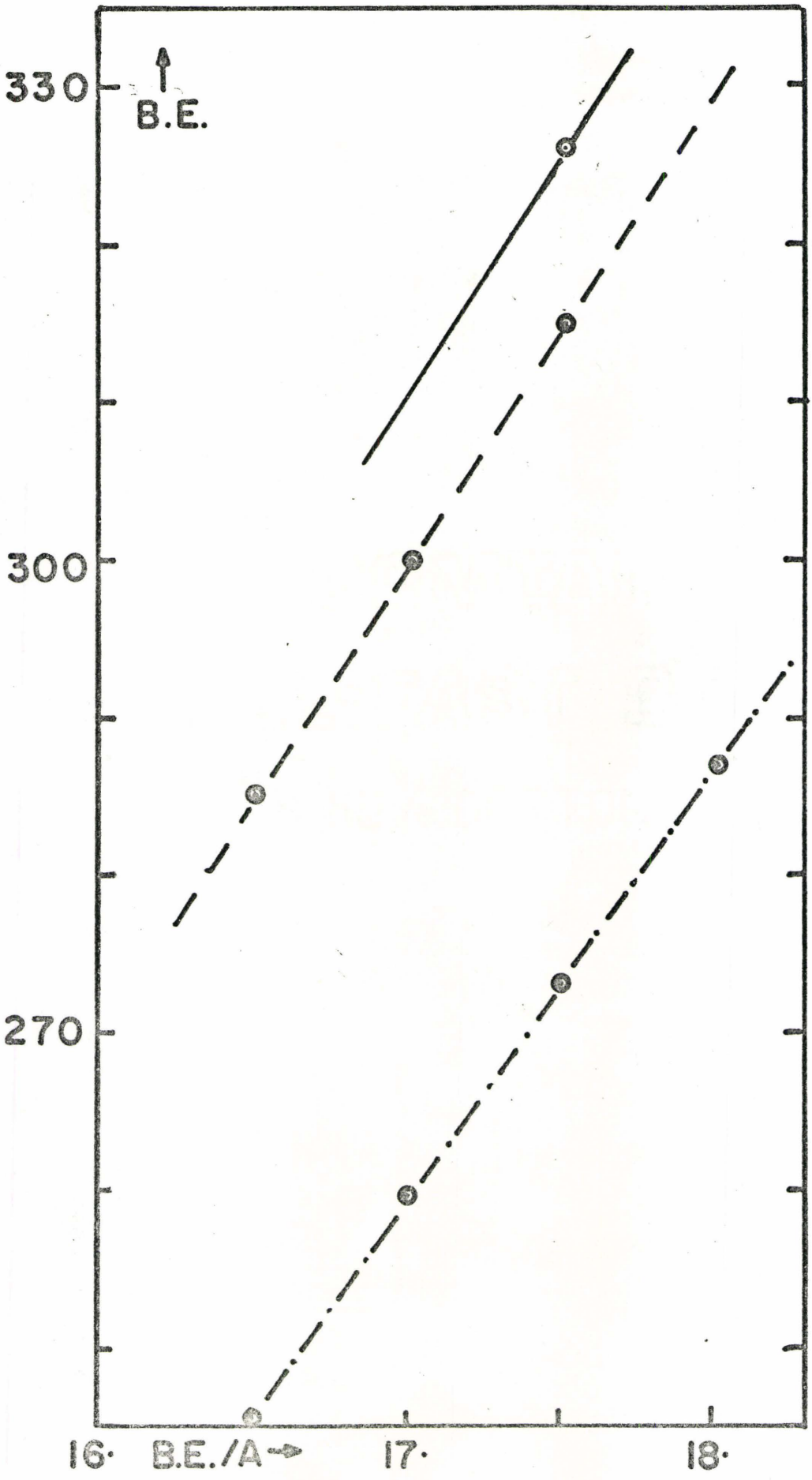

Figure 4.4

Figure 4.5

Radius in fm. of ^{40}Ca vs. E_s in MeV

(a) Solid line is for force G-0.

(b) Broken line is for force G-1.

(c) Alternating dots and dashes, G-3.

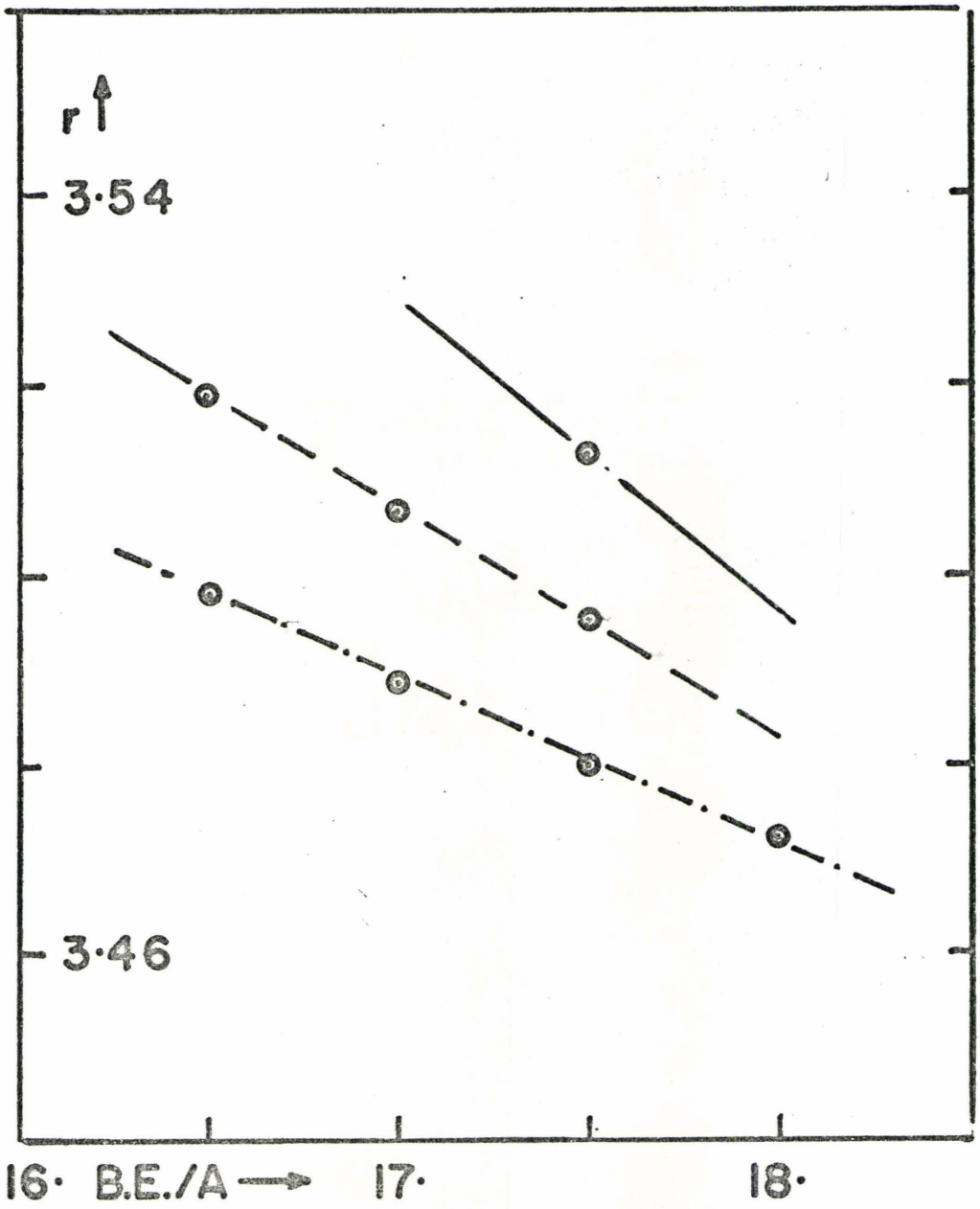

Figure 4.5

Figure 4.6

Binding energy of ^{16}O vs. E_s, both in MeV

(a) Solid line G-0, $k_s = 1.35$ fm^{-1}

(b) Broken line G-3, $k_s = 1.35$ fm^{-1}

(c) Alternating dots and dashes: G-3 $k_s = 1.30$ fm^{-1}.

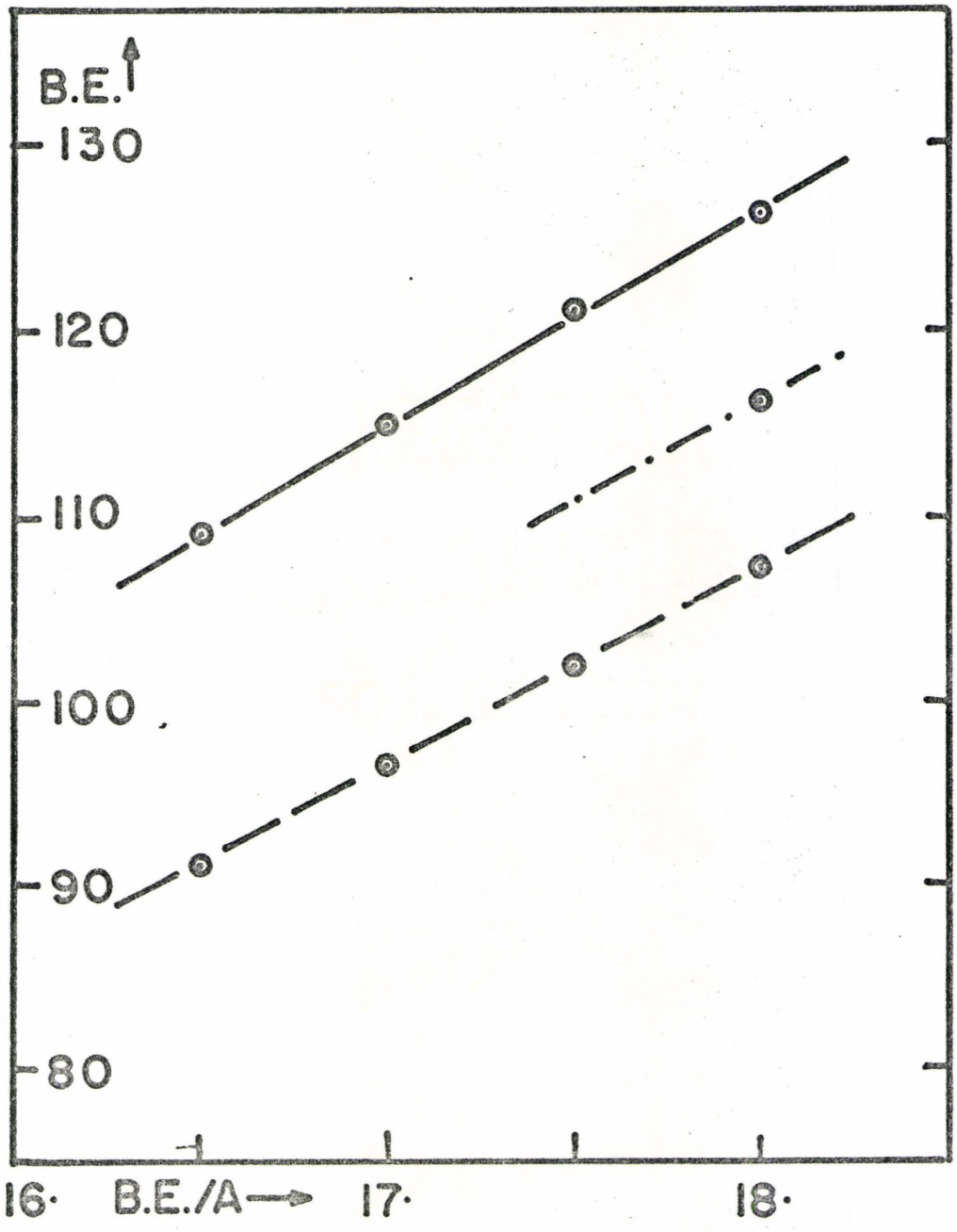

Figure 4.6

Figure 4.7

Radius in fm. of ^{16}O vs. E_s in MeV

(a) Solid line: G-0, $k_s = 1.35$ fm^{-1}

(b) Broken line: G-3, $k_s = 1.30$ fm^{-1}

(c) Dashes and dots: G-3, $k_s = 1.35$ fm^{-1}

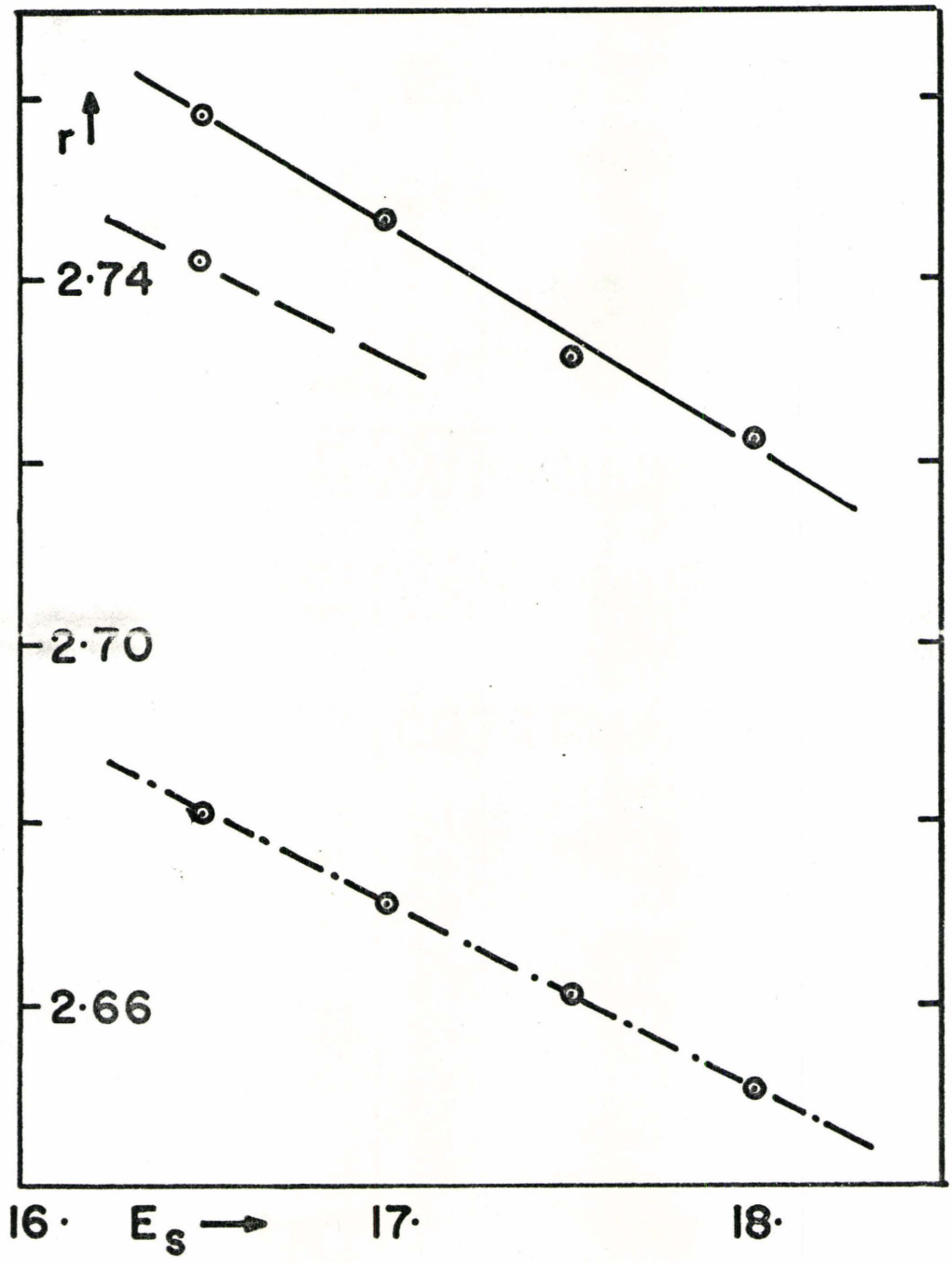

Figure 4.7

Figure 4.8

Binding energy of ^{40}Ca vs. E_s (both in MeV)

(a) Solid line G-3, $k_s = 1.35$ fm^{-1}

(b) Broken line G-3, $k_s = 1.30$ fm^{-1}

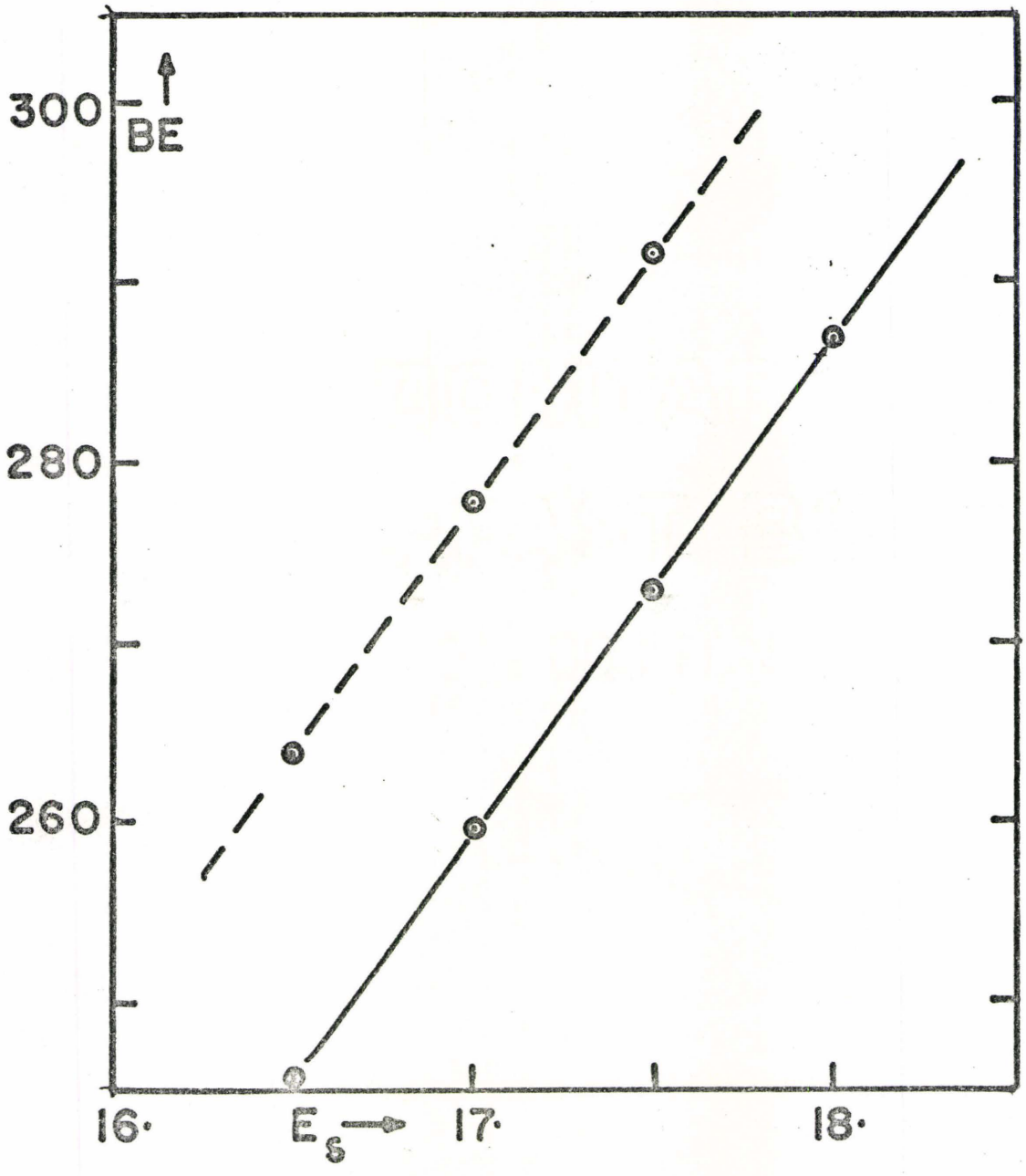

Figure 4.8

much improved over the k_s=1.35 fm^{-1} results. However they are still lower than the G-0 binding energies by the same amount as the improvement. This suggests that k_s=1.25 fm^{-1} would be a better choice.

If one looks at Fig.4.7 the k_s=1.30 fm^{-1} radii are quite close to the G-0 results and a value of k_s=1.39 would presumably line them up.

However the ^{40}Ca results are not so hopeful. The total binding energy of ^{40}Ca at E_s=17.5 in nuclear matter is only 293 MeV, about 50 MeV short of the experimental value. A very large change in saturation density would be necessary to approach the G-0 results. But what is more disturbing is Fig.4.9, which demonstrates that for k_s=1.30 the radii are already far too large. Any attempt to improve the total binding energy of ^{40}Ca by lowering the saturation density would result in far larger radii.

The results could perhaps be reconciled but only at a ridiculously large E_s in nuclear matter. This would make the ^{16}O results terrible. Thus we cannot get a "good" force G-3 which gives consistent results for both ^{16}O and ^{40}Ca. This is also assumed to be the case, to a lesser extent for G-1.

4.3 Symmetry Energy of Nuclear Matter

We will now study the character of force G-0 using different symmetry energy values. These forces were obtained

Figure 4.9

Radius in fm. of ^{40}Ca vs. E_s in MeV

(a) Solid line G-3, $k_s = 1.35$ fm^{-1}

(b) Broken line G-3, $k_s = 1.30$ fm^{-1}

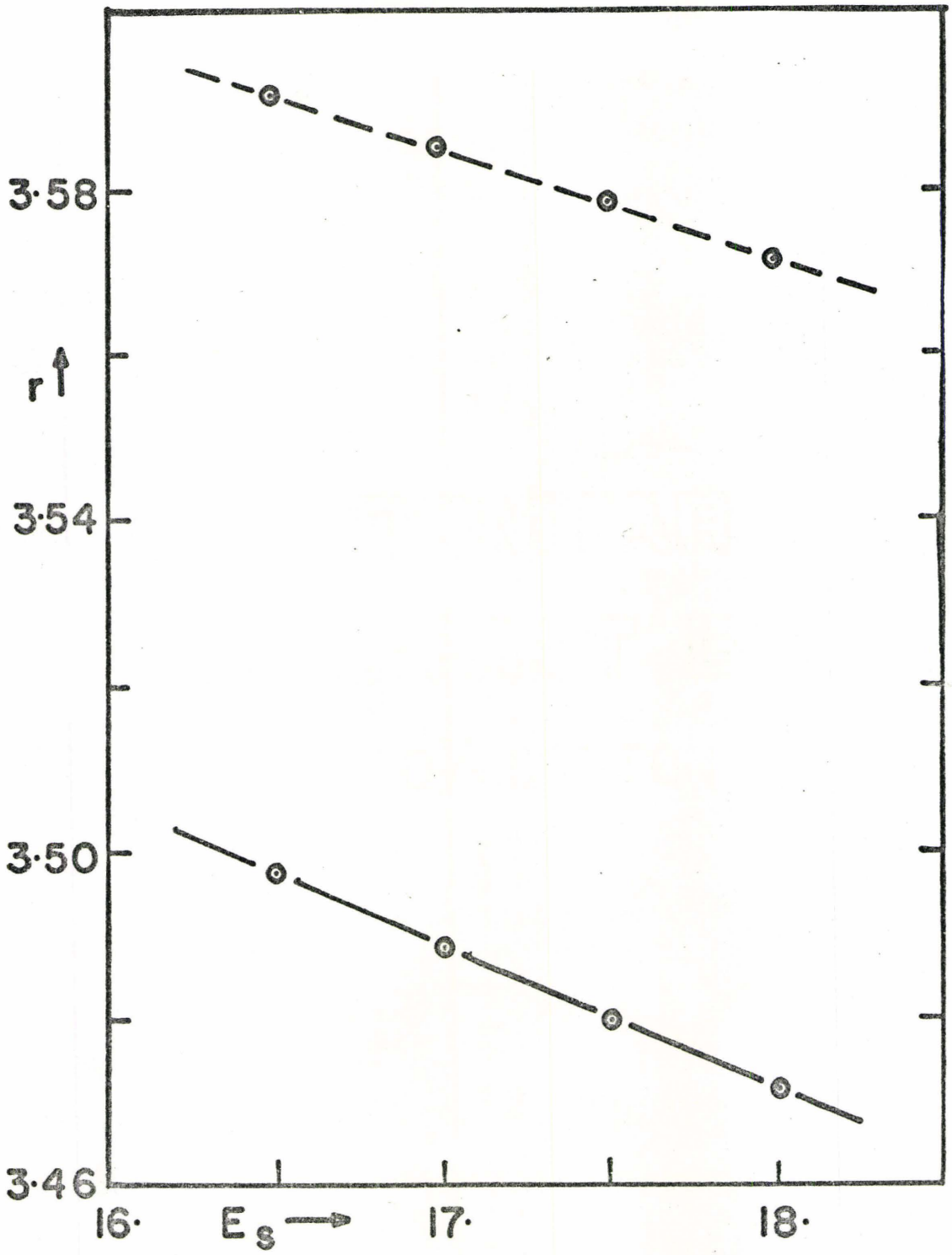

Figure 4.9

by normalizing the above force according to the following prescription.

Degree of Change	^1S Component renormalization	^3S Component renormalization
None (S = 34 MeV)	$\Delta(^1S)$	$\Delta(^3S)$
One (S = 36 MeV)	0	$2*\Delta(^3S)$
Two (S = 38 MeV)	$-\Delta(^1S)$	$3*\Delta(^3S)$

Basically the ^1S component is decreased by one unit and the ^3S increased by one unit for each degree of change. This is elaborated upon more completely by Sprung and Banergee (1971).

For various reasons it is justifiable to confine the renormalization to the ^3S state. One reason is the uncertainty in the ratio of the Tensor and central components of the basic nucleon force. Another is that the three body cluster is attractive in the ^3S state and repulsive in the ^1S state.

First we calculated ^{16}O using the three symmetry energy values. Table 4.7 gives the binding energies, radii, and crude single particle energies for each of these using our standard G-0 (17.5 MeV/A) force.

In nuclear matter the symmetry energy term will vanish for N=Z. Thus for finite nuclei, with N=Z not very much would be expected to happen as we change the symmetry energy. As is evident this simplified Hartree Fock approach

Properties of ^{16}O Calculated for different values of the Symmetry Energy of Nuclear Matter

TABLE 4.7

^{16}O E_s = 17.5 MeV/Particle k_s = 1.35 fm^{-1}

	S = 34 MeV	S = 36 MeV	S = 38 MeV
BE	-120.604	-120.668	-120.426
Coulomb Energy	13.022	13.020	13.020
Radii	2.7343	2.7346	2.7347
Neutron S.P. Energies			
1s	- 41.818	- 41.817	- 41.788
1p	- 25.938	- 25.944	- 25.912
Proton S.P. Energies			
1s	- 38.441	- 38.441	- 38.413
1p	- 22.723	- 22.729	- 22.698

does not distinguish between the different symmetry energy approximations. Similar results were observed for other binding energy per nucleon (16.5 MeV/A to 18.0 MeV/A) versions of force G-0. Thus it can be assumed spherical nuclei such as ^{16}O total binding energy, radii and our crude single particle energies are insensitive to the symmetry energy.

The deformed nuclei were then studied to see if this pattern of behaviour was also true for them. Three nuclei, ^{20}Ne, ^{24}Mg and ^{28}Si were calculated using each of the symmetry energy approximations. As can be seen from Table 4.8 the binding energies, and radii were insensitive to the degree of change in the symmetry energy approximation. The radii are especially insensitive.

Thus we see that in this type of calculation there is no preference as to which force is best. Therefore we settled on G-0 with one unit of change since this is the one which Campi found to be preferable for nuclei with $N \neq Z$ where the symmetry energy plays a much greater role.

In conclusion, G-0 force gives the best results when we select $k_s = 1.35$ fm^{-1} and $E_s = 17.5$ MeV. Force G-1 and G-3 give increasingly lower values for total binding energy and radii for ^{16}O and ^{40}Ca. In all cases as we increased BE/A, the binding energy in the finite nuclei rose linearly with a slope of ~ 1.2 and the radii decreased with a slope of 0.02. The attempt to correct

TABLE 4.8

Deformed Nuclei E_s = 17.5 MeV/A, k_s = 1.35 fm^{-1}

Symmetry Energy	34 MeV	36 MeV	38 MeV
Binding Energy			
Ne^{20}	-147.10	-147.19	-146.87
Mg^{24}	-171.05	-171.15	-170.78
Si^{28}	-218.08	-218.20	-217.75
Radii			
Ne^{26}	3.1470	3.1476	3.1474
Mg^{24}	3.2488	3.2492	3.2493
Si^{28}	3.3592	3.3596	3.3596

the poor results for G-3 at $k_s = 1.35$ by setting $k_s = 1.30$ was not successful. If a value of k_s was chosen to improve the total binding energy the radius would be unreasonably high. Finally the calculations we were doing were insensitive to changes in the symmetry energy value for both spherical and deformed nuclei. For the ensuing Hartree Fock calculations, the force G-0 with the symmetry energy adjusted by the "one unit" prescription was selected.

CHAPTER 5

5.1 Introduction

In this chapter the results of calculating the properties of the light nuclei using the Hartree Fock approach will be tabulated. As stated above, in Chapter four we shall use the force G-0 of Banergee and Sprung (1971) normalized to a saturation density of $k_s = 1.35$ fm^{-1} energy per nucleon $E_s = 17.5$ MeV, and symmetry energy S = 36 MeV. The spin orbit strength is 130 MeV fm^{-5}, the same as that used by X. Campi.

First, the spherical nuclei will be studied in order to determine the limitations of the present computer program, by comparing our results with those of other authors, especially X. Campi. These are of special interest because he also used the G-0 force of Sprung. He used the same parameters as above except for the energy per nucleon in nuclear matter. Campi's value was $E_s = 16.5$ MeV. We used a value 1 MeV higher than Campi because we did not have a starting energy term which contributed about 0.6 MeV per nucleon, in our Hamiltonian. In addition Campi's total binding energies tended to be about 0.4 MeV per nucleon low for the light nuclei. Assuming that our method is equivalent to Campi's, we should obtain very good energies for He, O and Ca.

Secondly, we studied the deformed nuclei, comparing them to the results of Lassey and Volkov (1972) and Zofka and Ripka (1971), This was done for each nucleus separately.

From these observations we will attempt to draw some conclusions about the force G-0 and the structure of light nuclei.

5.2 The Program

The Hartree-Fock program which has been used to obtain the results in this chapter is a modification of HARFO4S developed by Volkov, Manning and Lassey. The program was rewritten to accommodate up to a five gaussian density dependent force. With minor changes it could now be used for a force with any number of gaussians. The only limitation would be computer time. Space is conserved by summing the contributions of each gaussian and storing only one matrix for each of the Wigner, Majorana, Bartlett and Heisenberg exchange contributions. Momentum dependence of the range has been provided in order to accommodate the Volkov type forces. Each gaussian can have its own independent set of exchange parameters.

When tested, using Volkov's force 13 (or A in the notation of Lassey's thesis (1972)), Lassey's results were reproduced.

The first major difficulty encountered using this program was the approximation made by Lassey to the exchange part of the rearrangement energy. As has already been indicated in Chapter three, a constant λ was proposed as the approximation to the Slater exchange function. The mathematics suggested that the value of λ should not differ greatly from $\lambda = 0.5$.

Figure 5.1

Rearrangement Factor λ vs. Atomic Number A

(a) The solid line is Force B of Lassey's Thesis.

(b) The broken line is Force A of Lassey's Thesis.

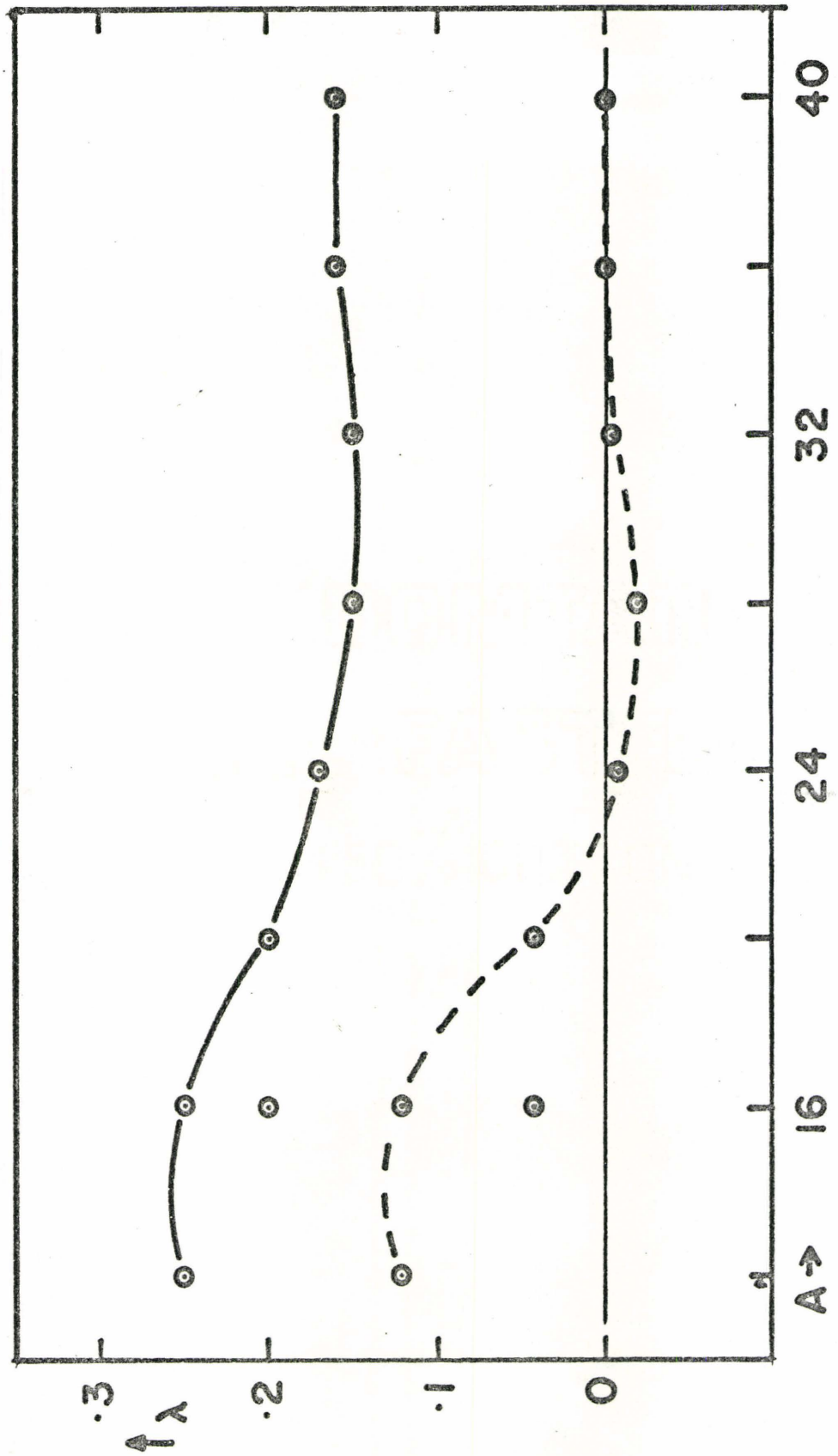

Figure 5.1

Indeed, for the delta function force λ was identical to 0.5.

However, Lassey thought that λ could be used as a variational parameter and varied to obtain the optimum total binding energy. Consequently the values of λ varied from 0.25 to -0.02 (Lassey 1972) for forces A and B. (See Fig. 5:1) The value of λ changed with atomic number, force and form of nucleus. (eg. different values were used for the ^{16}O ground state, and ^{16}O - 4 hole-4 particle excited state.)

However, varying λ I do not consider to be valid, since a change in λ is equivalent to changing the strength of the force for the exchange part of the rearrangement term. The problem is, what value to use.

For a given nucleus, the single particle energies varied with λ. It was first thought that if the single particle energies were sensitive to λ, perhaps these levels could be plotted as a function of λ, using Sprung's G-0 force and the values compared with those of X. Campi. Where the values intersected, this would be the appropriate value of λ.

Single particle energy levels are plotted as a function of λ for ^{16}O (See Fig. 5:2). The spin orbit splitting is about right and the $1p_{3/2}$, $1p_{1/2}$ and $1d_{5/2}$ levels were very close to Campi's especially for $\lambda \sim 0.5$. However the $1s_{1/2}$ level was high and would intersect Campi's value only if λ was about -0.1.

Figure 5.2

Single particle energy levels of ^{16}O vs. λ

(a) left-hand side - proton levels

(b) right-hand side - neutron levels

(c) dots are H.F.C. calculations

(d) faint lines- X. Campi calculations

(e) heavy black lines - experimental values

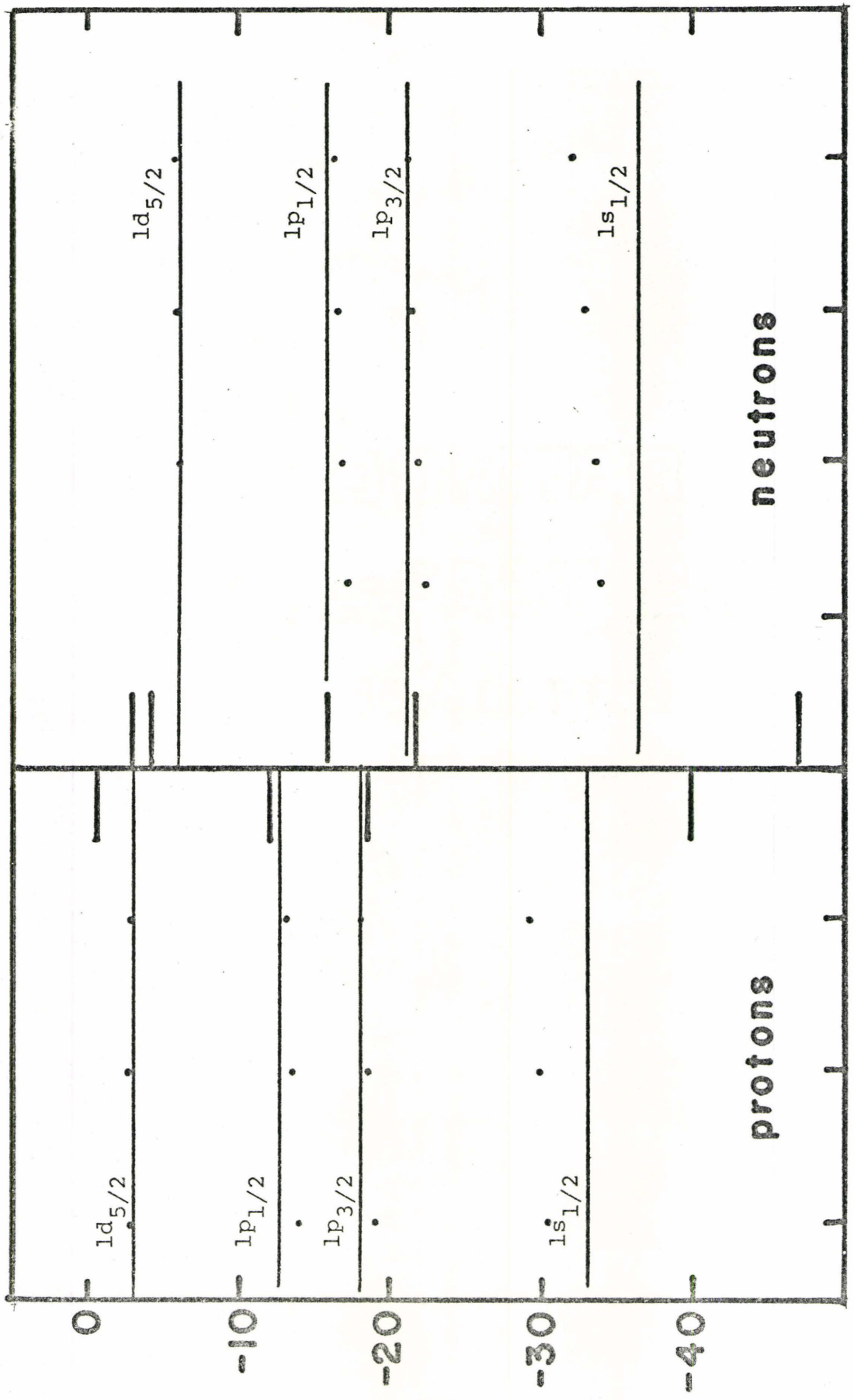
0
-10
-20
-30
-40
.2
.3
.4
λ
.1
.2
.3
.4
protons
neutrons
1d5/2
1p1/2
1p3/2
1s1/2
1d5/2
1p1/2
1p3/2
1s1/2

Figure 5.2

The high $s_{1/2}$ level, compared to Campi, is believed to be caused by the single gaussian approximation to the density. Oxygen has a depression in the density inside 1.5 fm. The single gaussian, fitted to the r.m.s. radius and atomic number of the nucleus would predict too high a density in the central (s-wave) region and perhaps a little too low a density in the limb (p-wave) region of the nucleus (See Fig. 5:3). This is consistent with the force being less attractive on the 1s state, than it would be if we properly used the actual density profile. We propose to improve on this aspect of the work in the future.

If this analysis was correct, ^{40}Ca should be less of a problem, since it had a maximum central density. In principle the s level should appear lower and coincide with Campi's energy levels, giving a value for λ.

As one can see from the proton levels (Fig. 5:4) the agreement is worse. The s levels agree at $\lambda \sim -0.5$, the p levels agree at $\lambda \sim 0.0$, and the d levels agree at $\lambda \sim 0.5$.

Thus no value of λ duplicates Campi's results for the single particle energies. This is not at all understood. Part of the problem could be that ^{40}Ca has filled the s-d shell with no opportunity to mix with a shell above it. However it is also believed that the constant λ approximation to the Slater exchange function is inadequate. It is recommended

Figure 5.3

Gaussian fit to oxygen density profile

(a) Solid line - Gaussian approximation

(b) Broken line - true density

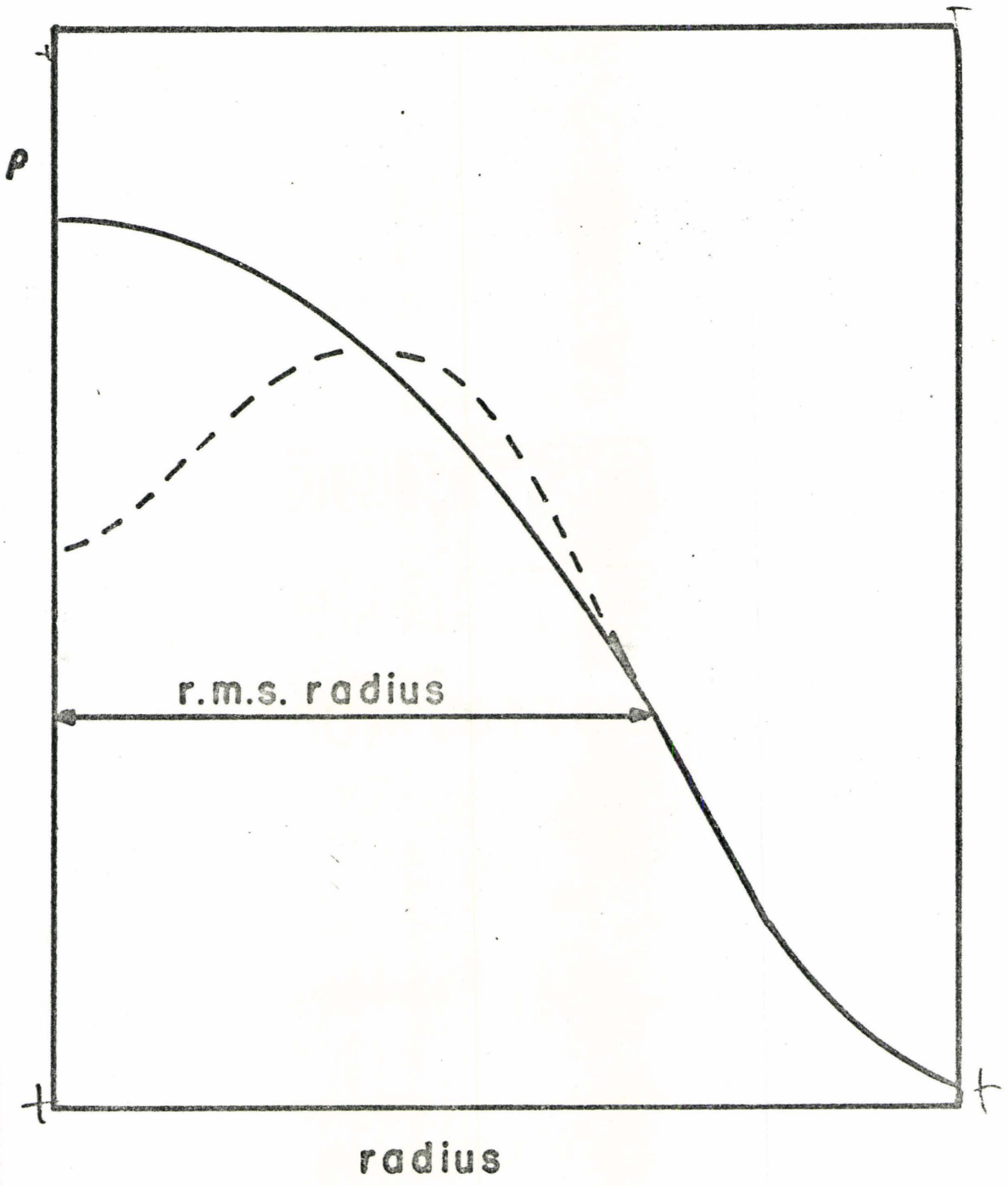

Figure 5.3

Figure 5.4

Proton single particle levels (in MeV) for ^{40}Ca vs. λ

(a) Heavy lines - HFC values

(b) Light lines - X. Campi values

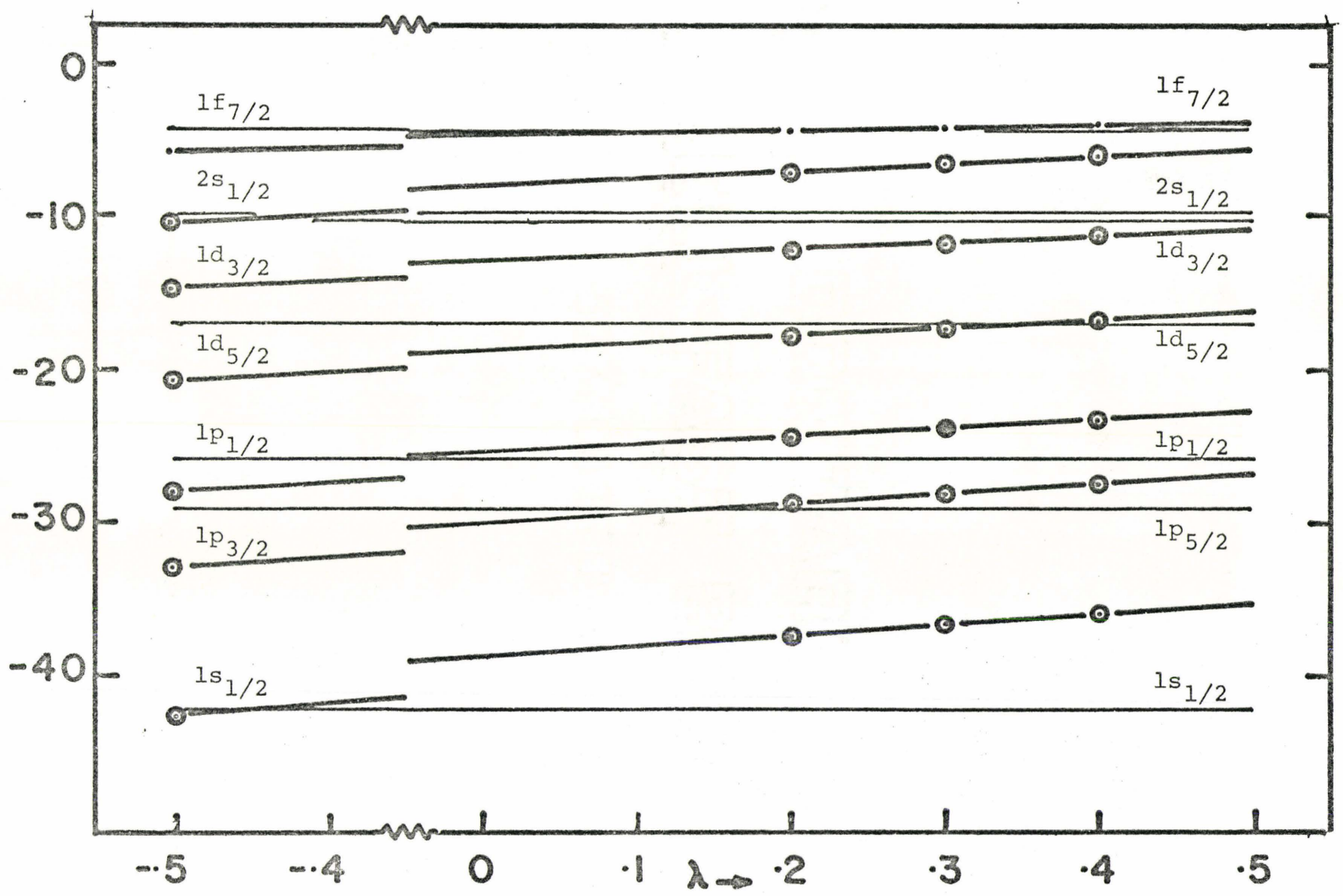
0
-10
-20
-30
-40
$1f_{7/2}$
$2s_{1/2}$
$1d_{3/2}$
$1d_{5/2}$
$1p_{1/2}$
$1p_{3/2}$
$1s_{1/2}$
$1f_{7/2}$
$2s_{1/2}$
$1d_{3/2}$
$1d_{5/2}$
$1p_{1/2}$
$1p_{5/2}$
$1s_{1/2}$
-.5
-.4
0
.1
λ
.2
.3
.4
.5

Figure 5.4

that the constant be replaced by a guassian approximation.

Further it was observed that total energy decreased with λ, while all measurements of radii r_p, r_n, r_m increase linearly with λ. (Fig. 5:5) The radius of ^{40}Ca is less sensitive to λ than ^{16}O. Later it will be demonstrated that for deformed nuclei the quadrupole moment is insensitive to λ, therefore the volume increases with λ.

This numerical experiment to determine λ has been inconclusive. A value of $\lambda=0.4$ was chosen since it was consistent with λ being close to 0.5, and it does not produce violent conflict between the single particle levels obtained, and those of X. Campi. (except for the 1s levels already noted).

5.3 Spherical Nuclei

In this section we shall compare the spherical nuclei in particular. By "spherical" we mean the closed shell nuclei ^4He, ^{16}O and ^{40}Ca, rather than those such as ^{32}S for which there has been some speculation that it could also be spherical. (Zofka and Ripka, 1971).

For each of these nuclei a spherical basis has been used. This guarantees sphericity and avoids the necessity of projecting out the spherical solution.

The basis was made spherical by constraining the oscillator constants as follows:

$$\alpha_i = \beta_i$$

$$\alpha_+ \neq \alpha_-$$

$$\beta_+ \neq \beta_-$$

Figure 5.5

Radii and binding energy with λ

(a) Upper left: Binding energy of ^{16}O vs. λ

(b) Lower left: Radius of ^{16}O vs. λ

(c) Upper right: Binding energy of ^{40}Ca vs. λ

(d) Lower left: Radius of ^{40}Ca vs λ

Radii in fm.

Binding energies in MeV

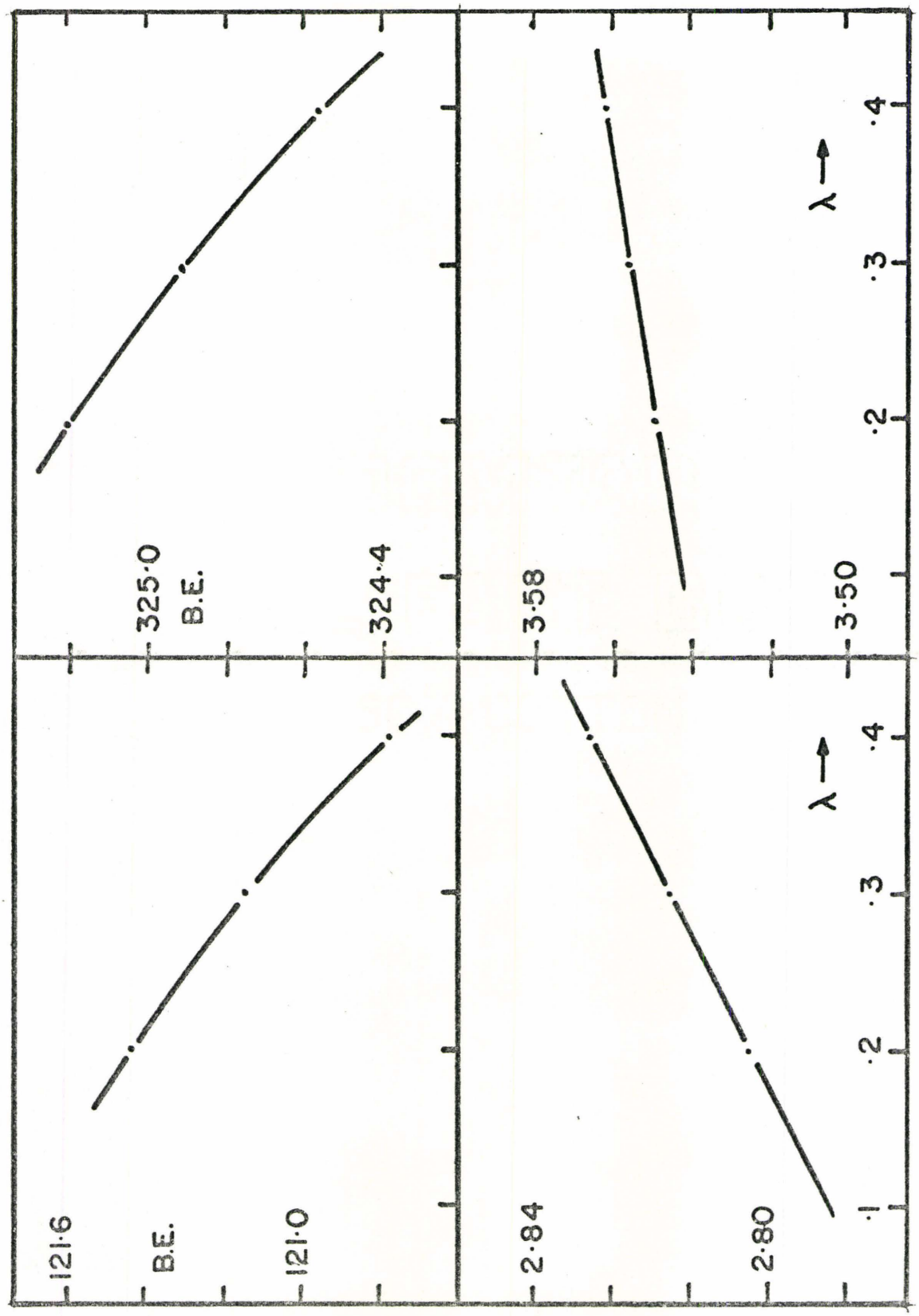

Figure 5.5

where + or - refer to the parity of the state.

5.3.1 Oxygen 16

With λ fixed at 0.4 the Hartree Fock calculation was done for ^{16}O. As is obvious from the density map of ^{16}O (Fig. 5:6); it is indeed spherical. This, plus the density profile show the pronounced dip in density in the interior of the nucleus, which has become characteristic of ^{16}O (Fig. 5.7).

Comparing this result with the profile of Campi, one observes that his central density is about 0.02 fm^{-3} greater than our central density. The maximum is 0.1 fm closer to the origin, and there is less density at the surface than in our solution. This is consistent with an over-estimation of the central density by the single gaussian density approximation and the subsequent compensation for this by the HF procedure. Since this has shifted the density outward one would expect an increased radius.

This is confirmed by the table of radii (Table 5.1). Our radius is close to that of Force A (henceforth called V-LA) of Volkov and Lassey (Lassey 1972). Of course Lassey had the same problem with the density approximation. However the results of X. Campi are closer to the results of Zofka and Ripka (1971), using forces Lineg and B1.

It should be noted here that Lineg is an approximation

Figure 5.6

Density Distribution of ^{16}O

Contour labelled as following in units of fm^{-3}

A	0.01
B	0.02
C	0.04
D	0.06
E	0.08
F	0.10
G	0.12
H	0.14
I	0.16
J	0.18
K	0.20

Border markings are at intervals of 0.1 fm.

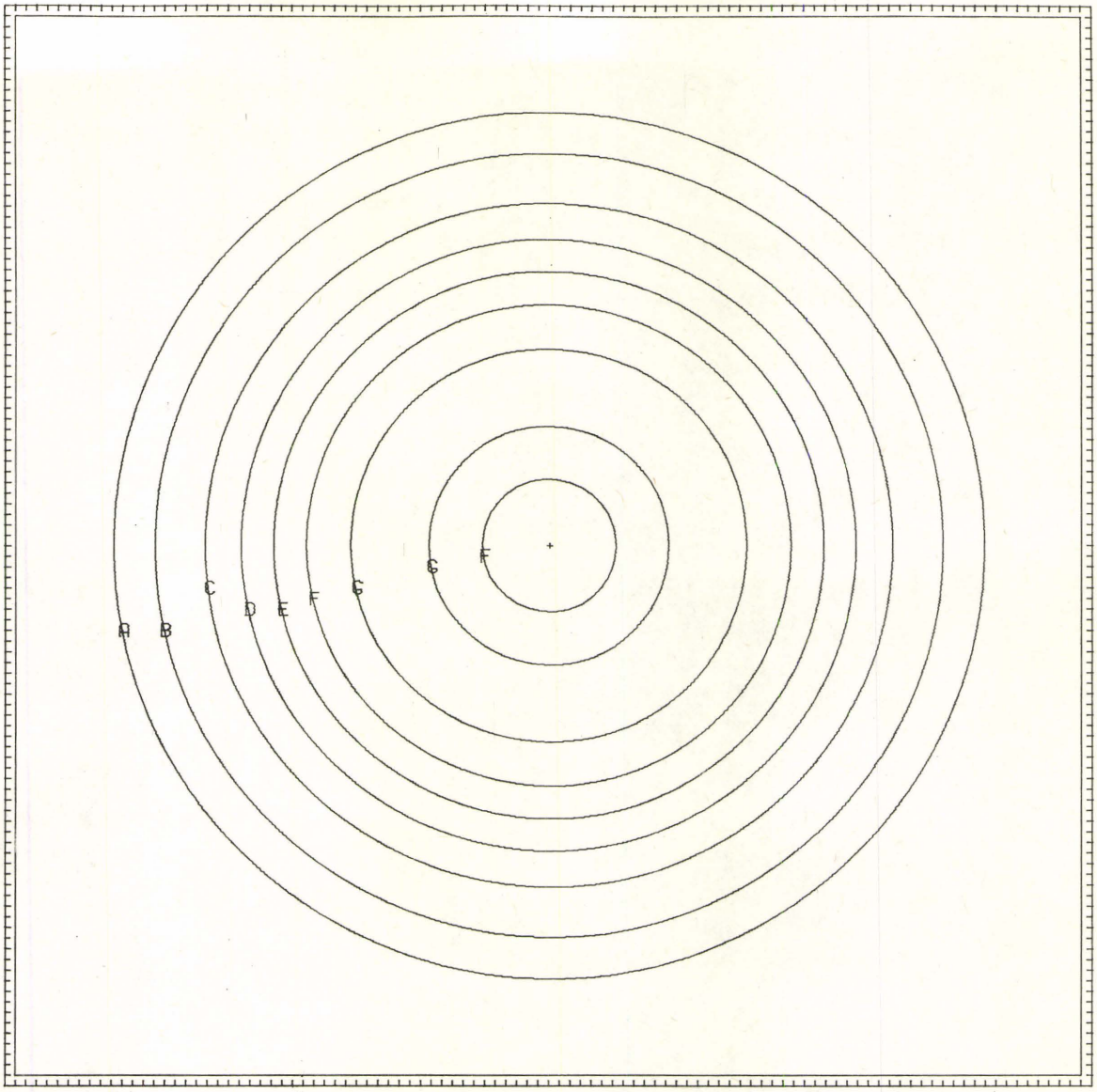

Figure 5.6

Figure 5.7

Density profile of ^{16}O. Density in fm^{-3} vs. radius in fm.

(a) Solid line is HFC profile

(b) Broken line is X. Campi profile

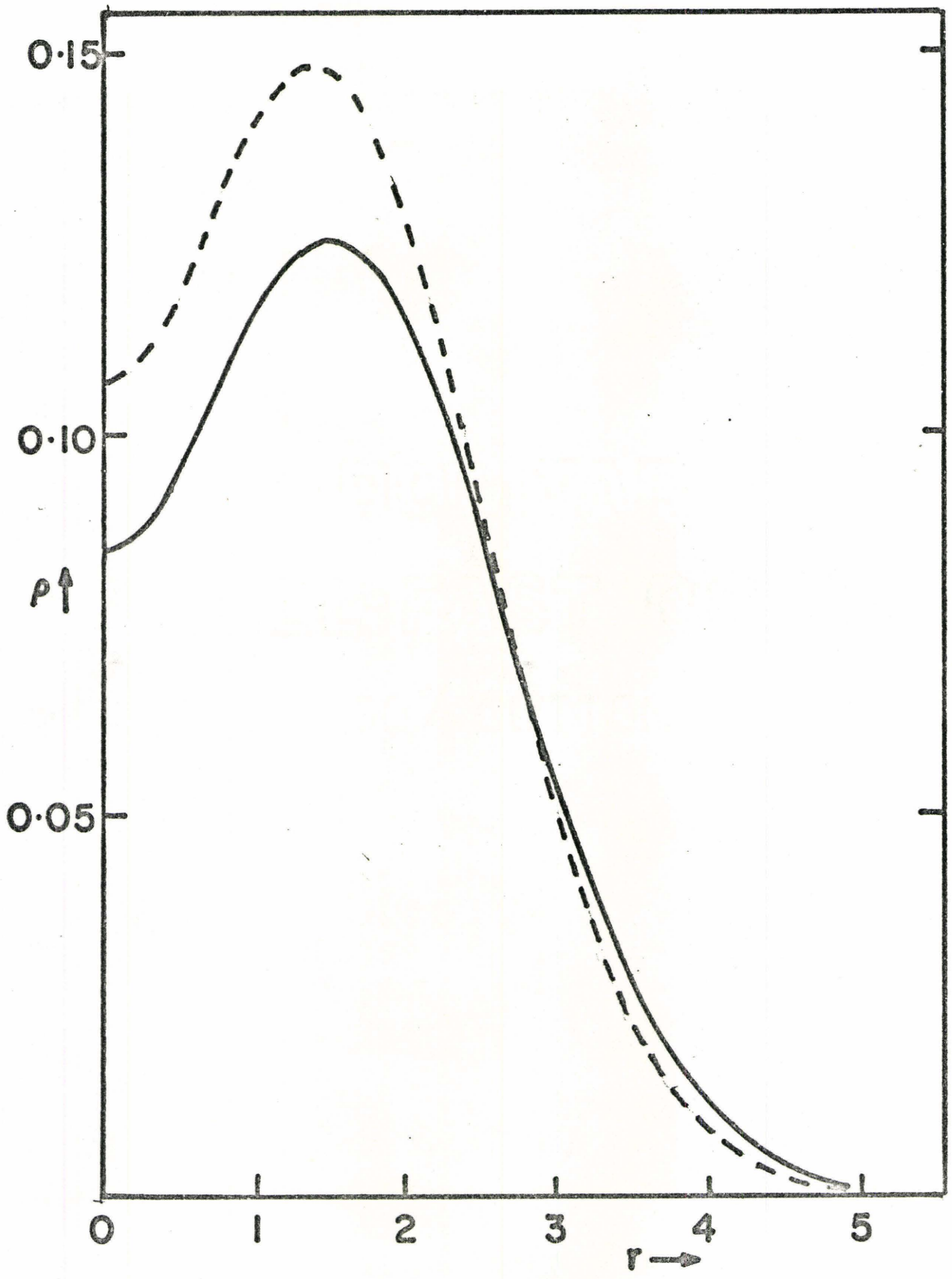

Figure 5.7

to the effective interaction of Negele (1970) which has been modified to make it linearly dependent on the density and identical to the interaction of Negele at $k_1 = 1.0$ fm^{-1} and $k_2 = 1.4$ fm^{-1} (Zofka and Ripka (1971)). B1 is the density independent force of Brink and Boeker (1967).

The density profile of the V-LA force is very similar to our Hartree-Fock result, (Henceforth called HFC), with a central density of about 0.05 fm^{-3} and a maximum density of about 0.12 fm^{-3} at 1.5 fm. However the Negele profile has a central density of 0.12 fm^{-3} and the maximum of 0.17 fm^{-3} has shifted in to about 1.2 fm. This is more similar to the results of X. Campi.

Clearly our program is giving central densities low by 25-30%, larger radii and extra density on the surface for ^{16}O.

In contrast the binding energies and the single particle energies are remarkably similar (Table 5:1(b) and (c)). The binding energies are all about the same except that of B1. It appears that one cannot obtain both the radii and binding energies near the experimental values without density dependence (Zofka and Ripka 1971).

The single particle energies of the various density dependent forces are very similar. As has been discussed previously, X. Campi's single particle levels are similar to ours except for the $1s_{1/2}$ level. The V-LA results are lower than

TABLE 5.1(a)

Radii of ^{16}O

	Mindet	HFC	X. Campi	V-LA	Lineg	Bl
Total	2.73	2.827	2.68	2.89	2.64	2.64
Proton	-	2.838	2.69	2.90	2.66	2.66
Neutron	-	2.815	2.67	2.87	2.62	2.61
Charge	-	(2.91)†	2.75	2.97	2.72	2.72

TABLE 5.1(b)

*Binding Energies of ^{16}O

Total	120.67	120.78	122.88	122.18	119.84	94.56
Proton	53.82	54.60	-	55.56	-	-
Neutron	66.84	66.19	-	66.62	-	-
BE/A	7.54	7.55	7.68	7.64	7.49	5.91

* All signs of Binding Energies and Single Particle Energies are reversed.

† Obtained by adding 0.08 fm to the mass radius. This is the increase calculated by most other sources.

TABLE 5.1(c)

*Single Particle Energies of ^{16}O

Protons	Mindet	HFC	X. Campi	V-LA	Lineg	Bl
$1s_{1/2}$	38.44	29.17	33.16	34.50	33.	43.5
$1p_{3/2}$	22.73	17.98	18.13	20.82	16.5	18.
$1p_{1/2}$		13.32	12.78	15.78		
$1d_{5/2}$	-	2.53	3.33	3.09	-0.5	-5.3
GAP	-	10.79	9.45	12.68	17.0	23.
Neutrons						
$1s_{1/2}$	41.82	32.25	36.38	37.46	-	-
$1p_{3/2}$	25.95	21.05	21.25	23.77	-	-
$1p_{1/2}$		16.32	15.81	18.66	-	-
$1d_{5/2}$	-	5.66	6.29	6.12	-	-
GAP	-	10.66	9.52	12.54	17.03	23.3

* All signs of Single Particle Energies reversed.

Figure 5.8

Proton single particle levels of ^{16}O in MeV

(a) Mindet calculation

(b) HFC calculation

(c) X. Campi calculation

(d) V-LA calculation (dots show values for $\lambda = 0.40$)

(e) Lineg of Zofka and Ripka

(f) Bl of Zofka and Ripka

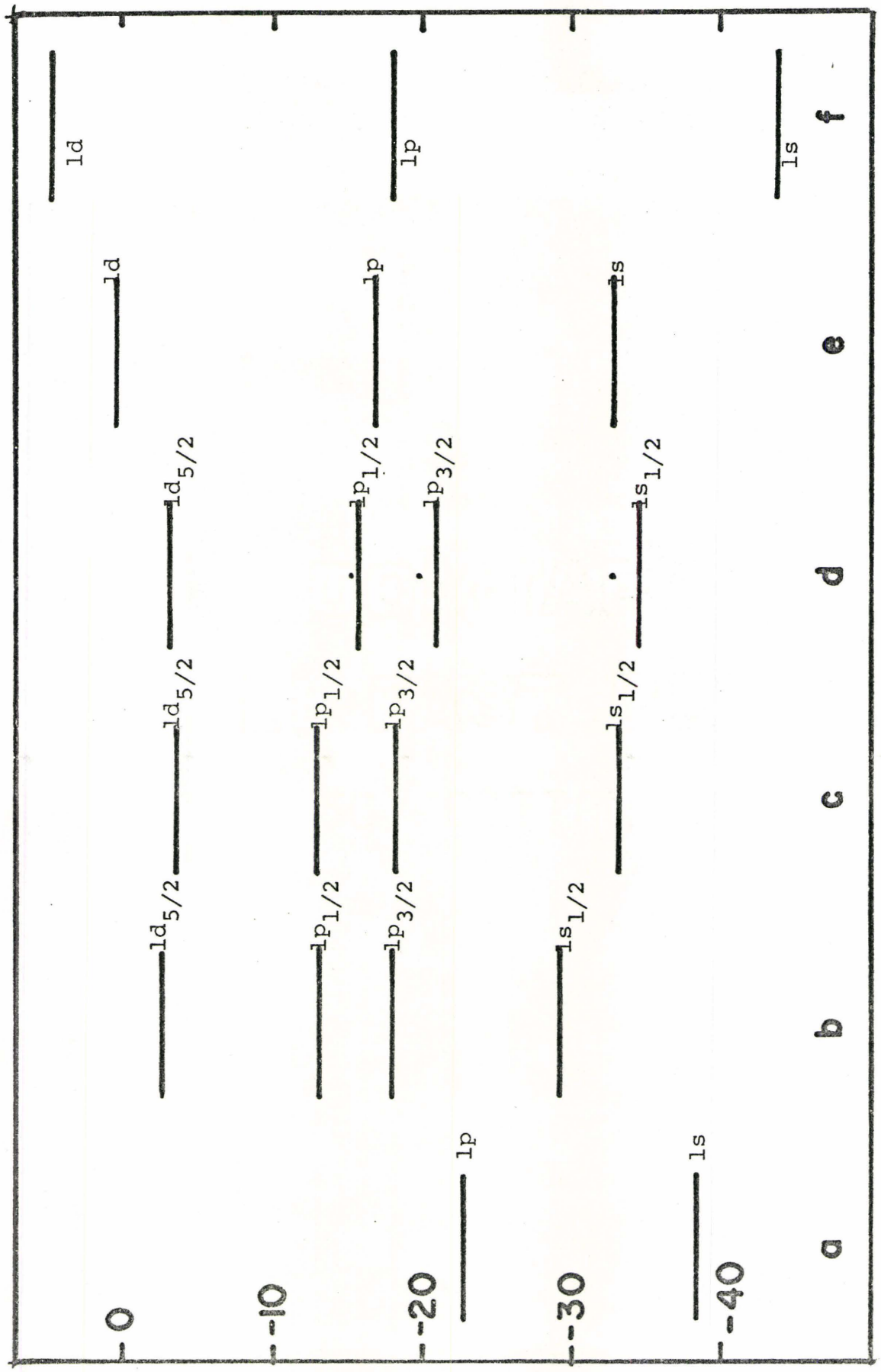

Figure 5.8

Figure 5.9

Neutron single particle levels for ^{16}O

(in MeV)

(a) Mindet

(B) HFC

(c) X. Campi

(d) V-LA

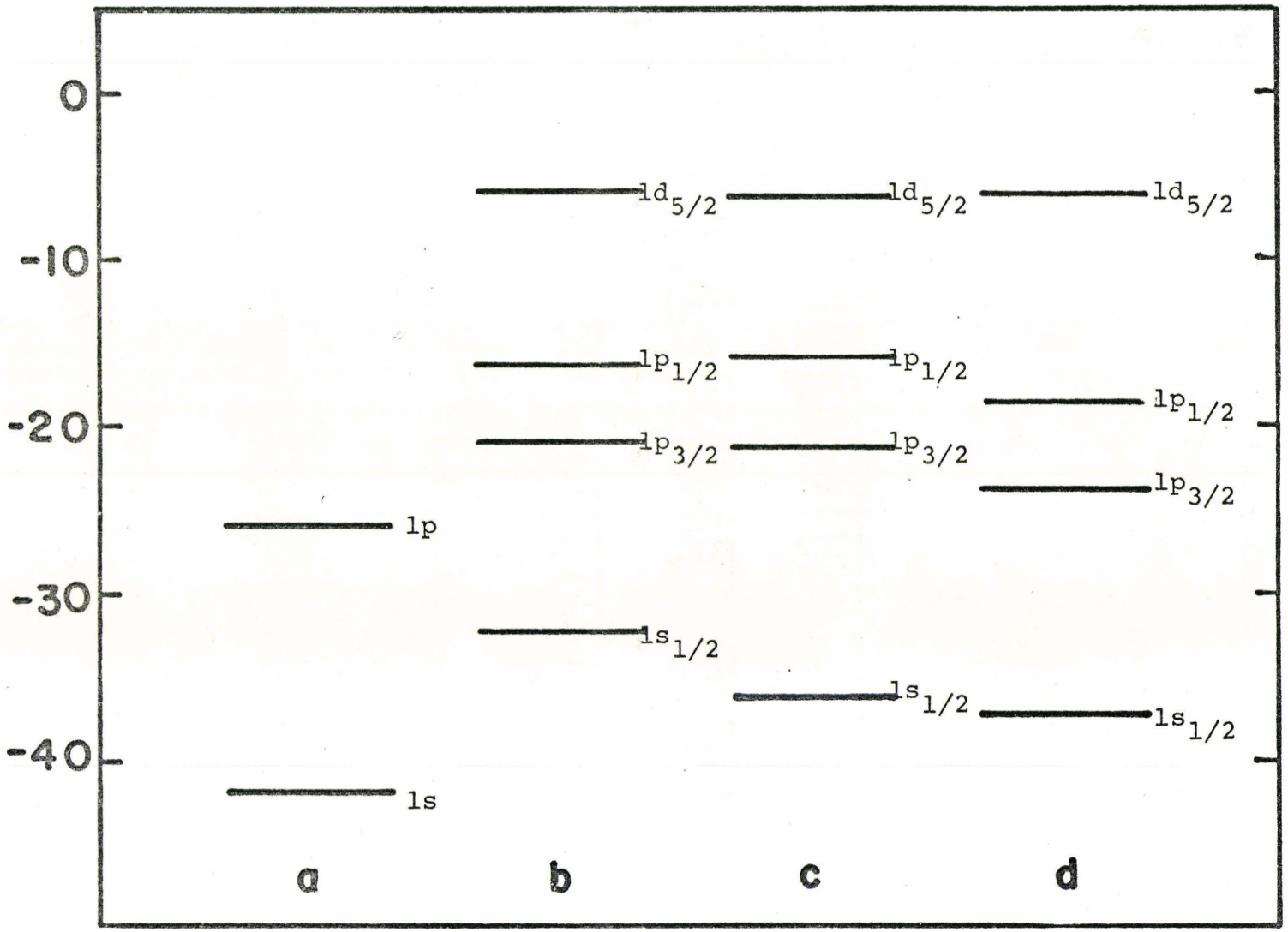
0
-10
-20
-30
-40
1p
1s
1d5/2
1p1/2
1p3/2
1s1/2
1d5/2
1p1/2
1p3/2
1s1/2
1d5/2
1p1/2
1p3/2
1s1/2
a
b
c
d

Figure 5.9

our results. However had $\lambda = 0.4$ been used the single particle levels would have become:

	Proton		Neutron	
	λ=0.12	λ=0.4	λ=0.12	λ=0.4
$1s_{1/2}$	34.5	32.5	37.5	35.0
$1p_{3/2}$	20.8	19.5	23.8	22.5
$1p_{1/2}$	15.8	15.0	18.7	17.8
$1d_{5/2}$	3.1	2.6	6.1	5.5

These are closer to, but still not as high as our values. The single particle energies of Lineg are also not significantly different. If a spin orbit force had been incorporated by Zofka and Ripka the 1p and 1d levels would have split appropriately and the resulting $1d_{5/2}$ level would have dropped about 2 or 3 MeV.

The neutron single particle energies form a similar pattern but are about 3 MeV lower owing to the absence of the Coulomb repulsion. (See Figs. 5.8 and 5.9).

The gap energy, ie the energy difference between the highest occupied and lowest unoccupied single particle levels, is about the same for both protons and neutrons. The different gap energies of different authors form no neat pattern. However the values of HFC, X. Campi, and V-LA tend to be low and those of Ripka and Zofka tend to be high. The experimental gap energy for both the neutrons and protons is 11.5 MeV. The Lineg gap energy of Zofka and Ripka would improve if a spin orbit term was included in their Hamiltonian.

5.3.2 Calcium 40

Like Oxygen, Calcium is spherical. However instead of a density depression in the interior of the nucleus, there is a central maximum (Fig. 5:10 and 5:11). The HFC calculation has a central density of 0.222 fm^{-3} then drops off to a shoulder or plateau at 2.25 fm with a density of 0.13 fm^{-3}. Then the density drops off more or less linearly again until at 5 fm the density is about 0.015 fm^{-3}.

This central density is too high. One reason for this is that the wave functions are unable to mix with states above the s-d shell. The p-f shell is of opposite parity and we supply no others above it. (Lassey 1972). Secondly, owing to the plateau, a gaussian approximation to the density, fit to the r.m.s. radius of about 3.56 fm, (which is well below the shoulder) will overestimate the shoulder density and possibly underestimate the central density. Thus the program will try to compensate by increasing the density in the central region at the expense of the plateau region.

These combined effects may be seen by comparing our density profile with that of X. Campi. Campi has a lower central density, a higher plateau and reduced density on the surface outside 3.75 fm.

Owing to the r^2 weighting of the density, the height of the plateau is of crucial importance to the root mean square radius. Since the plateau is inside the r.m.s. radius, the higher the plateau the lower the radius. The relative

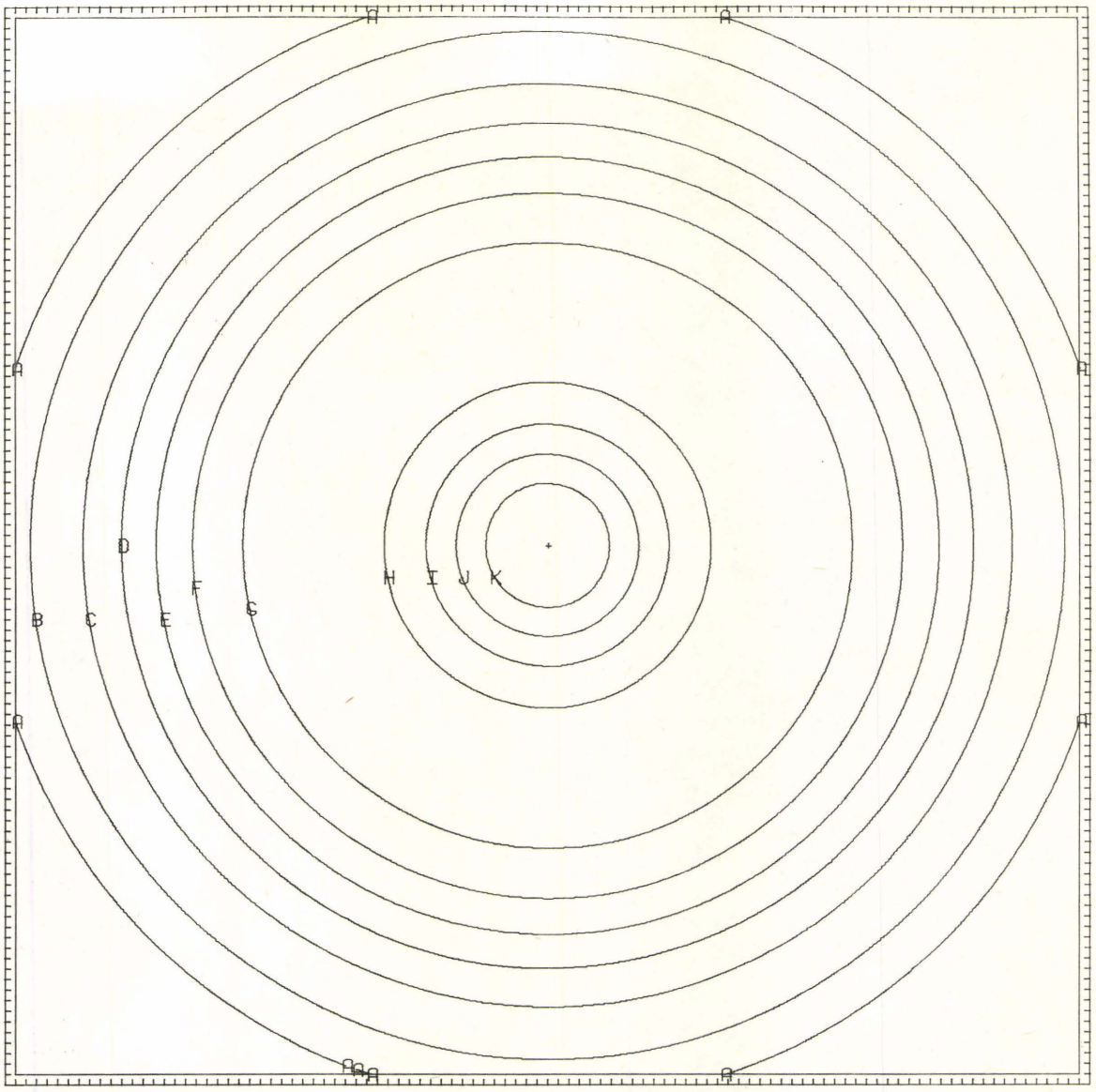

Figure 5.10

Density Distribution of ^{40}Ca

Figure 5.11

Density profile of ^{40}Ca. Density in fm^{-3} vs. radius in fm.

(a) Solid line - HFC

(b) Broken line: X. Campi

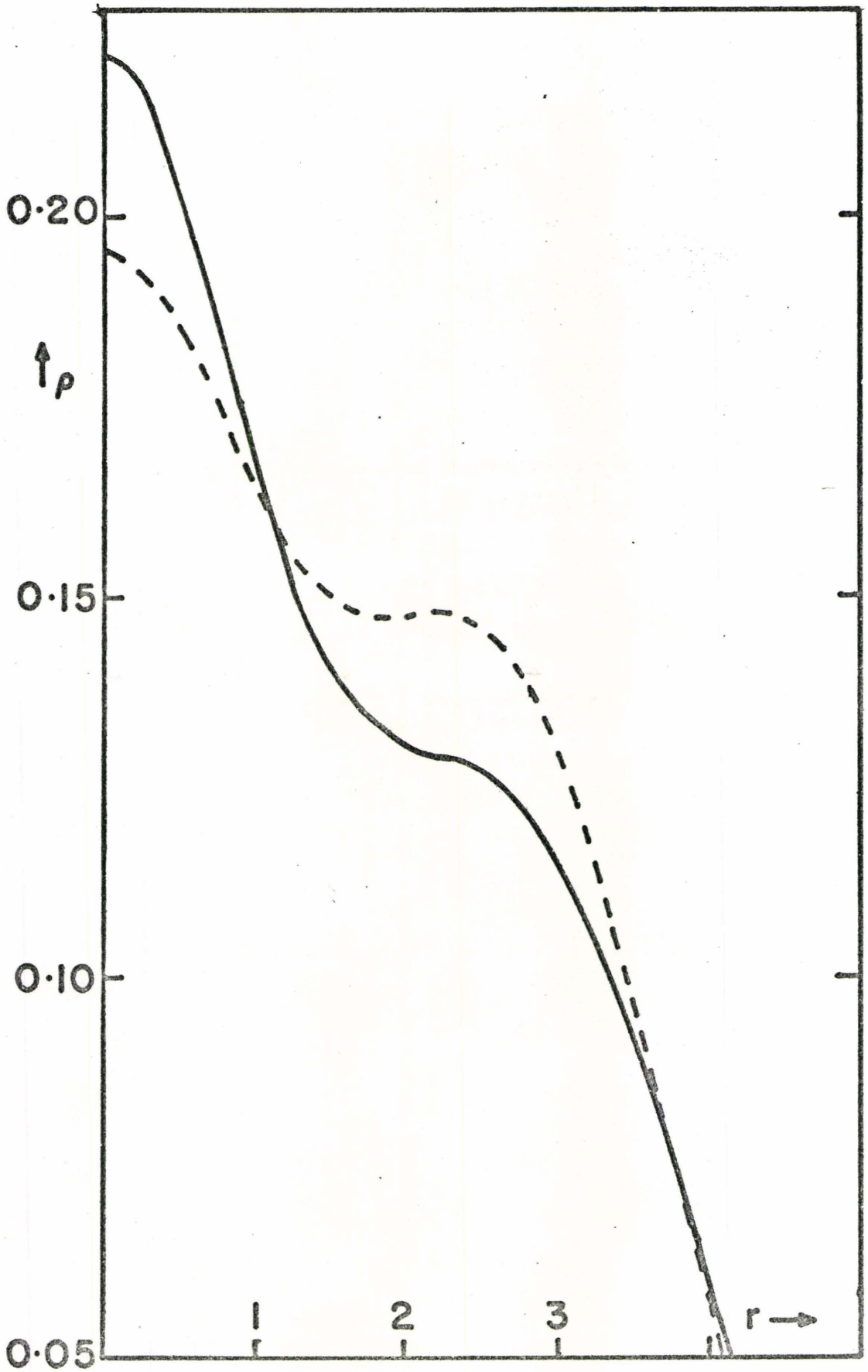

Figure 5.11

TABLE 5.2(a)

Radii of ^{40}Ca For Various Calculations

	Mindet	HFC	X. Campi	V-LA	Lineg	Bl
Total	3.52	3.561	3.41	3.62	3.38	3.39
Proton	-	3.570	3.43	3.63	3.43	3.43
Neutron	-	3.551	3.38	3.61	3.33	3.35
Charge	-	(3.64)†	3.49	3.70	3.50	3.50

† Charge radius estimated by adding 0.08 fm to the mass radius.

TABLE 5.2(b)

*Binding Energies of ^{40}Ca

Total	324.80	324.17	333.2	354.33	326.8	254.
Proton	127.76	128.37	-	144.35	-	-
Neutron	197.45	195.80	-	209.99	-	-
BE/A	8.12	8.10	8.33	8.86	8.17	6.35

* The signs of the binding energies have been changed for convenience.

TABLE 5.2(c)

	Mindet	HFC	Campi	V-LA	Lineg	Bl
Proton						
$1s_{1/2}$	46.56	36.03	42.36	45.03	39.8	60.
$1p_{3/2}$	35.00	27.39	29.08	34.66	27.5	36.
$1p_{1/2}$		23.23	25.69	29.83		
$1d_{5/2}$	21.49	16.90	16.68	20.87	13.5	14.
$1d_{3/2}$	19.56	11.22	10.58	14.93		
$2s_{1/2}$	17.63	5.68	9.99	11.79	10.5	12.
$1f_{7/2}$	-	3.55	4.14		-	-
GAP	-	2.13	5.85	8.3	-	-
Neutron						
$1s_{1/2}$	54.44	43.09	49.48	51.99	-	-
$1p_{3/2}$	42.08	34.25	36.03	41.43	-	-
$1p_{1/2}$		29.94	32.58	36.47	-	-
$1d_{5/2}$	28.24	23.58	23.39	27.36	-	-
$1d_{3/2}$	26.35	17.90	17.16	21.42	-	-
$2s_{1/2}$	24.47	13.05	16.73	18.77	-	-
$1f_{7/2}$	-	9.94	10.56	10.4	-	-
GAP	-	3.11	6.17	8.4	13.2	20.6

height of the central density is of lesser importance.

Thus the high plateau of Ripka and Zofka (1971) of 0.15 fm^{-3} results in a low r.m.s. mass radius of 3.35 fm. Both our HFC and V-LA calculations give a low plateau of 0.13 fm^{-3} and a higher r.m.s. radius of about 3.6 fm. Campi's results give a plateau at 0.147 fm^{-3} and a r.m.s. radius of 3.41 fm, both close to the experimental values. (Ripka and Zofka.)

The central densities do not form a neat pattern. In addition to the factors previously mentioned, their height clearly depends on the nature of the force such as the attractive/repulsive strength at short range.

This comparison of the binding energies of ^{40}Ca shows fewer regularities than in the case of ^{16}O. As before the binding energy obtained using force B1 is far too low, even though the radius is not unreasonable. Again it appears density dependence is useful in reconciling these data.

The effective forces used in the HFC, Lineg, and X. Campi calculations all give similar results. They are all underbound. However X. Campi's calculation is not as underbound as ours, possibly owing to the starting energy term in his Hamiltonian.

The phenomenological force V-LA however is overbound.

Why the binding energy did not drop for the HFC calculation over the Mindet is somewhat problematic. One would not expect it to drop much, because the s-d shell is filled,

and mixing would be minimal. However it should drop a little. The HFC result however is less bound. This is because the Mindet program ignored the exchange part of the rearrangement term. This is equivalent to the λ=0.0 calculation which gives an extra 1 MeV to the total binding energy (see section 5.2). Thus the Mindet total binding energy should be 323.8 MeV, while mixing would allow the total binding energy to drop another 0.4 MeV. A similar argument would account for the very small decrease in the binding energy for ^{16}O when mixing was allowed.

The single particle spectrum (Fig. 5:12 and 5:13) of ^{40}Ca reveals a pattern that was also true for ^{16}O. The B1 force of Zofka and Ripka which has no density dependence produced a spread out spectrum with a very low 1s level. Our results which use the strongly density dependent Sprung force produced a compact and generally higher spectrum, while the Volkov force which employs a weak density dependence gives an intermediate spectrum.

The explanation is in terms of the density dependence and rearrangement term. If there is no density dependence and therefore no rearrangement term the binding energy per particle is

$$E/A = \frac{1}{2A} \sum_{i}^{A} (t_i + \varepsilon_i)$$

where t_i is the kinetic energy of particle "i" and ε_i is

Figure 5.12

Proton single particle levels of ^{40}Ca (in MeV)

(a) Mindet

(b) HFC

(c) X. Campi

(d) V-LA

(e) Lineg

(f) Bl

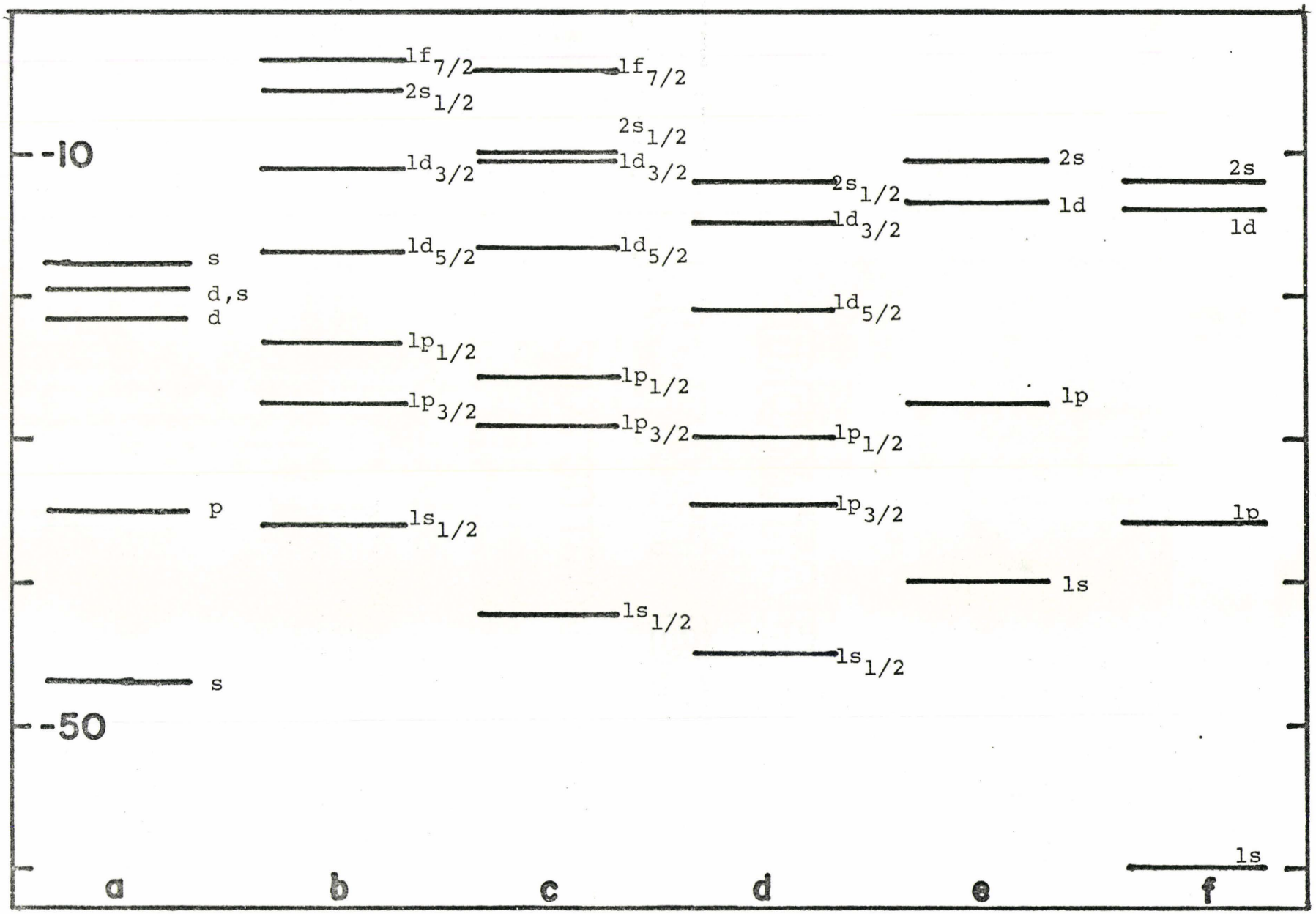
-10
-50
s
d,s
d
p
s
$1f_{7/2}$
$2s_{1/2}$
$1d_{3/2}$
$1d_{5/2}$
$1p_{1/2}$
$1p_{3/2}$
$1s_{1/2}$
$1f_{7/2}$
$2s_{1/2}$
$1d_{3/2}$
$1d_{5/2}$
$1p_{1/2}$
$1p_{3/2}$
$1s_{1/2}$
$2s_{1/2}$
$1d_{3/2}$
$1d_{5/2}$
$1p_{3/2}$
$1p_{1/2}$
$1s_{1/2}$
2s
1d
1p
1s
2s
1d
1p
1s
a
b
c
d
e
f

Figure 5.12

Figure 5.13

Neutron single particle levels for ^{40}Ca (in MeV)

(a) Mindet

(b) HFC

(c) X. Campi

(d) V-LA

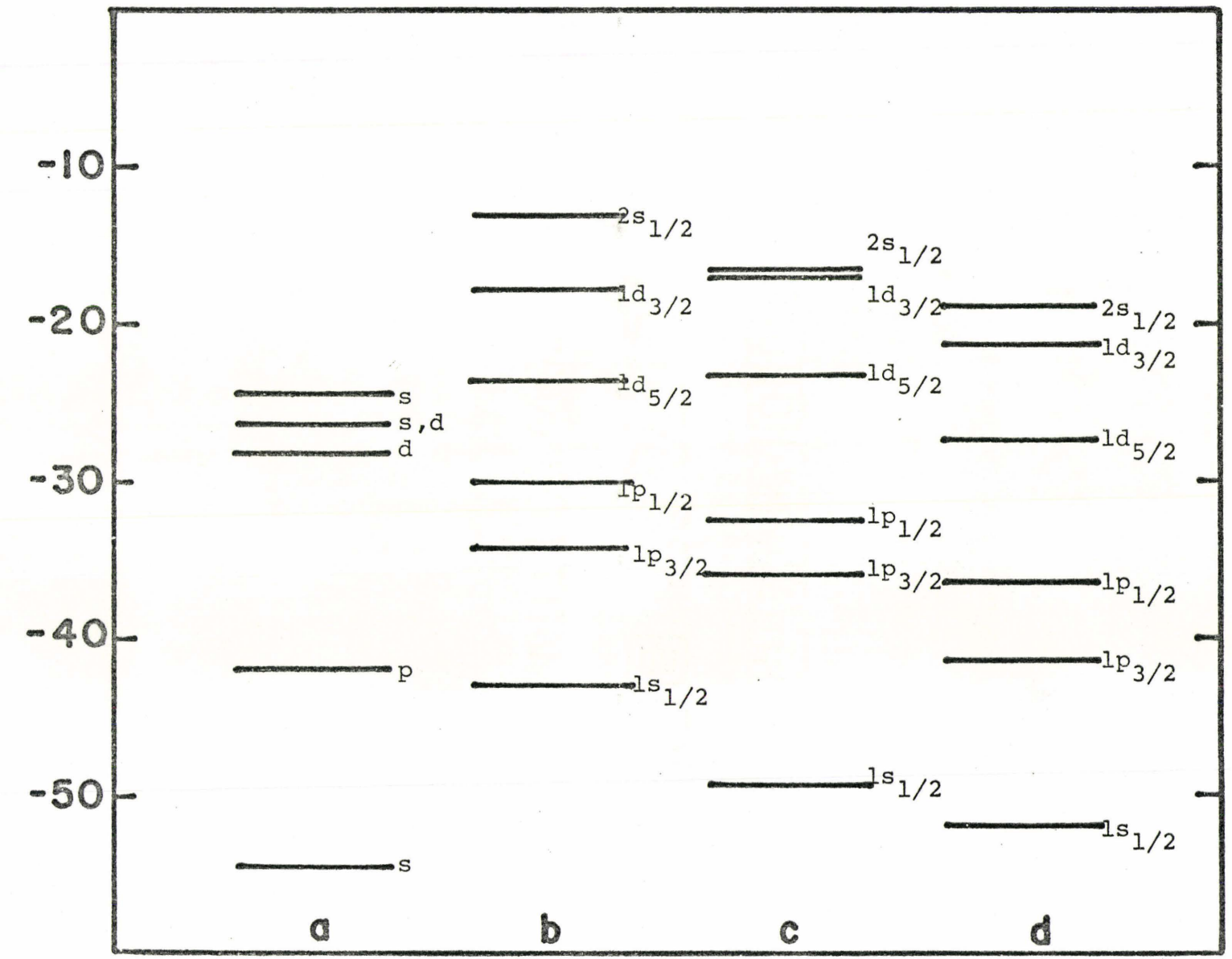
-10
-20
-30
-40
-50
s
s,d
d
p
s
2s1/2
1d3/2
1d5/2
1p1/2
1p3/2
1s1/2
2s1/2
1d3/2
1d5/2
1p1/2
1p3/2
1s1/2
2s1/2
1d3/2
1d5/2
1p1/2
1p3/2
1s1/2
a
b
c
d

Figure 5.13

the single particle energy of particle "i". Now E/A is about -8 MeV. The kinetic energy term contributes about +8 MeV

ie $$\frac{1}{2A}\sum_{i}^{A} t_i = \frac{1}{2A}\sum^{A} (16\ \text{MeV}) = \frac{1}{2A}(16\ A)\ \text{MeV} = 8\ \text{MeV}$$

The single particle term must then contribute about -16 MeV. Thus the average of the single particle energies must be about -32 MeV. Therefore some levels must be quite low, at say -60 MeV and thus more spread out.

If there is density dependence the binding energy per particle will contain an additional rearrangement term ΔE_R.

$$E/A = \frac{1}{2A}\sum_{i} (t_i + \varepsilon_i) + \Delta E_R$$

This contributes about -4 MeV. (Campi and Sprung 1972) Because the radius is still the same, the kinetic energy term still contributes +8 MeV, leaving -12 MeV to be provided by the single particle energies. Therefore the single particle energies must now average only -24 MeV. The spectrum then will be higher and less spread out.

This also partially explains the decrease in the values of the single particle levels as λ decreases. As λ decreases, the exchange portion of the rearrangement energy is decreased. This means the average of all the single particle energies must become more negative in order to maintain a constant binding energy. Consequently they move downward.

The Lineg spectrum, the HFC and Campi single particle values are similar. The application of a spin orbit term in the Lineg Hamiltonian would have split the 1p and 1d levels and made it appear even more similar. This is consistent since each uses an effective force derived from a realistic force.

One feature is different. From a comparison of our HFC spectrum with that of X. Campi we see the $1s_{1/2}$ and $2s_{1/2}$ levels are abnormally high. The V-LA spectrum also shares a high $2s_{1/2}$ level. This could be due to the s levels not being able to mix with higher even shells. However the most important cause must be that the density is overestimated in the region of the plateau by the single gaussian density approximation. Whether the central density is overestimated or underestimated by the gaussian is of little consequence since the plateau which extends from 1.5 to 2.5 fm, a considerable width in terms of the nucleus, is weighted by r^2. Since the density is overestimated in this region the program will attempt to compensate by removing density from this region, outward toward the surface hence the low plateau for HFC and V-LA, and the large radius. The same reasoning can be used to explain the slightly higher 1p levels in the HFC spectrum than in that of X. Campi, since the plateau region would be composed, in large measure of 1p density.

Finally the V-LA spectrum should be 2-3 MeV higher on the whole since $\lambda=0.0$ was used.

A comparison of our HFC single particle values with experiment at first would indicate they should come down, or spread a little. Certainly the 2s should come down, probably below the $1d_{3/2}$ level, but definitely to produce a wider gap between the $2s_{1/2}$ and $1f_{7/2}$ level, consistent with a closed shell nucleus.

However the single particle eigenvalues are only an approximation to the separation energies. It would be better to calculate ^{39}K or ^{39}Ca and look at the difference in binding energy between them and ^{40}Ca. However, even if you did that, the wave function for ^{40}Ca less one particle may contain a fair amount of "spurious centre of mass motion". This would be considerably more than in the case of ^{40}Ca. Thus one should correct for this. Becker of Oak Ridge claims the correction for the $1s_{1/2}$ level may be as high as 10 MeV.

This, in addition to the large experimental errors associated with the observed single particle energies indicates, that the calculated levels are not hopelessly incompatable with experiment.

5.3.3 Helium 4

Most authors, including Jofka and Ripka do not include ^{4}He in a study of light nuclei. However a comparison of the calculations of Volkov and Lassey, X. Campi and this author for ^{4}He is included for completeness.

The HFC density profile of ^{4}He is basically a gaussian. (See Fig. 5.14 and 5.15)

$$\psi = 0.9998\ \phi_{000} + 0.00381\ \phi_{002} + 0.00538\ \phi_{100}$$

The form of ϕ_{000} is a gaussian (See Appendix 1) Campi's density profile is very similar to ours, but deviates slightly at the top. This indicates that the density of ^{4}He is not quite a gaussian. Even for this small a nucleus the basis may not be large enough to allow fine adjustments, or perhaps the gaussian density approximation inaccurately estimates the density just enough to cause the program to over-compensate by accumulating extra density inside 0.7 fm and outside 2.0 fm.

The radii tabulated in Table 5.3(a) are very similar. Our radius is slightly smaller than the radius of X. Campi, reflecting the slight excess of density on the surface. The V-LA radius demonstrates, as we have already observed, a tendency of that force to produce large radii.

All the forces produce too large a radius when compared to experiment. Our calculated mass radius should be increased for proton size but decreased for centre of mass motion. Thus the mass radius should be slightly larger (perhaps 0.03 fm) than experiment. However our radii are about 10-20% larger than

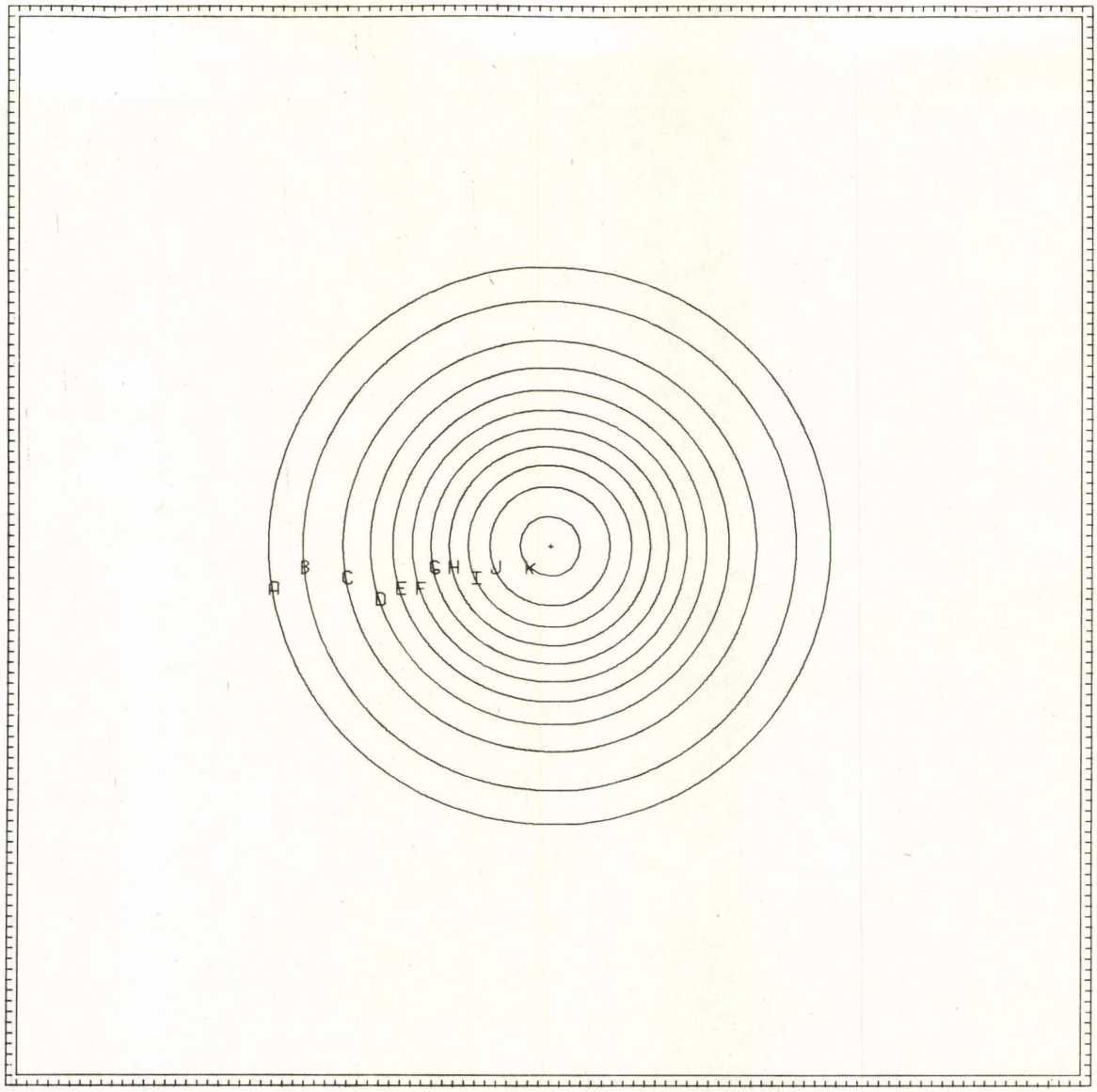

Figure 5.14

Density Distribution of ^4He

Figure 5.15

Density Profile of ^{40}Ca

Density in fm^{-3} vs. radius in fm

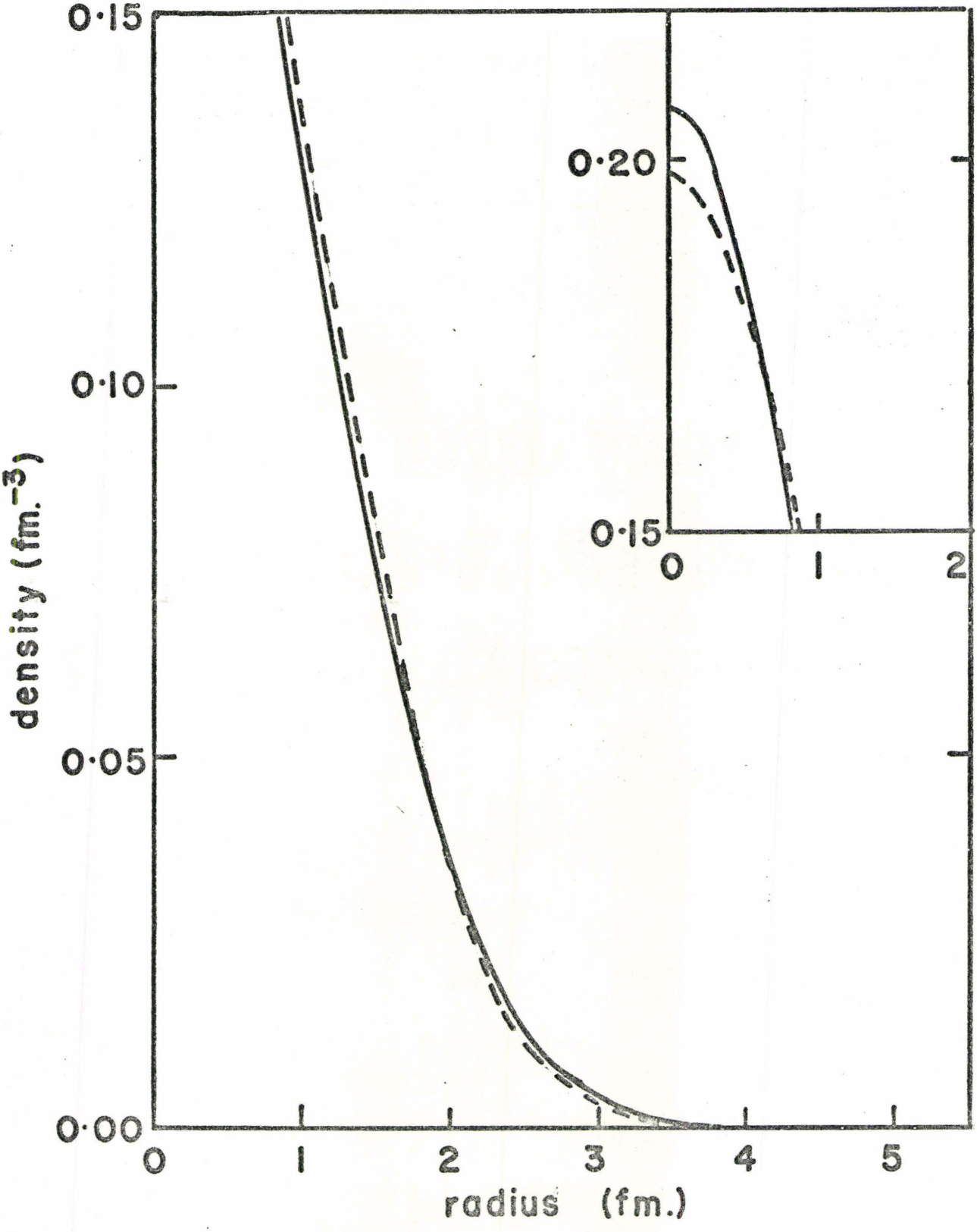

Figure 5.15

TABLE 5.3(a)

Radii of ^{4}He

	Mindet	HFC	X. Campi	V-LA	Exp
Total	1.866	1.853	1.83	2.025	
Proton	-	1.856		2.028	
Neutron	-	1.851		2.021	
Charge					1.67±.04

TABLE 5.3(b)

Binding Energies of ^{4}He

Total	29.755	29.746	27.72	25.61	28.295
Proton	14.501	14.534		12.50	
Neutron	15.254	15.212		13.11	
BE/A	7.43	7.43	6.93	6.40	7.074

TABLE 5.3(c)

Single Particle Energies of ^{4}He

Proton	24.55	18.866	19.55	19.56	19.813
Neutron	25.30	19.593	20.28	20.23	20.577

Figure 5.16

Proton and Neutron Single Particle Energy Levels in MeV of ^{4}He

(a) Mindet Calculation

(b) HFC Calculation

(c) X. Campi Calculation

(d) V-LA Calculation

(e) Exp.

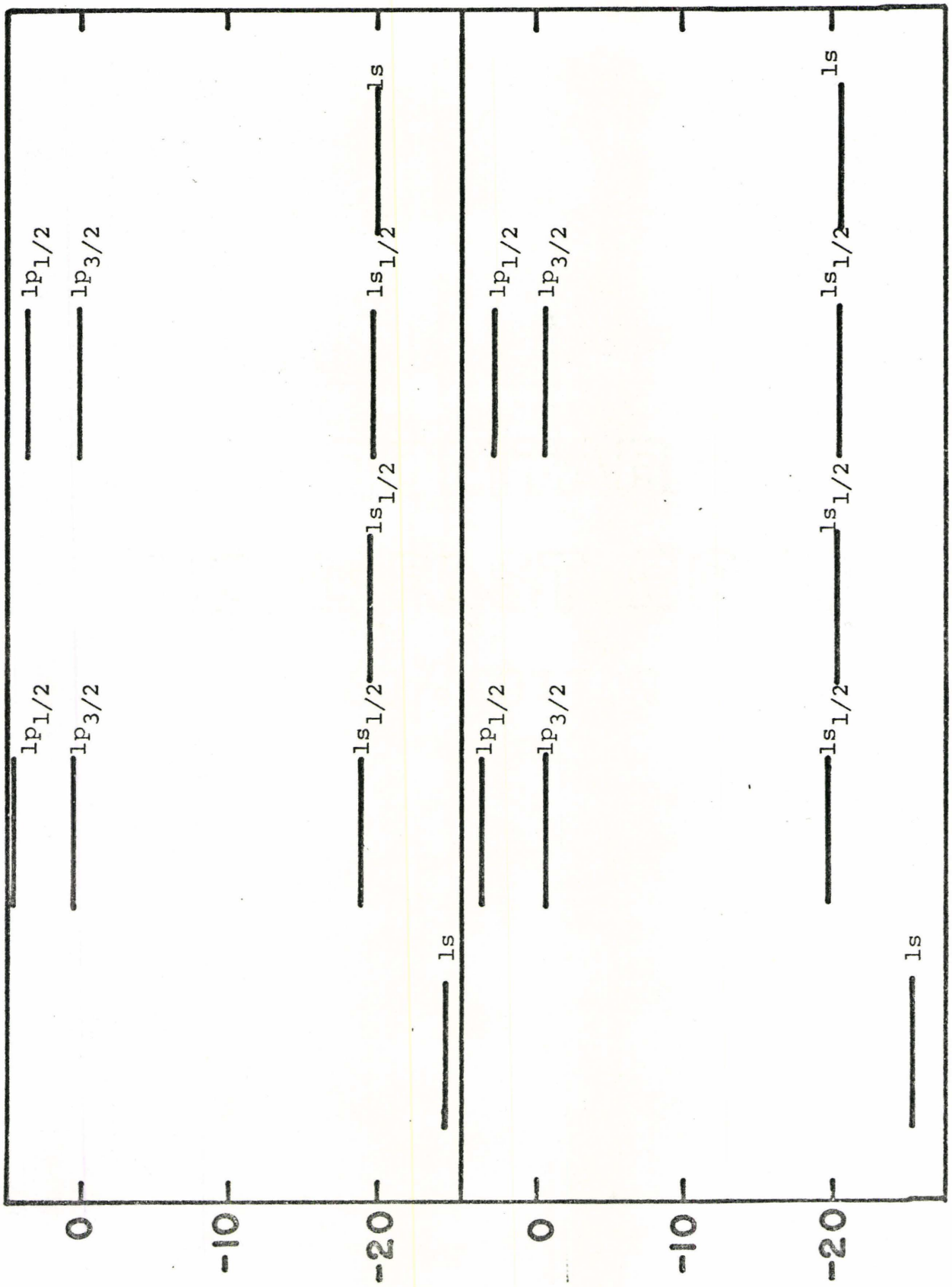

Figure 5.16

experiment. This may reflect a difficulty with the Local Density Approximation. This treats the density statistically, yet there are only four particles. In addition the density decreases rapidly within two fm making any approximation prone to error.

The single particle energies are all very similar. As usual the HFC level is higher than the other 1s single particle levels. This again could reflect a tendency of the density approximation to produce higher single particle levels since the density is underestimated by up to 0.05 fm^{-3} between 0.7 fm and 2.0 fm. It could also reflect an incorrect value of λ or the effect of the starting energy term being absent.

The separation energies are very close to the "experimental" values quoted. These values were calculated from the difference in the binding energies of ^4He and ^3He, then ^4He and ^3He for the proton and neutron respectively. Consistent with experiment the proton and neutron single particle energy levels differ by about 0.7 MeV.

5.3.4 Conclusions

In this section we have studied the limitations of the HFC program by calculations of the spherical nuclei.

For the exchange part of the rearrangement term λ=0.4 was chosen. This may not be the best value, (and indeed it ought to be improved by replacing the Slater exchange function with a guassian), but the results are not in violent disagreement with those of X. Campi.

In general the radii and subsequently the volume increased with λ. The total binding energy, while almost constant decreases slightly. The single particle levels rise with λ, and with the strength of the density dependence.

The systematic tendencies of the nuclei were invariably connected to the density dependence. The single gaussian would consistently overestimate the density in the s-wave region. The program would attempt to compensate by removing density to the surface. In ^{16}O this meant a lower central density, in ^{40}Ca a lower plateau, but in all cases it produced greater density on the surface and an increased root mean squared radius. In addition the s levels were high compared to X. Campi.

The total binding energy shows a tendency to be low, except for ^{4}He. ^{4}He is difficult because the L.D.A. may not be very reliable (See Chapter 3). At the other extreme ^{40}Ca has not been given a large enough basis to allow sufficient mixing.

Finally calculations were made for symmetry energies S = 34 MeV and S = 38 MeV in addition to the S = 36 MeV results listed above. As expected these nuclei were insensitive to changes in the symmetry energy.

We have found several systematic similarities and differences between the forces and the programs. Now we shall study the deformed nuclei.

5.4 Deformed Nuclei

In this section we shall examine the deformed nuclei up to ^{40}Ca comparing our result for each nucleus, with results of other, similar, calculations. We shall then look for systematic patterns in the observations over the entire range of our nuclei.

Certain nuclei were omitted from this thesis because the calculations refused to converge. These were ^{8}Be, ^{12}C and $^{16}O^{*}$ (4 particle-4 hole configuration). Each of these had in common a dumbell-like density distribution along at least one axis and little or no density along the others. As a result the gaussian density approximation cannot properly represent the density. This difficulty was not critical for Volkov and Lassey since their forces had a weak density dependence. However the large errors in the density approximation coupled with the strong density dependence of the Sprung force combined to cause a rotation of the density distribution of the nucleus. The result was that the iterative procedure would not converge.

Similar difficulties were encountered for many of the nuclei, however this problem was overcome by constraining,

$$\langle m|H|m'\rangle = 0 \qquad \text{for } m \neq m'$$

(where $m = J_z$).

The axial symmetry imposed by this constraint at the outset of the calculation was considered sufficient to maintain axial symmetry throughout the entire iteration. This was not precisely

true. However for most nuclei this procedure gave reasonable results. However, the triaxial nuclei, ^{24}Mg and ^{32}S, did rotate slightly. The values quoted for these nuclei are believed to be close to the converged values.

Since we are dealing with deformed nuclei, there must be some quantitative way of expressing this departure from sphericity. The root mean square radius of protons (neutrons) is defined as the square root of

$$R_p^2 = \frac{1}{Z}\int \rho_p(\underset{\sim}{r}) r^2 d^3r = \frac{1}{Z} \langle r^2 \rangle_p$$

(p→n, Z→N for neutrons).

The mass r.m.s. radius is

$$R^2 = \frac{1}{A}(Z\ R_p^{\ 2} + NR_n^{\ 2})$$

$$= \frac{1}{A}(\langle r^2 \rangle_p + \langle r^2 \rangle_n)$$

$$R = \frac{1}{\sqrt{A}} \langle r^2 \rangle^{1/2}$$

The intrinsic quadrupole moment is defined as

$$Q_o = (3\langle z^2 \rangle - \langle r^2 \rangle)$$

This may be defined for the proton or neutron in an analagous fashion. However this value increases with A rather than being only shape dependent. Thus we renormalize:

$$D_o = Q_o/AR^2 = Q_o/\langle r^2 \rangle$$

with analagous expressions for the protons and neutrons.

$$D_o^p = Q_o^p/Z\ R_p^{\ 2} = Q_o^p/\langle r^2\rangle_p$$

$$D_o^n = Q_o^n/NR_n^{\ 2} = Q_o^n/\langle r^2\rangle_n$$

If the nucleus is prolate, (is longer along the z symmetry axis than the radius in the ρ direction), the quadrupole moment will be positive. If the nucleus is oblate having

$$2\langle z^2\rangle < \langle x^2\rangle + \langle y^2\rangle$$

then the quadrupole moment will be negative.

If the nucleus is not axially symmetric, this asymmetry is measured by

$$Q_2 = \langle x^2\rangle - \langle y^2\rangle$$

with appropriate $Q_2^{\ p}$ and $Q_2^{\ n}$ for the protons and neutrons respectivelv. The renormalization has been done in two different ways by different authors. Volkov and Lassey define the mass asymmetry as

$$D_2^V = \frac{\langle x^2\rangle - \langle y^2\rangle}{\langle x^2\rangle + \langle y^2\rangle} = \frac{Q_2}{\langle \rho^2\rangle}$$

while Zofka and Ripka define it alternatively as

$$D_2^{ZR} = \frac{Q_2}{\langle r^2\rangle}$$

The transformation from one to the other is (Lassey 1972):

$$D_2^{ZR} = \frac{1}{3}(Z-D_o)D_2^{\ V}$$

In this thesis D_2 will mean D_2^{ZR} with the same convention for the protons and neutrons.

The r.m.s. charge radius is best compared with the experimental radius which is often calculated from electron scattering. Two corrections are made to the proton r.m.s. radius; one for the centre of mass, the other for the finite proton radius.

$$R_c^2 = R_p^2 + \langle r^2 \rangle \text{ proton} - (2\bar{a}^{-2} + \bar{b}^{-2})/A$$

where $\langle r^2 \rangle^{1/2}_{\text{proton}} = 0.76$ fm.

For large enough nuclei the centre of mass correction is neglegible, but not for A<40. For ^{4}He this correction helps to reduce the excessively large radius. However cancellation due to the finite proton size leaves only a 2% overall reduction.

The single particle states we use, and hence the single particle levels do not have a good m_ℓ. However the z component of angular momentum $k = m_\ell + m_s$ is a good quantum number, and states of $\pm k$ are degenerate. For comparision with Jofka and Ripka we will list both $|k|$ and $|m_\ell'|$, where m_ℓ' is the m_ℓ value of the largest component of the state. Where there are two large components, both m_ℓ's will be listed, with the largest being first. For asymmetric nuclei only parity π will be a good quantum number, however for comparison the above procedure will be also used.

5.4.1 Neon 20

From the density map of ^{20}Ne (Fig 5.17) it is evident

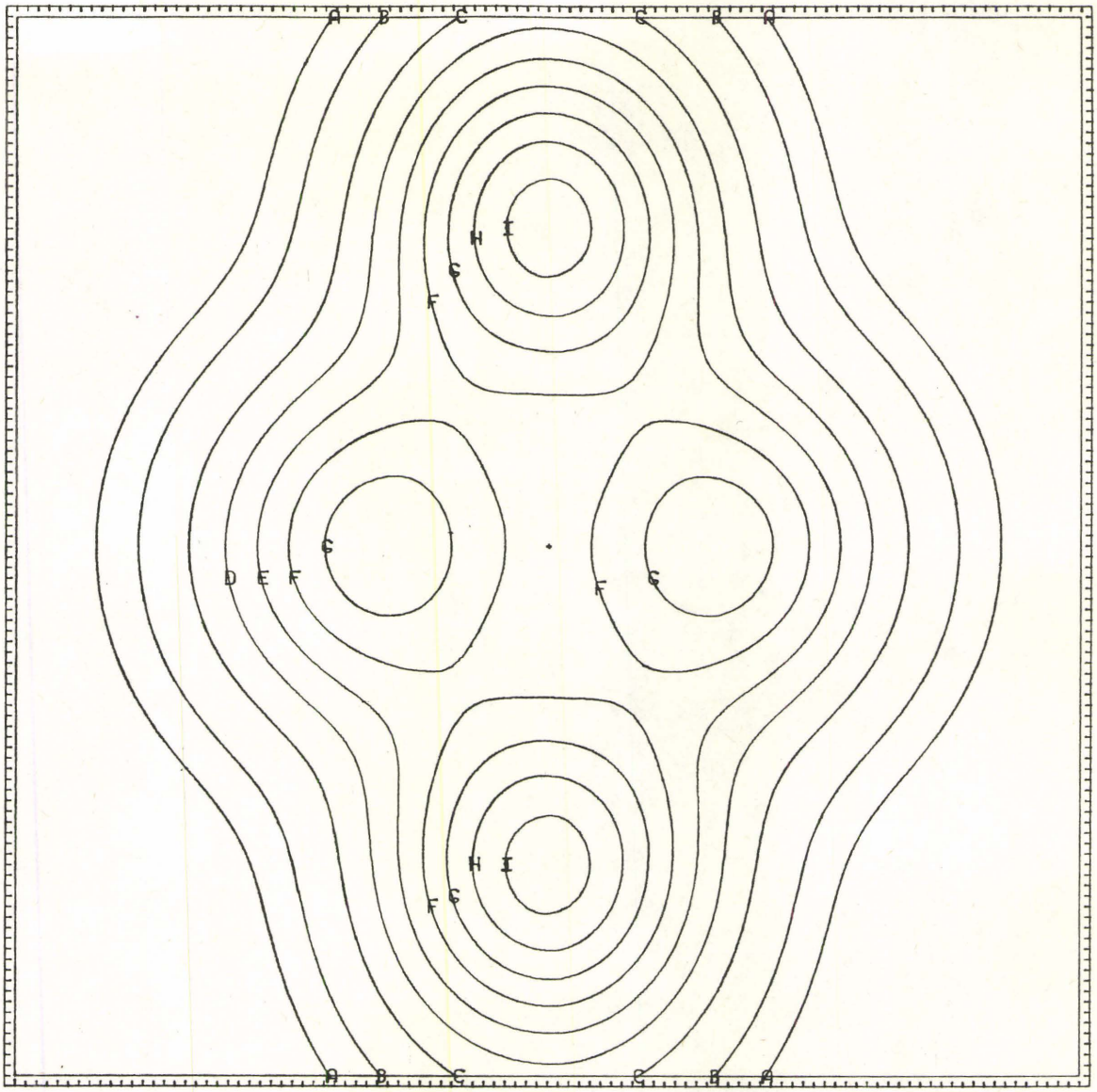

Figure 5.17

Density Distribution of ^{20}Ne

that the nucleus is prolate, with several prominant clusters of density. A close examination of this map suggests that the density be interpreted as five alpha-particles in the configuration of a trigonal bipyramid. Since any orientation about the z-axis is equally probably, the density appears as a ring of three alpha-particles in the x-y plane, with one alpha particle above and another below this plane on the z axis. The interpretation of the density in terms of alpha-particles is reinforced by a direct comparison of the outer contours of ^{20}Ne with those of ^{4}He (Fig 5.18) as shown by Lassey.

Volkov and Lassey have reported (1972) that clustering is enhanced by

(a) mixing states, which bring an admixture contributions from excited states to the core.

(b) saturation resulting from odd state repulsion owing to the exchange combination, and

(c) saturation due to the strength of the density dependence.

Clustering is minimized by saturation effects depending on the strength of the momentum dependence in the range,

$$\lambda(k) = \lambda^{o}[1 + C_1 (k - C_2)^2]$$

Sprung's force is a Serber type with weak odd state repulsion. It has no momentum dependence. The clustering must be largely dependent on the density dependence which is stronger than that of Volkov.

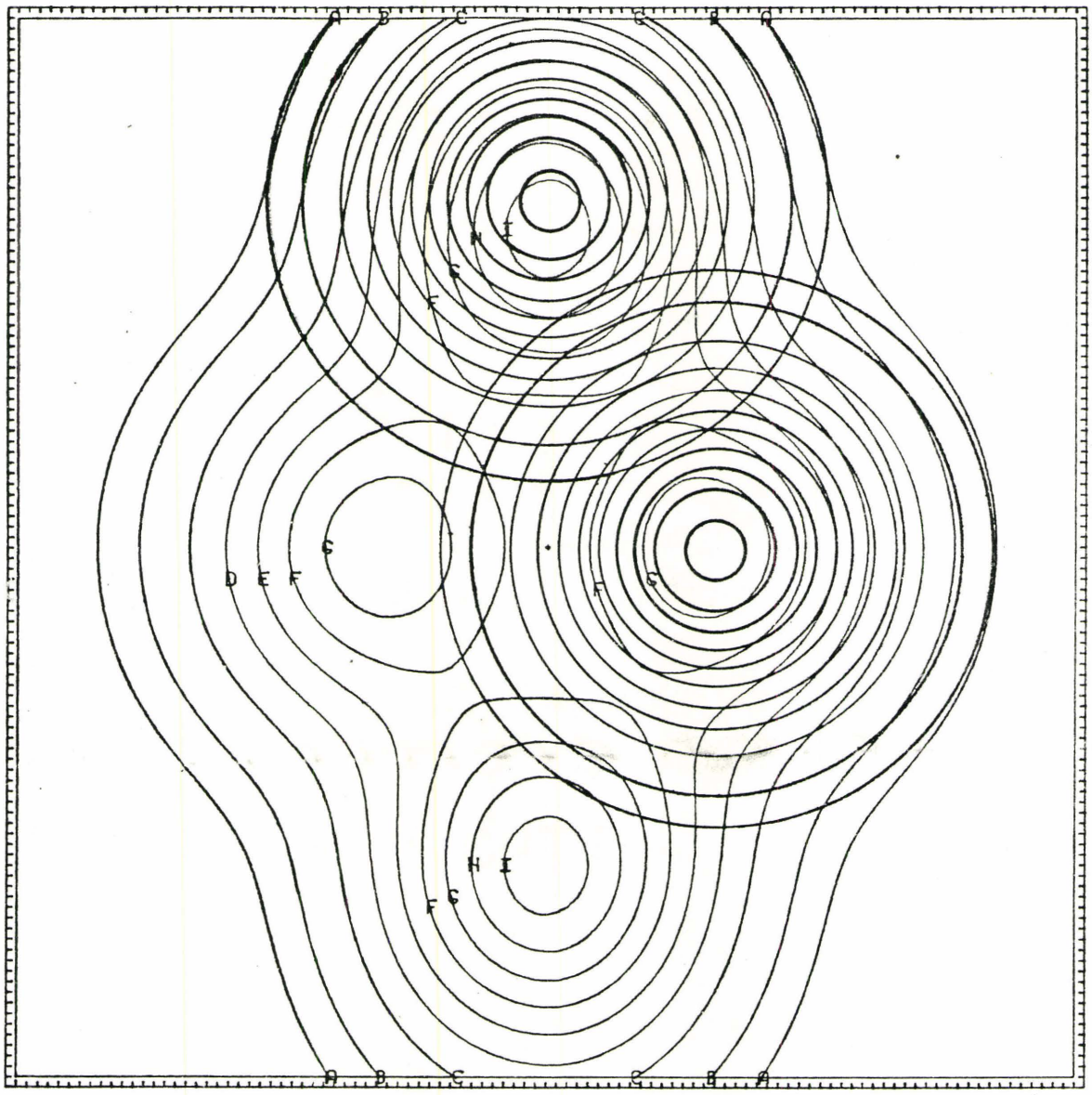

Figure 5.18

Density Distribution of ^{20}Ne with ^{4}He Density Superimposed

Enhancement of clustering may also be induced in nuclei with a depression in the centre by the gaussian density approximation overestimating the density and then compensating for this by moving the density toward the surface. This could give low central densities, high 0+ single particle levels and large radii, as argued in the previous chapter.

^{20}Ne was analysed as a function of λ. As with spherical nuclei the single particle levels and the radii increased linearly with λ. The binding energy remained relatively constant, but increased slightly with λ. However the shape, or quadrupole moment remained invariant. (Table 5.4(a)).

Compared with the other forces; both the HFC and V-LA radii were larger (Table 5.5(a)). This is in keeping with the density approximation. The shape parameters are similar with HFC being slightly more prolate.

The binding energies of both the HFC and V-LA are remarkably similar as are the other parameters mentioned above. The total binding energy is greater than LINEG and much greater than B1 (see Table 5.5(c)).

The single particle levels (Fig. 5.19 and Table 5.5(d)) follow a predictable pattern. HFC are compact, while B1 is spread out. The V-LA levels would be about 2.5 MeV higher had λ=0.40 been used instead of λ=0.04. Owing to the prolateness of the nucleus the 0^- state, which has z dependence is lower

(see 142)

TABLE 5.4(a)

λ	-0.5	0.0	0.4
Radius			
Mass	3.088	3.164	3.233
Proton	3.098	3.175	3.245
Neutron	3.079	3.153	3.222
Binding Energy			
Total	-152.54	-152.90	-151.91
Proton	- 67.33	- 67.73	- 67.41
Neutron	- 85.21	- 85.17	- 84.50
Quadrupole Moment	6.189	6.187	6.183
Single Particle Energies			
Proton 0+	- 35.97	- 32.31	- 29.62
Neutron 0+	- 39.83	- 36.05	- 33.25

TABLE 5.5(a)

Radii of ^{20}Ne in fm.

	Mindet	HFC	V-LA	Lineg	Bl
Mass	3.148	3.234	3.220	2.96	2.97
Proton		3.245	3.230	2.99	2.99
Neutron		3.222	3.211	2.92	2.94
Charge		(3.31)	3.300	3.05	3.04

Expt Charge Radius is 2.91 fm.

TABLE 5.5(b)

Shape Parameters for ^{20}Ne

$\langle r^2 \rangle^{1/2}$ (fm)	3.148	3.234	3.220	2.96	2.97
$\langle \rho^2 \rangle$ (fm^2)	4.385	4.909	5.057	4.183	4.249
$\langle z^2 \rangle$ (fm^2)	5.522	5.546	5.313	4.549	4.542
D_o (fm^2)	0.672	0.591	0.537	0.563	0.545
D_2 (fm^2)	0.0	0.0	0.0	0.0	0.0

TABLE 5.5(c)

Binding Energies for ^{20}Ne

	Mindet	HFC	V-LA	Lineg	Bl
Total	147.19	151.91	151.45	143.0	112.4
Proton	64.20	67.41	67.36	-	-
Neutron	82.99	84.50	84.09	-	-
BE/A	7.36	7.58	7.57	7.15	5.62

TABLE 5.5(d)

Single Particle Energies of ^{20}Ne

k^π	$m_\ell{}^\pi$	Mindet	HFC	V-LA	Lineg	Bl
Proton						
$1/2^+$	0^+	39.49	29.62	36.59	34.1	45.
$1/2^-$	0^-	26.85	21.85	25.31	22.0	26.
$3/2^-$	1^-	25.46	18.55	22.30	16.7	18.
$1/2^-$	1^-	21.19	14.98	17.93		
$1/2^+$	0^+	19.44	15.07	14.05	10.7	12.
$3/2^+$	1^+	-	2.80	5.45	3.5	-3.
GAP		-	12.18	8.6	6.7	15.
Neutrons						
$1/2^+$	0^+	43.52	33.25	40.19		
$1/2^-$	0^-	30.45	25.31	28.77		
$3/2^-$	1^-	29.32	22.21	25.89		
$1/2^-$	1^-	25.05	18.57	21.45		
$1/2^+$	0^+	22.90	18.45	17.34		
$3/2^+$	1^+	-	6.46	9.13		
$5/2^+$	2^+	-	6.63	7.54		
GAP		-	11.83	8.21	6.93	15.21

Figure 5.19

Proton Single Particle Energy Levels of ^{20}Ne

(a) Mindet Calculations

(b) HFC Calculations

(c) V-LA Calculations

(d) Lineg Calculations

(e) Bl Calculations

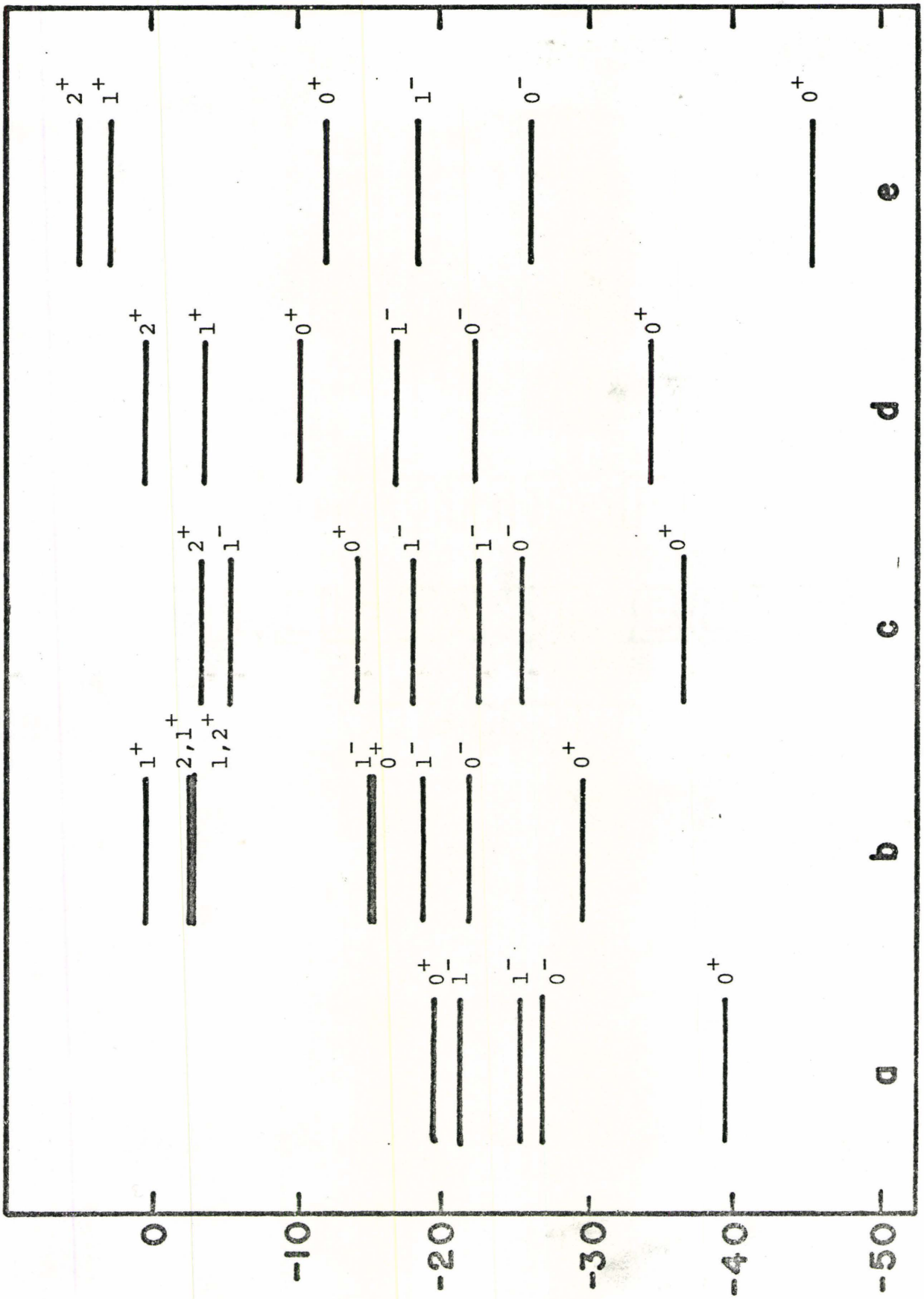

Figure 5.19

Figure 5.20

Neutron Single Particle Energy Levels of ^{20}Ne

(a) Mindet Calculations

(b) HFC Calculations

(c) V-LA Calculations

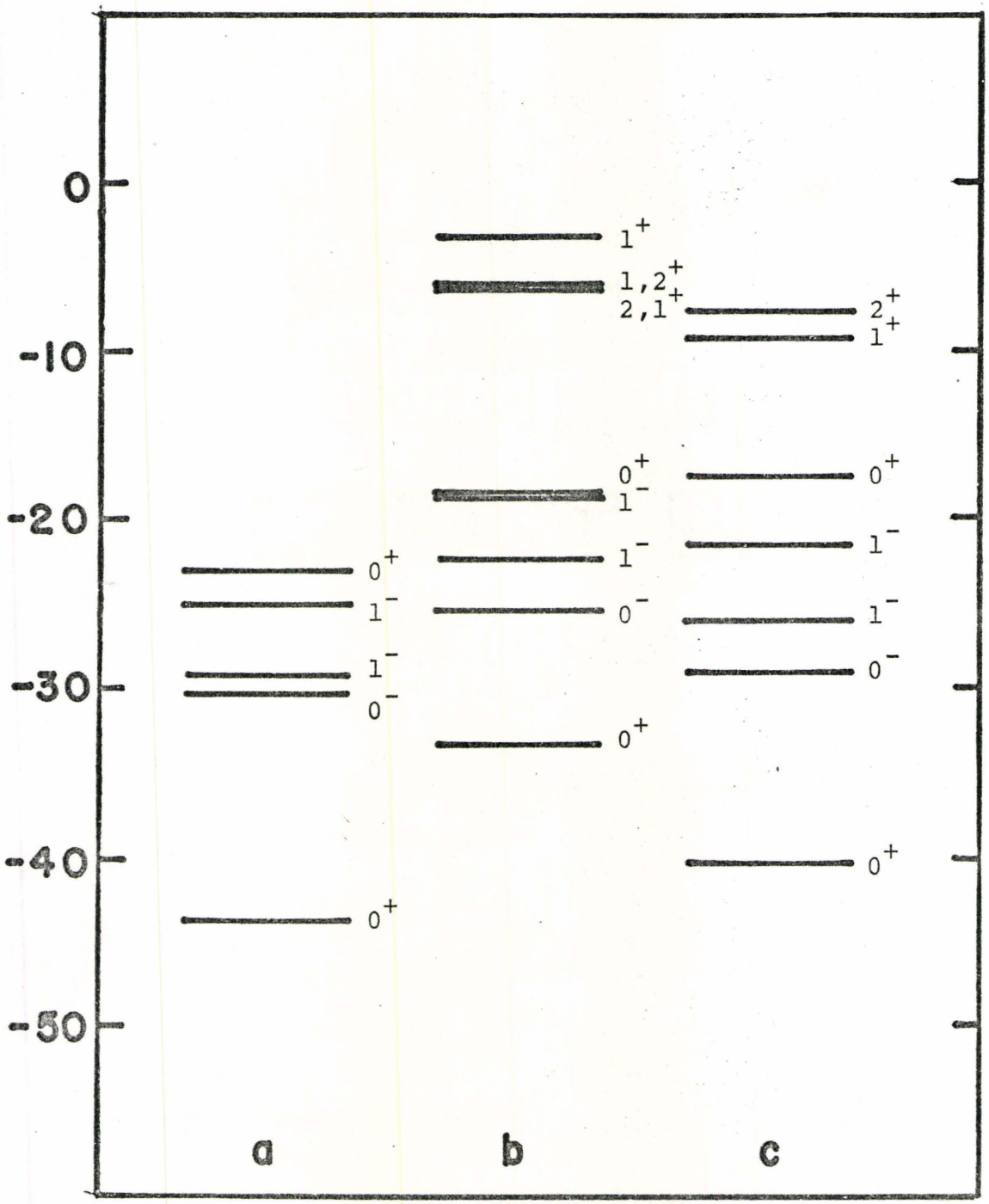

Figure 5.20

than the two 1^- levels which have a ρ dependence. The most obvious anomaly is that the d state 0^+ level has dropped down below the 1^- level. The 0^+ state is mainly prolate with a z^2 dependence.

The HFC density of ^{20}Ne shows very strong clustering on the z axis at about ± 3 fm, having a value of about 0.171 fm^{-3} compared to the central density 0.093 fm^{-3}. This is clearly not well represented by a gaussian. The central density will be overestimated and the cluster density will be underestimated. Density will be removed from the centre toward the surface. The cluster will seem very attractive giving an excessively low s type 0^+ level while the S type 0^+ level rises.

The neutron levels are 3-4 MeV lower than the proton single particle levels.

A comparison of the HFC calculations for the three symmetry energy values showed no changes which could be attributed to anything more than the error in renormalizing.

5.4.2 Magnesium 24

The density map of ^{24}Mg (Fig.5.21)resembles a bitetrahedral configuration of six alpha-particles. Two alphas on the x-axis touching each other at r=0 , with two above and two below in the y-z plane touching each other on the z axis ± 2.5 fm from the origin. Clustering is more pronounced for the upper and lower regions of the nucleus than along the x axis. As with ^{20}Ne the system seems to favour building up density in the prolate

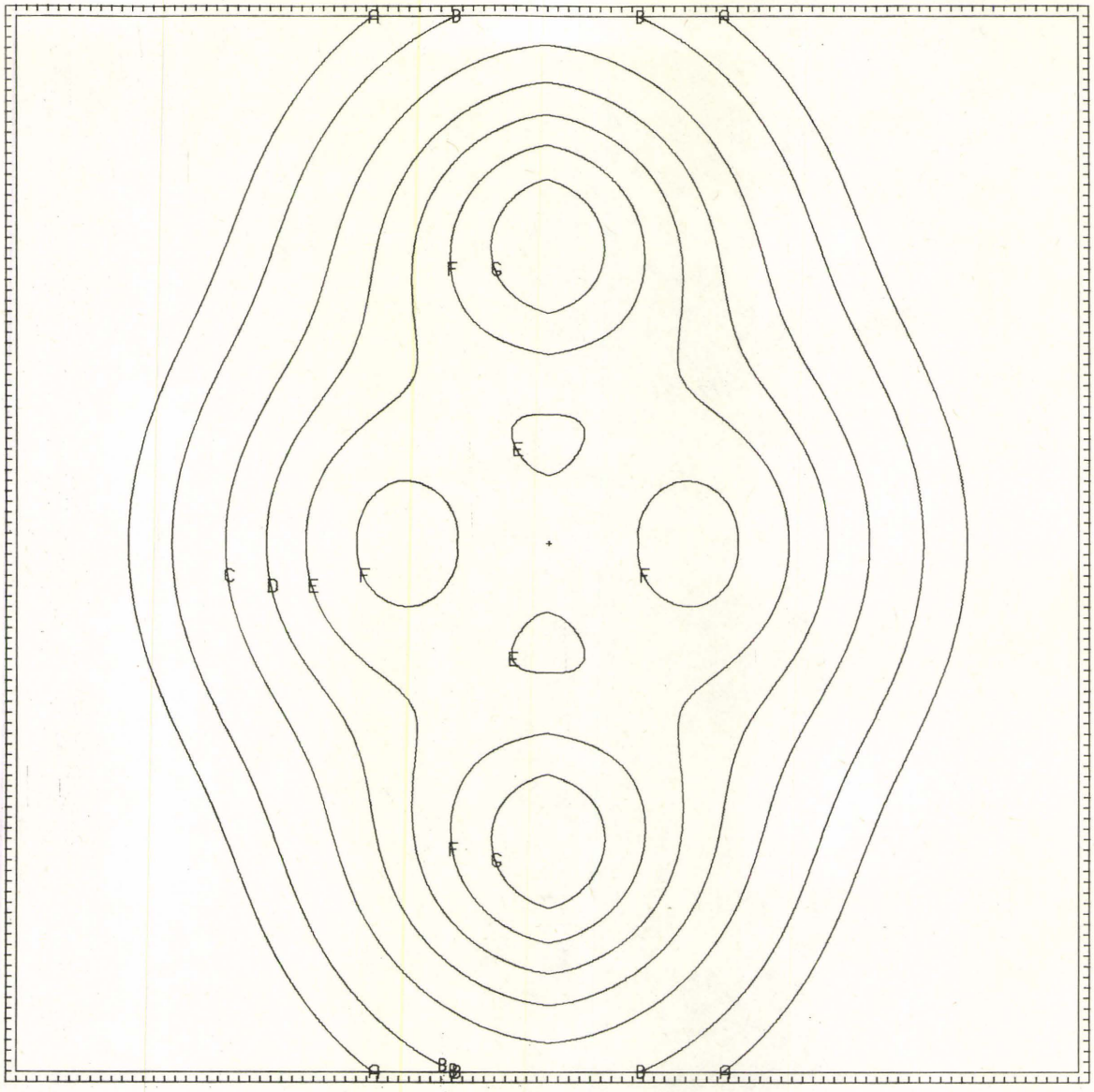

Figure 5.21(a)

Density Distribution of ^{24}Mg in the x-z plane

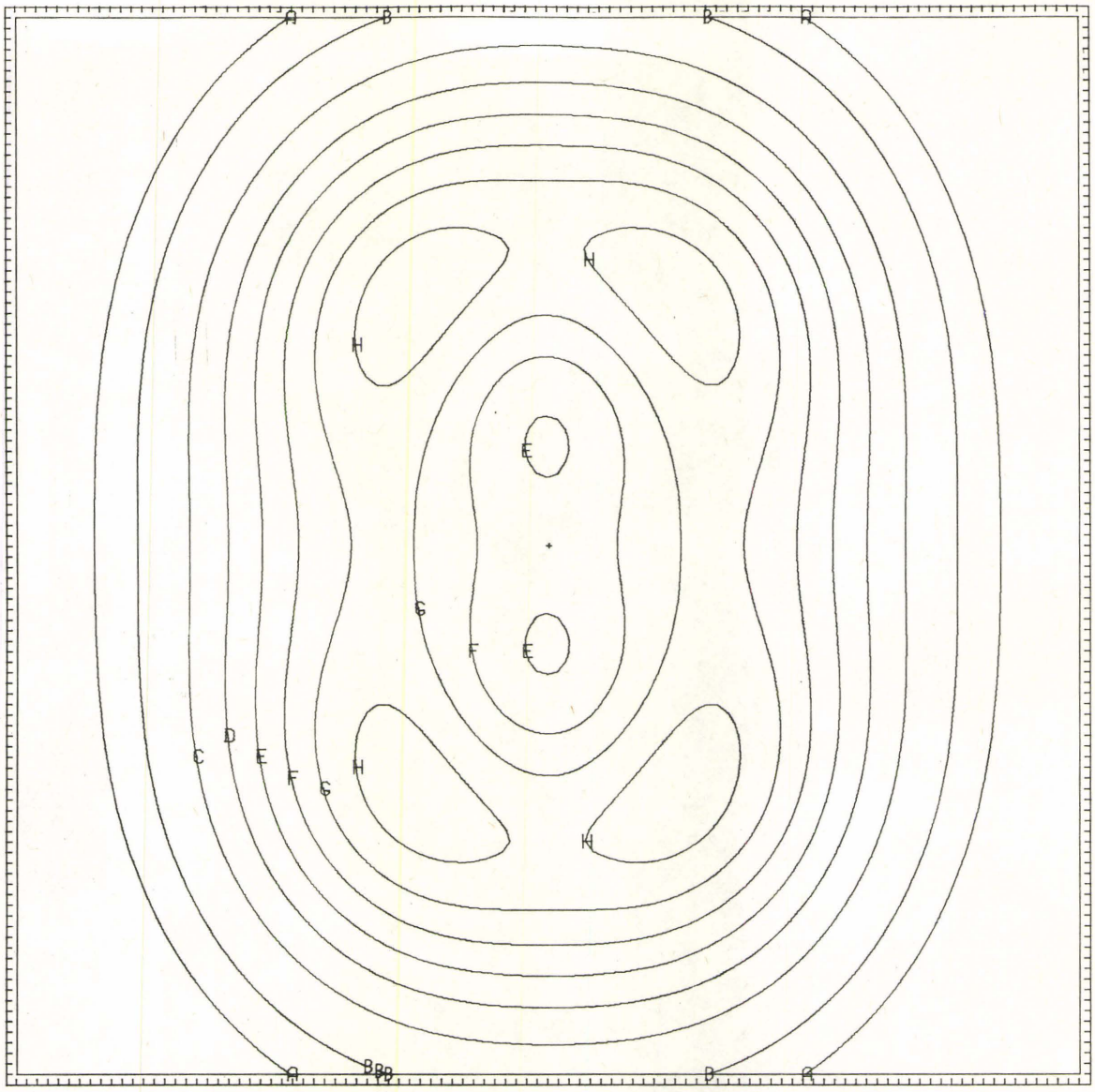

Figure 5.21(b)

Density Distribution of ^{24}Mg in the y-z plane

region at the expense of other regions, in this case both the s and p regions.

The size parameters (Table 5.6 (a) and (b)) reveal that the radii tend to be larger for both HFC and V-LA than for Lineg and B1. For Lineg, Mg is a little more prolate but not nearly as asymmetric. One would wonder if our approach is favouring asymmetry. This is not inconceivable since the program has shown a tendency to move density toward regions of high density and the surface.

The binding energies are similar, HFC being a little more bound than Lineg, and B1 being extremely underbound. A pattern is developing where V-LA is slightly more bound than HFC.

The single particle levels (Fig. 5.22) reveal the typical 0+, 0-, 1-, 1-... pattern for prolate nuclei with B1 spread out and HFC less so. However, HFC differs in that the s-d (0+) level has come down below one of the p(1-) levels. This is indicative of low density in the p region, hence the 1- level rising and high density in the d(0+) region dropping that level. The filling of the d state in the y-z plane gives the off-axis clustering. The usual poverty of density in the centre causes the high 0+ s state. On the whole the s.p. levels are not greatly different from those of Lineg; however, there is strong evidence of greater asymmetry. The V-LA levels would be 2-3 MeV higher if λ=0.4 had been used instead of λ=0.01. The 1- level is not as high, which is in agreement with the higher

TABLE 5.6(a)

Radii of ^{24}Mg for Various Calculations

	Mindet	HFC	V-LA	Lineg	Bl
Mass	3.246	3.35	3.38	3.14	3.16
Proton	-	3.36	3.39	3.18	3.19
Neutron	-	3.34	3.37	3.10	3.13
Charge	-	(3.43)	3.46	3.24	3.24

TABLE 5.6(b)

Share Parameters of ^{24}Mg

$\langle r^2 \rangle^{1/2}$	3.246	3.35	3.38	3.14	3.16
$\langle \rho^2 \rangle$	4.88	5.44	5.57	4.70	4.83
$\langle z^2 \rangle$	5.67	5.80	5.85	5.16	5.16
D_o	0.612	0.548	0.537	0.570	0.552
D_2	-	0.164	-0.141	-0.088	-0.089

TABLE 5.6(c)

Binding Energies for ^{24}Mg

Total	171.15	184.24	186.53	172.8	133.7
Proton	72.28	80.00	81.33	-	-
Neutron	98.87	104.24	105.20	-	-
BE/A	7.13	7.68	7.77	7.20	5.16

TABLE 5.6(d)

Single Particle Energies of ^{24}Mg

Proton

$(m_\ell)\pi$	Mindet	HFC	V-LA	Lineg	Bl
0^+	40.49	31.64	38.77	36.	47.
0^-	32.41	25.78	29.38	24.	30.
1^-	25.12	21.46	25.06	20.	23.
1^-	22.78	13.92	19.29	17.	18.
0^+	20.31	15.00	16.30	12.	13.
1^+	15.49	12.28	13.53	10.	11.
1^+	-	4.33	5.98	5.	- 1.5
GAP	-	7.95	7.55	5.	13.5

Neutron

$(m_\ell)\pi$	Mindet	HFC	V-LA	Lineg	Bl
0^+	45.31	35.85	43.00	-	-
0^-	36.81	29.92	33.49		
1^-		25.31	29.23		
1^-		18.46	23.45		
0^+		18.97	20.31		
1^+		16.37	17.50		
1^+		8.98	10.25		
GAP		7.39	7.25	4.83	12.14

Figure 5.22

Proton Single Particle Energy Levels of ^{24}Mg

(a) Mindet Calculations

(b) HFC Calculations

(c) V-LA Calculations

(d) Lineg Calculations

(e) Bl Calculations

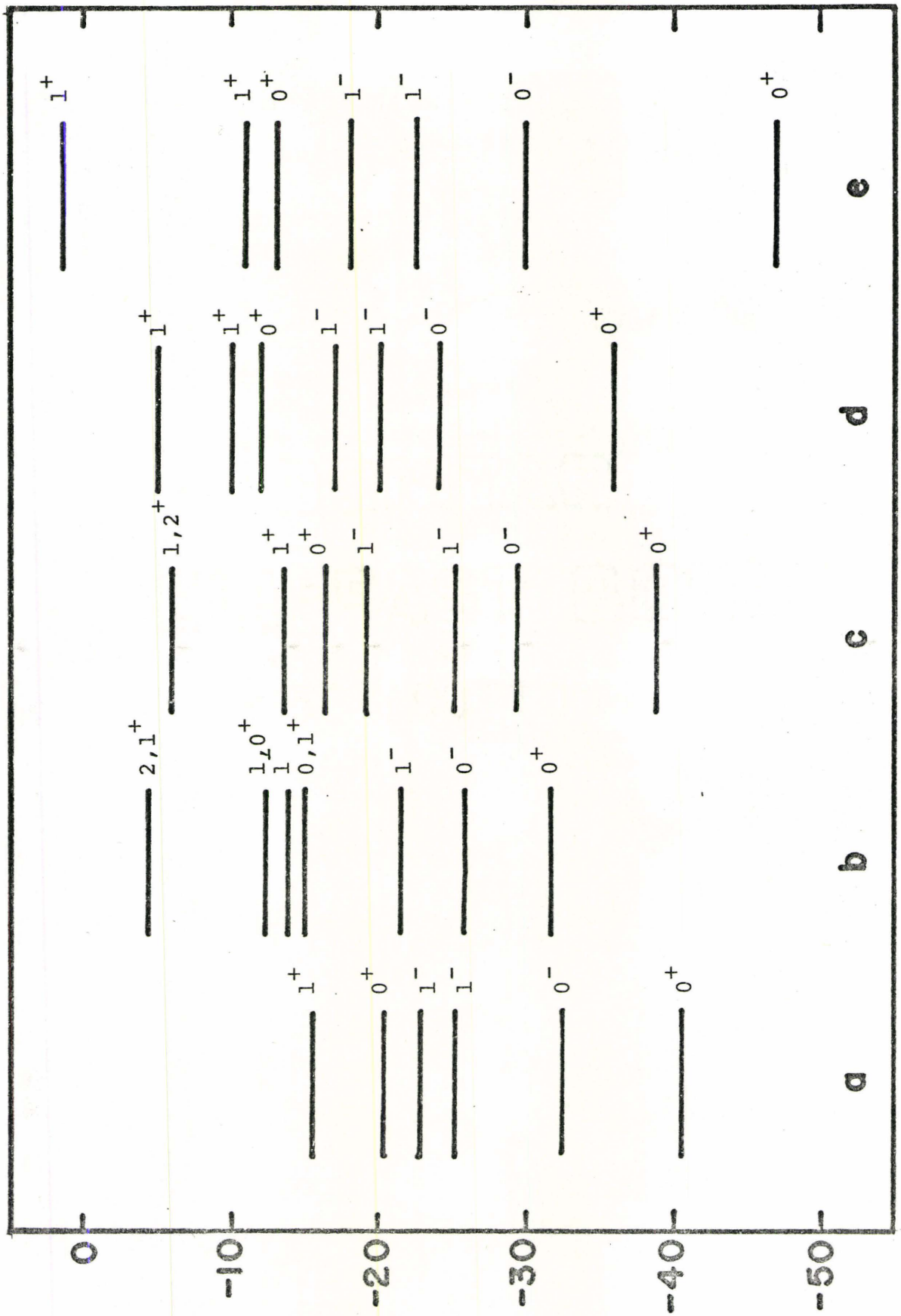
0
-10
-20
-30
-40
-50
a
b
c
d
e
1+
1+ 0+
1- 1-
0-
0+
2,1+
1,0+ 1+ 0,1+
1- 0-
0+
1,2+
1+ 0+ 1- 1- 0-
0+
1+ 0+ 1- 1- 0-
0+
1+ 0+ 1- 1- 0-
0+

Figure 5.22

density of the p region clusters that they obtain.

5.4.3 Silicon 28

Silicon 28 has two low level forms, one prolate the other oblate. The prolate (Fig. 5.23) is composed of two rings of three alpha particles above and below a central one. The oblate (Fig. 5.25) has the configuration of a ring of five alpha particles surrounding two axial alpha particles touching at z=0.

First we shall study the prolate form. Our radii are 5% larger than for Lineg. The shape parameter D_o indicates that HFC and V-LA give not quite as prolate a solution. The energies are again highest for V-L A and a little lower for HFC. The nuclei of Zofka and Ripka are less bound (see Tables 5.7 (a), (b) and (c)).

The single particle levels show the typical prolate lower levels ordering. However the d(1+) level has dropped below the 0+ level. This is indicative of the strong clustering off the z-axis in the d region. The p(1-) levels are high owing to little density in the x-y plane. The 1s(0+) level is also high consistent with the relatively low density ar r=0, the region of another alpha particle. (Fig. 5.24 and Table 5.7(d)).

The HFC levels would be similar to the Lineg levels if spin orbit were added to the latter. The V-LA results should be 3-4 MeV higher if λ=0.4 was used instead of λ=-0.02.

The gaps would all be similar if spin orbit were added to Lineg. The neutron single particle levels are about 5 MeV

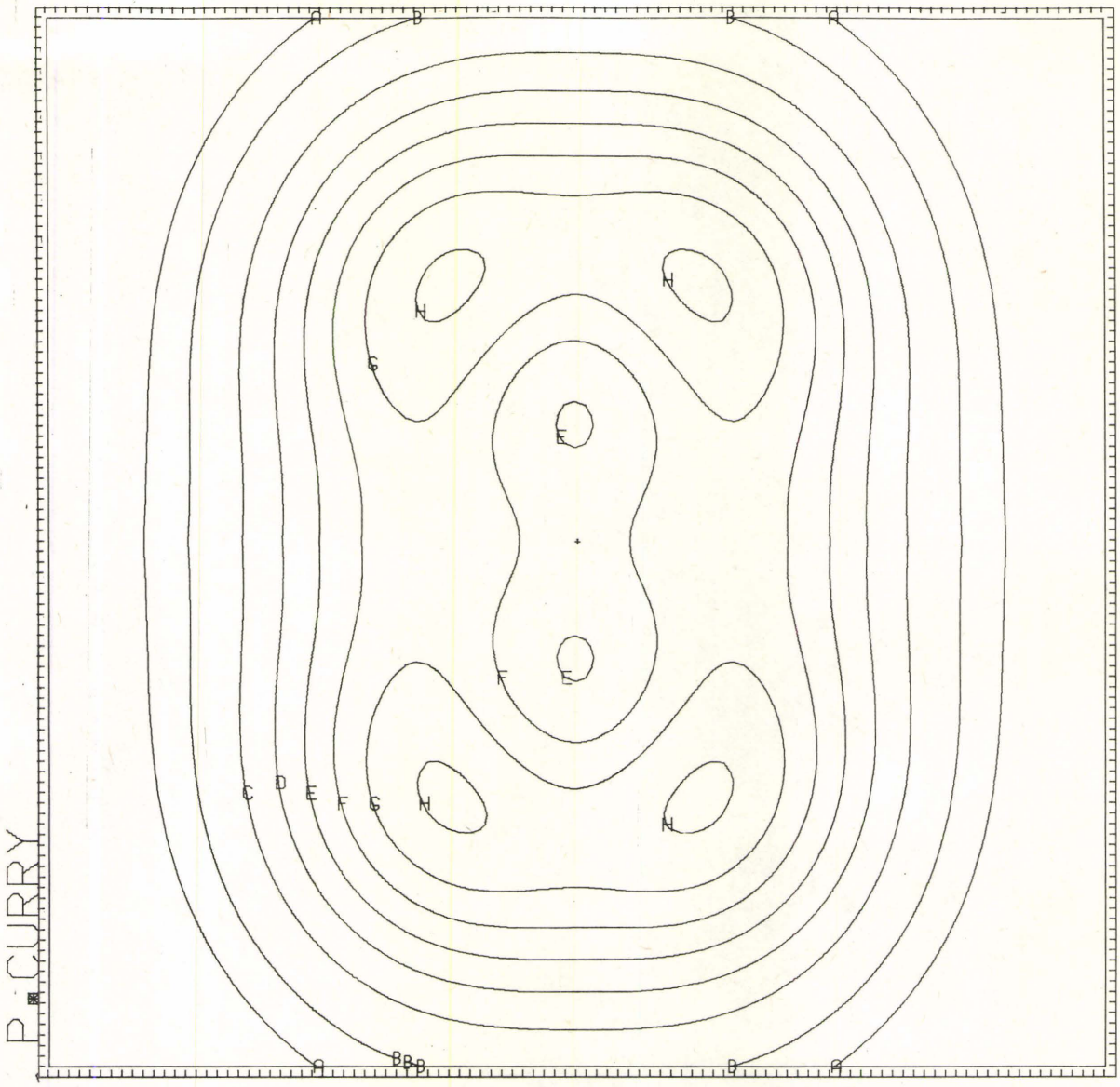

Figure 5.23

Density Distribution of Prolate ^{28}Si

TABLE 5.7(a)

Radii of Silicon 28 Prolate

	Mindet	HFC	V-LA	Lineg	Bl
Mass	3.360	3.440	3.495	3.28	3.32
Proton		3.452	3.504	3.32	3.35
Neutron		3.428	3.486	3.23	3.28
Charge		(3.52)	3.57	3.38	3.40

TABLE 5.7(b)

Shape Parameters of ^{28}Si Prolate

$\langle r^2 \rangle^{1/2}$	3.360	3.440	3.495	3.28	3.32
$\langle \rho^2 \rangle$	5.223	5.640	5.863	5.023	5.095
$\langle z^2 \rangle$	6.064	6.236	6.351	5.703	5.894
D_o	0.612	0.581	0.560	0.595	0.609
D_2	-	0.0	0.0	0.0	0.0

TABLE 5.7(c)

Binding Energies of ^{28}Si Prolate

Total	218.20	219.08	224.94	209.4	161.
Proton	91.35	92.88	96.32	-	
Neutron	126.85	126.20	128.61	-	
BE/A	7.78	7.824	8.034	7.48	5.75

TABLE 5.7(d)

Single Particle Levels of ^{28}Si Prolate

Protons

$k\pi$	$m_\ell \pi$	Mindet	HFC	V-LA	Lineg	Bl
$1/2^+$	0^+	41.21	33.12	40.92	37.	49.
$1/2^-$	0^-	36.24	28.05	32.95	27.	35.
$3/2^-$	1^-	28.40	21.09	26.45	20.	23.
$1/2^-$	1^-	24.21	17.44	22.21		
$1/2^+$	0^+	22.67	15.24	18.58	14.	15.
$3/2^+$	1^+	21.65	15.34	16.92	11.	11.
$1/2^+$	1^+	18.43	10.43	12.84		
$5/2^+$	2^+	-	5.59	7.20	2.5	-2.5
GAP		-	4.84	5.64	8.5	13.5

Neutrons

$1/2^+$	0^+	46.76	38.04	45.80	-	-
$1/2^-$	0^-	41.32	32.90	37.70	-	-
$3/2^-$	1^-	33.51	26.00	31.28	-	-
$1/2^-$	1^-	29.32	22.26	26.96	-	-
$1/2^+$	0^+	27.60	20.16	23.31	-	-
$3/2^+$	1^+	26.51	20.11	21.50	-	-
$1/2^+$	1^+	23.29	15.30	17.46	-	-
$5/2^+$	2^+	-	10.65	12.00	-	-
GAP		-	4.65	5.46	8.35	13.54

Figure 5.24

Proton Single Particle Energy Levels of Prolate ^{28}Si

(a) Mindet Calculations

(b) HFC Calculations

(c) V-LA Calculations

(d) Lineg Calculations

(e) Bl Calculations

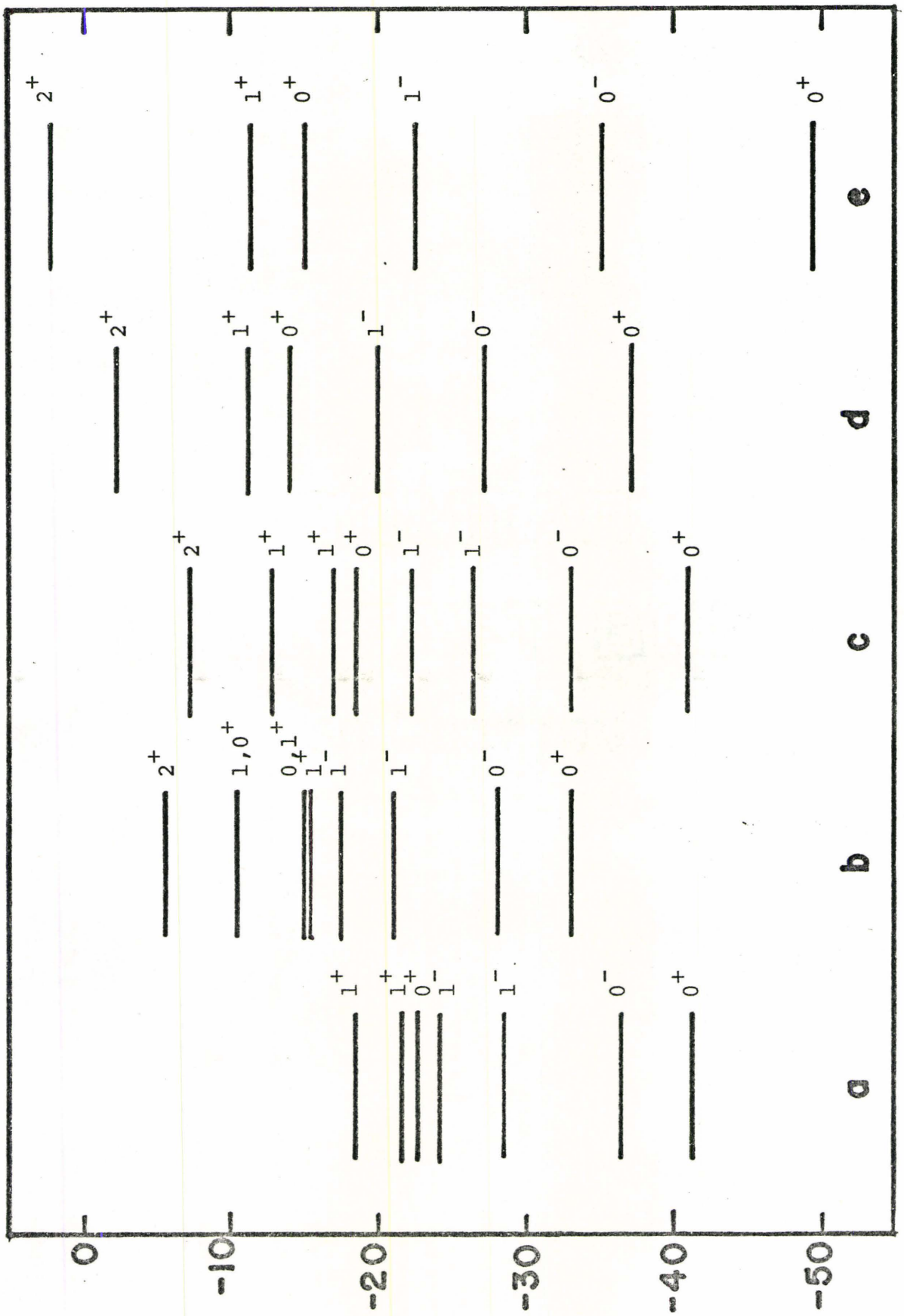

Figure 5.24

lower than the proton levels.

The oblate form of ^{28}Si (Fig 5.25) is reputed to be the ground state. The HFC and V-LA calculations show the oblate to be the ground state by 0.5 and 0.2 MeV respectively. The B1 and Lineg forces indicate that the prolate is the ground state by 2.0 and 3.0 MeV respectively.

From table 5.8 we see that our radii are about 0.25 fm larger than those of Zofka and Ripka. The HFC radii are larger for the oblate, the V-LA are both similar, while the Lineg and B1 radii are larger for the prolate state. However our quadrupole moment, D_o is not as large as the other ones. (See Table 5.8(b)). The V-LA nucleus is most bound, HFC is 5 MeV less bound with Lineg and B1 quite underbound compared to the experimental value of 236.53 MeV.

The HFC quadrupole moment is less negative owing to the central clusters being at larger z than V-LA. This is consistent with the previously mentioned z-axis density build-up at the expense of the core.

The oblate single particle levels show a distinctly different pattern than do the prolate levels. The 0- level is now above the two 1- levels. The 1+ level moves up and the 2+ levels move down. This is consistent with the density being localized nearer the x-y plane than the z axis.

The pattern of the levels is fairly uniform from force to force, except for compactness and the "λ-depression" of

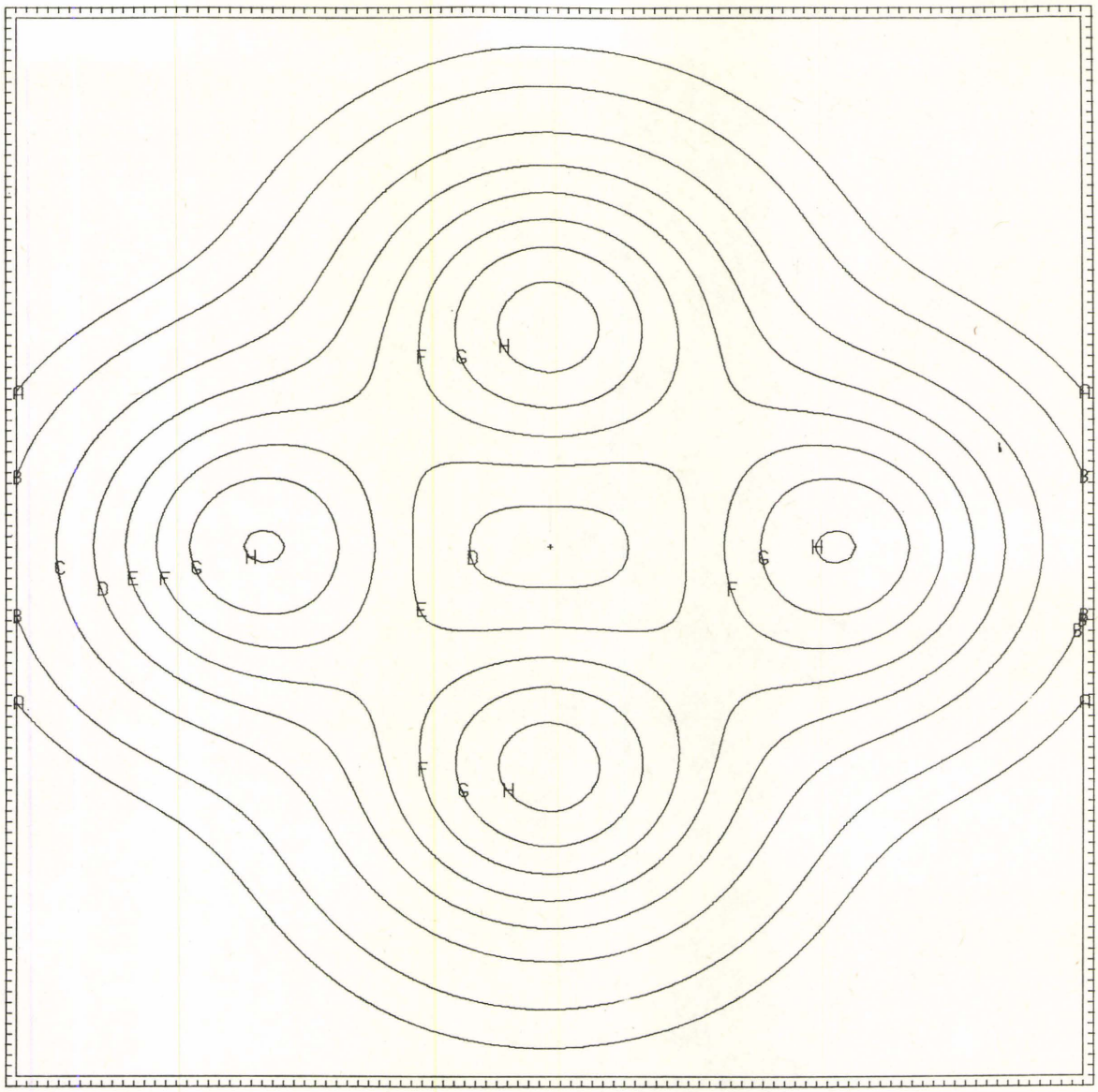

Figure 5.25

Density Distribution of Oblate ^{28}Si

TABLE 5.8(a)

Radii of ^{28}Si Oblate For Various Calculations

	Mindet	HFC	V-LA	Lineg	Bl
Mass	3.393	3.496	3.496	3.25	3.26
Proton		3.507	3.504	3.29	3.29
Neutron		3.486	3.487	3.20	3.23
Charge		(3.58)	3.58	3.35	3.35

TABLE 5.8(b)

Shape Parameters of ^{28}Si Oblate

$\langle r^2 \rangle^{1/2}$	3.393	3.496	3.496	3.25	3.26
$\langle \rho^2 \rangle$	9.607	9.520	9.808	8.708	8.775
$\langle z^2 \rangle$	1.903	2.703	2.414	1.822	1.853
D_o	-0.504	-0.337	-0.408	-0.481	-0.477
D_2	0.0	0.0	0.0	0.0	0.0

TABLE 5.8(c)

Binding Energies of ^{28}Si Oblate

Total	208.08	220.24	225.09	206.4	159.0
Proton	86.48	93.92	96.53	-	-
Neutron	121.59	126.31	128.56	-	-
BE/A	7.43	7.87	3.04	7.34	5.68
EXP	236.53				

TABLE 5.8(d)

Single Particle Levels of ^{28}Si Oblate

Protons

k	$m_e\pi$	Mindet	HFC	V-LA	Lineg	Bl
1/2	0^+	42.16	31.56	40.50	37.	50.5
3/2	1^-	31.53	24.97	30.12	25.	30.
1/2	1^-	-	23.56	28.72		
1/2	0^-	22.06	19.13	22.53	18.	
5/2	2^+	19.95	15.84	17.34	12.5	12.
1/2	0^+	17.70	14.00	15.02	11	13.
3/2	2^+		12.99	14.54	12.5	12
3/2	1^+		4.30	6.53	5.	-2.
GAP		-	8.69	8.01	6.5	14.

Neutrons

1/2	0^+	47.69	36.36	45.39		
3/2	1^-	36.55	29.70	34.86		
1/2	1^-		28.27	33.46		
1/2	0^-	27.21	23.93	27.36		
5/2	2^+	24.74	20.50	21.77		
1/2	0^+	22.25	18.68	19.63		
3/2	2^+		17.64	19.07		
3/2	1^+		9.26	11.39		
GAP		-	8.38	7.68	6.41	13.82

Figure 5.26

Proton Single Particle Energy Levels of Oblate ^{28}Si

(a) Mindet Calculations

(b) HFC Calculations

(c) V-LA Calculations

(d) Lineg Calculations

(e) Bl Calculations

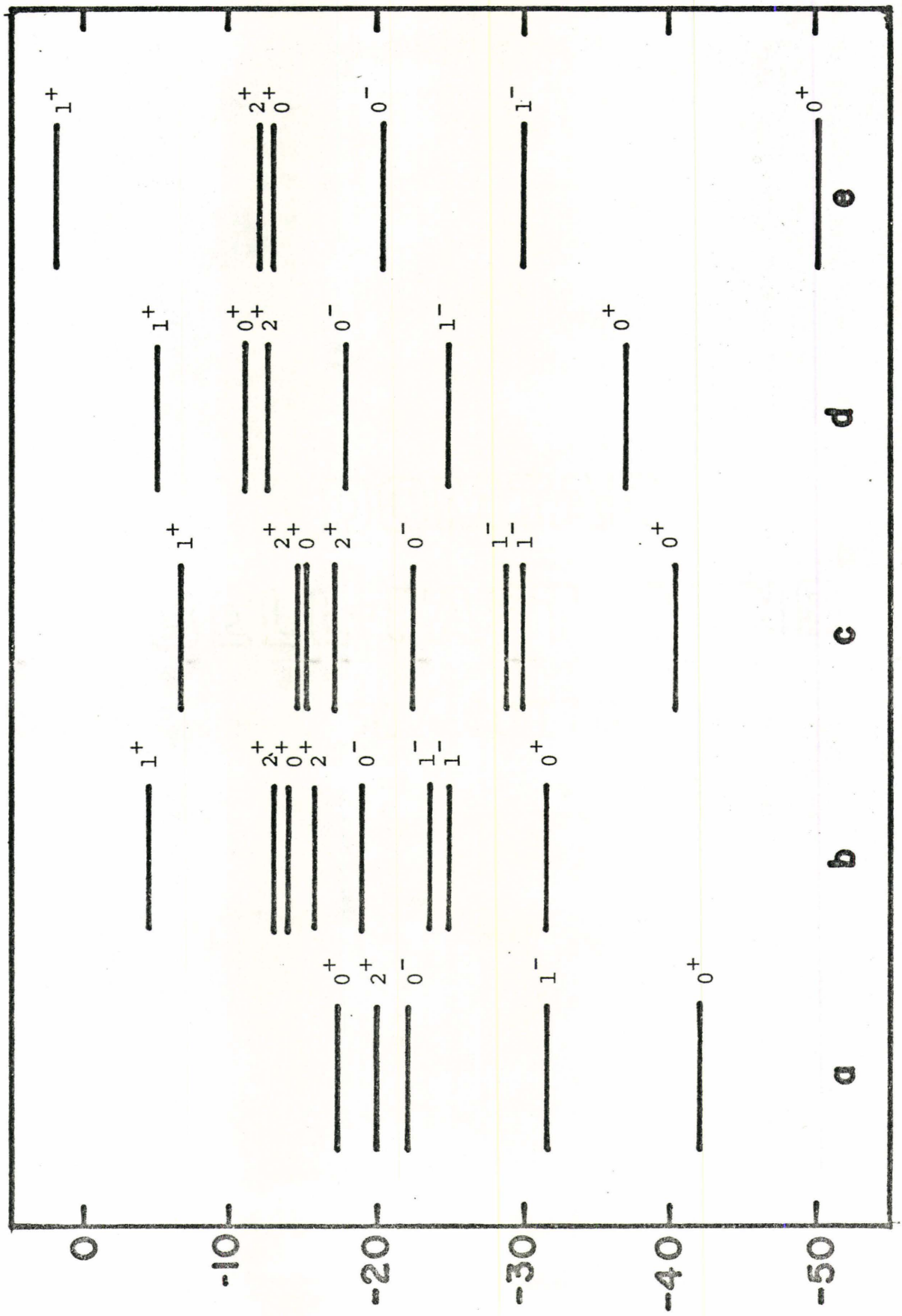

Figure 5.26

V-LA. In both HFC and V-LA the 2+ levels are a bit lower than Lineg and B1. This could mean more clustering in our nuclei. The 0+ is too high for HFC indicating a strong central density depression.

The energy gaps are similar for HFC and V-LA. Spin orbit force will decrease the gap of both Lineg and B1 making the former smaller than the others.

The neutron levels are about 5 MeV lower than the proton single particle levels.

5.4.4 Sulphur 32

Most Hartree Fock calculations, including those of Volkov and Lassey (1972), and Zofka and Ripka (1971) predict a triaxial ground state for ^{32}S. However there appears to be several low lying configurations. Nakai et al of Berkley (1970), using the reorientation effect in projectile Coulomb excitation, with beams from the Berkley Hilac, measured the static quadrupole moment of ^{32}S and found it to be prolate.

HFC calculations have been done for prolate (Fig. 5.27) oblate (Fig 5.28) and triaxial (Fig. 5.29) configurations of ^{32}S. The triaxial form, is first compared with the other calculations.

^{32}S, the clown nucleus (Fig. 5.30), has the configuration of two diamonds one above and one below the x-y plane, with an alpha particle at each vertex. This is triaxial, the longer dimension being along the y-axis.

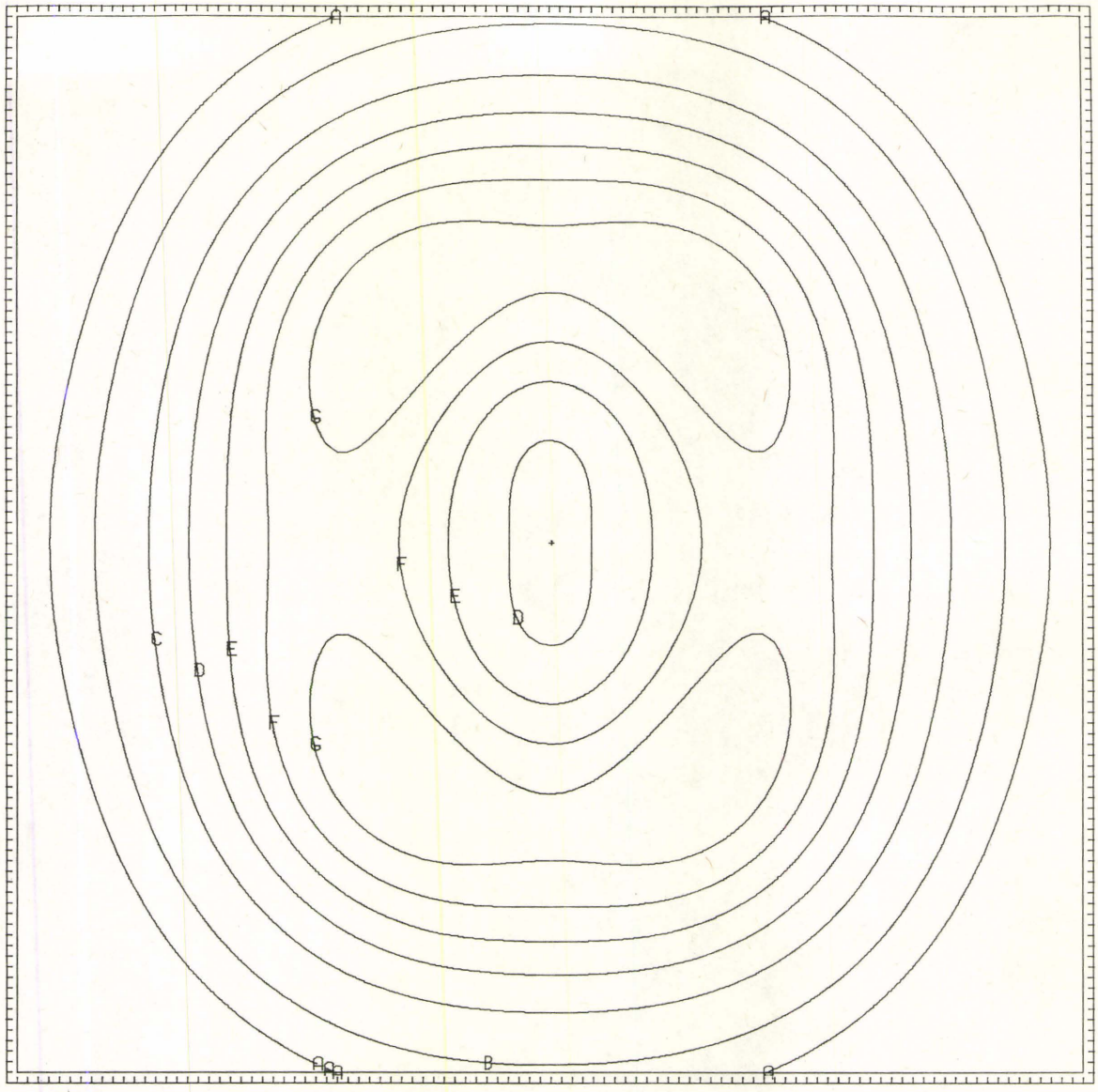

Figure 5.27

Density Distribution of Prolate ^{32}S

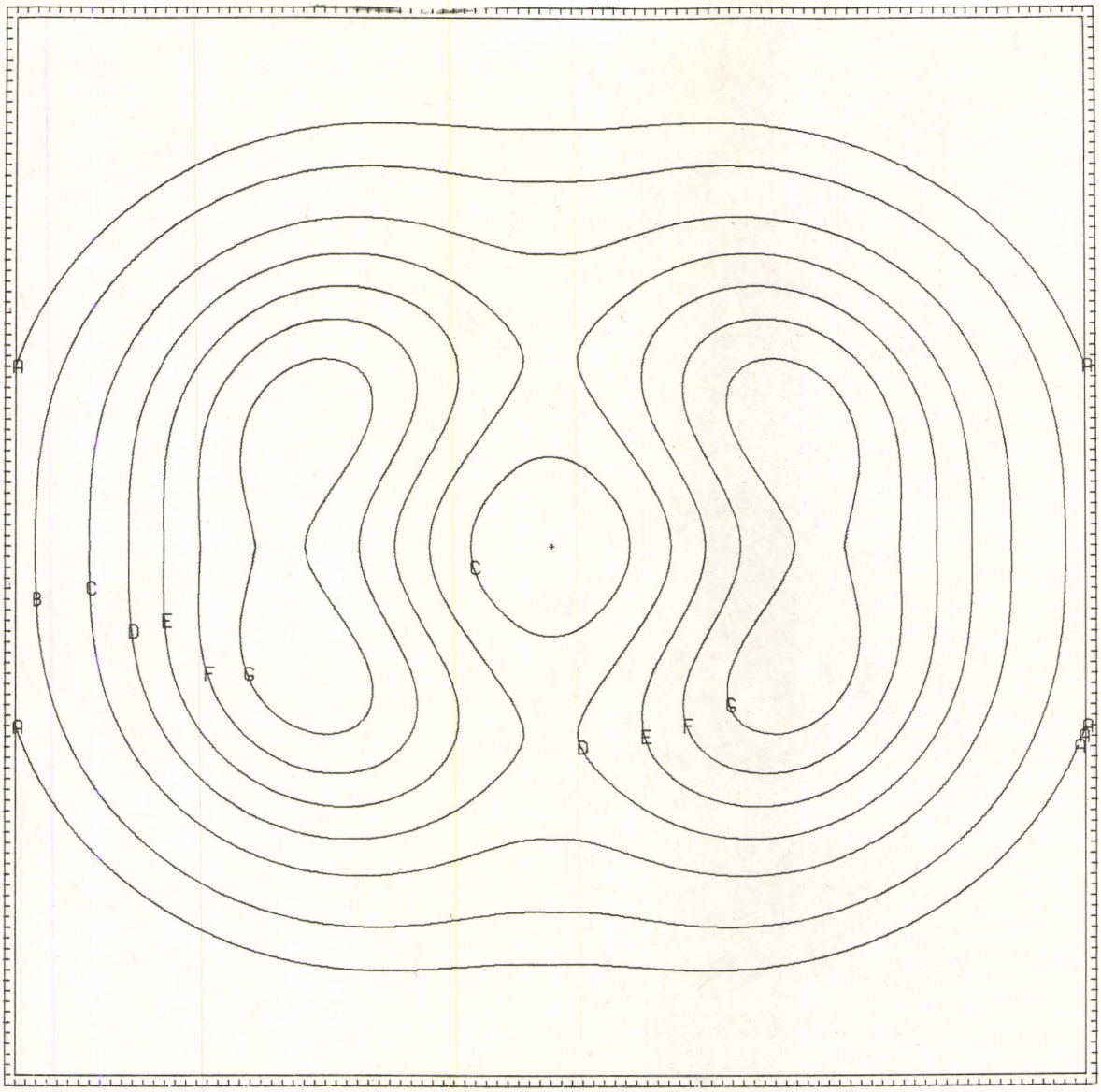

Figure 5.28

Density Distribution of Oblate ^{32}S

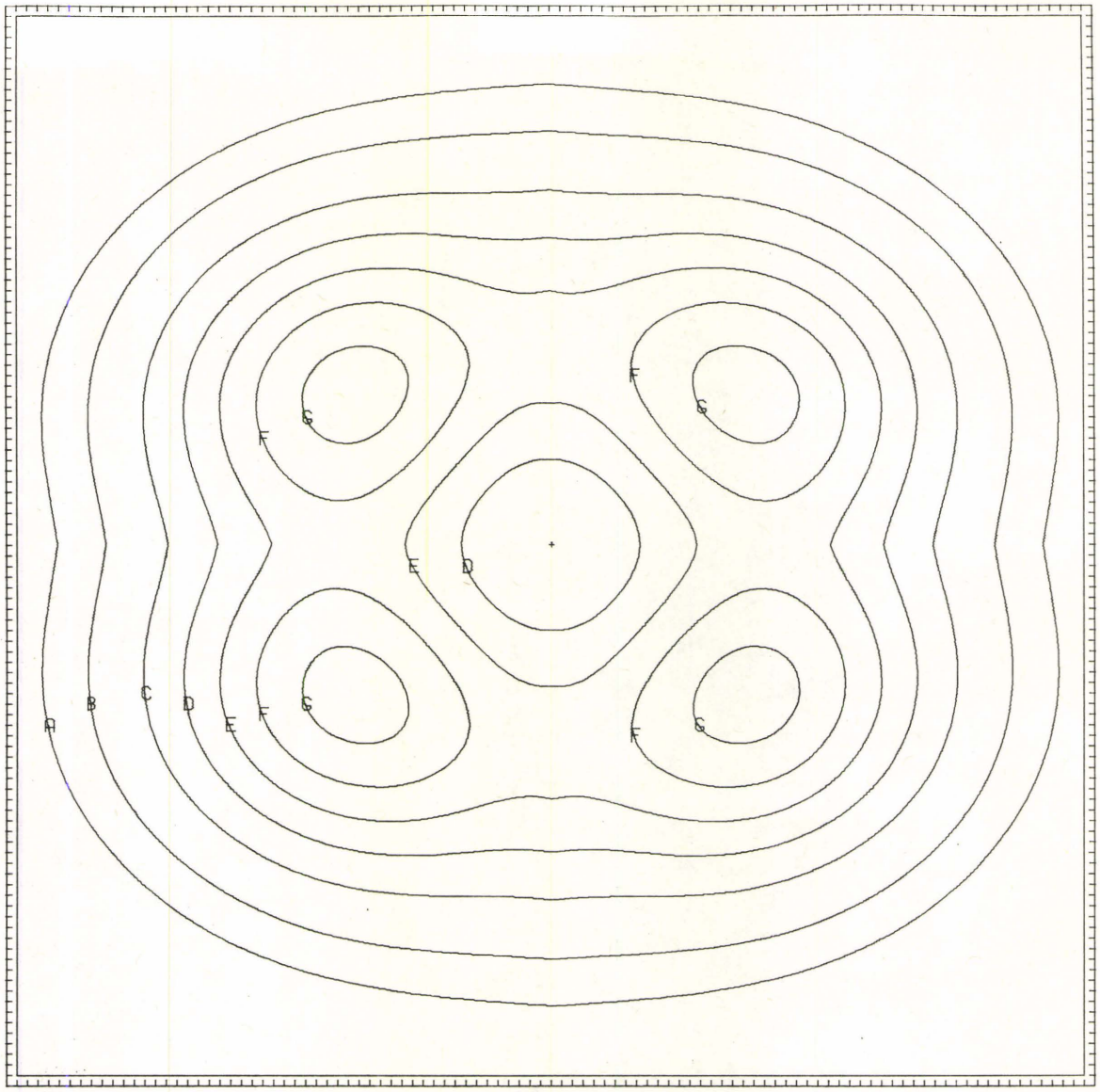

Figure 5.29(a)

Density Distribution of Triaxial

^{32}S in the x-z plane

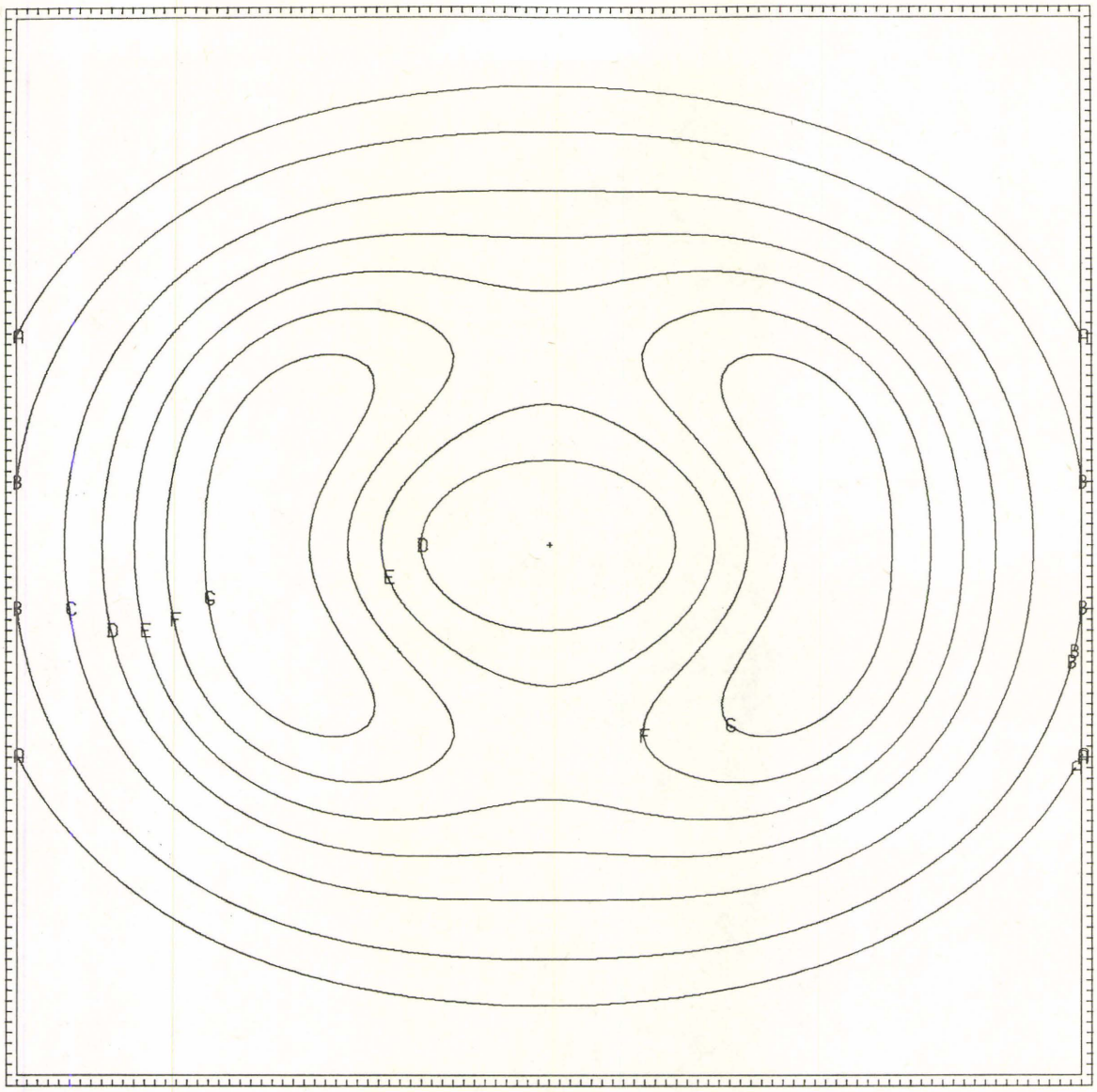

Figure 5.29(b)

Density Distribution of Triaxial

^{32}S in the y-z plane

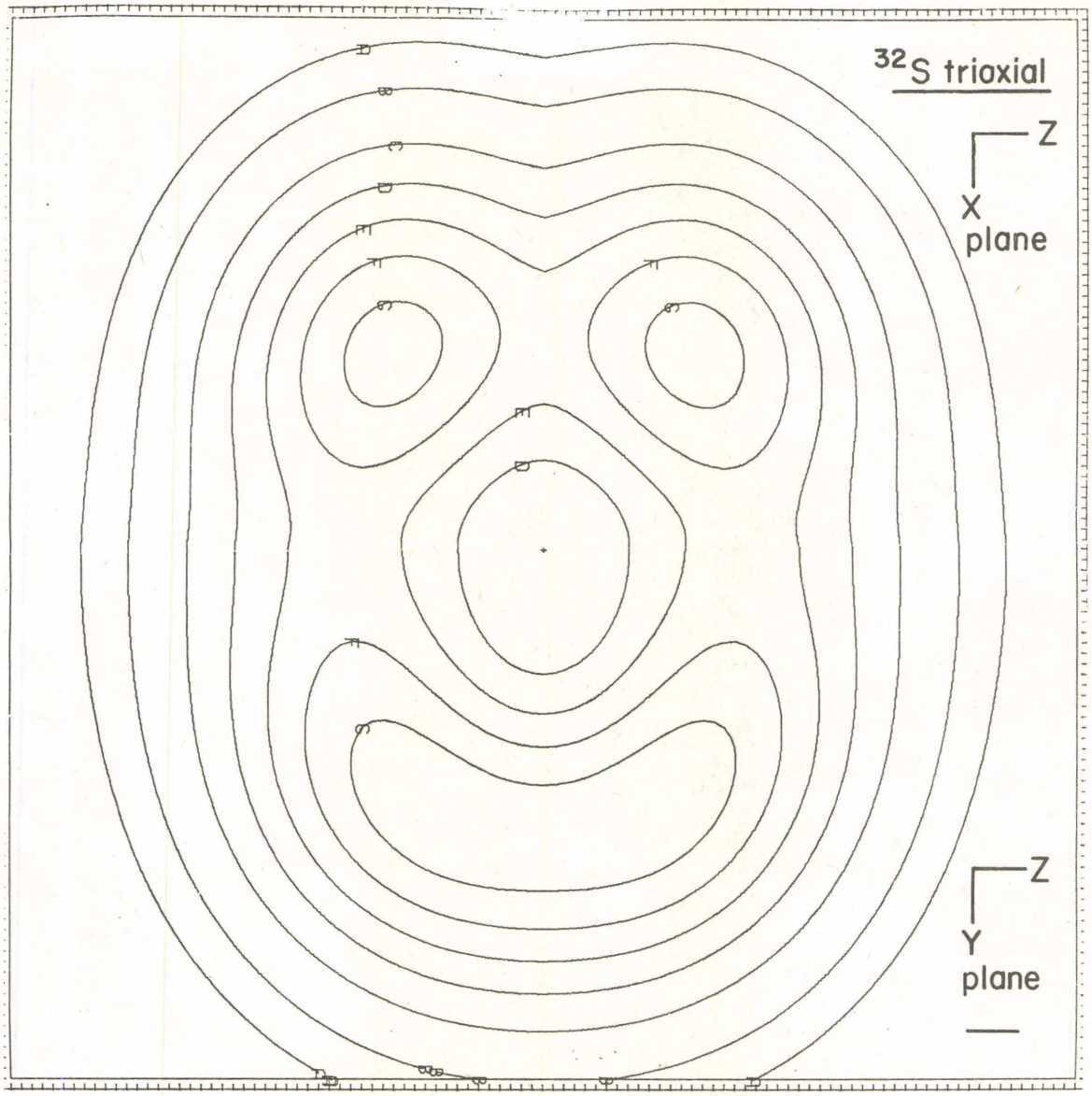

Figure 5.30

Composite of Triaxial ^{32}S

The radii follow the established pattern. The HFC and V-LA radii are larger than those of Zofka and Ripka. The shape parameters however, are quite different. (Table 5.9b) The asymmetry D_2 is small for Zofka and Ripka, larger for V-LA and largest for HFC. The quadrupole moment D_o however is vice-versa.

The binding energies compare well with the experimental value of 271.77 MeV with the exception of B1.

The single particle levels are quite interesting. In each case we have the typical oblate pattern 0+, 1+, 1-, 0-, (when only the parity is a good quantum number, the m_ℓ is that of the largest component of the linear combination which makes up our state). The order of the remaining levels changes from calculation to calculation. The HFC configuration has a hole at $r \sim 0$ which is consistent with the high, unoccupied 0+ state. The V-LA configuration (Lassey 1972) is a plane of 6 alpha particles in the y-z plane, with one alpha on either side of the plane on the x-axis. In contrast to HFC, the V-LA single particle level has a 1+ unoccupied state, the 0+ having come down, owing to no central minimum. The Zofka and Ripka spectra are most similar to the V-LA results. The configuration is probably most similar to Lassey's. However the two low 2+ levels probably indicate a more uniform density distribution in the $\langle x^2 \rangle$ and $\langle y^2 \rangle$ regions. Hence the lower D_2. In any event one would not expect a central minimum for either Lineg or B1. (Fig. 5.31).

TABLE 5.9(a)

Radii of Triaxial ^{32}S

	Mindet	HFC	V-LA	Lineg	Bl
Mass	3.427	3.536	3.549	3.31	3.34
Proton	-	3.546	3.558	3.36	3.37
Neutron	-	3.525	3.541	3.26	3.30
Charge	-	(3.62)	3.62	3.42	3.44

EXP 3.24±0.02

TABLE 5.9(b)

Shape Parameters for Triaxial ^{32}S

$\langle r^2 \rangle^{1/2}$	3.427	3.536	3.549	3.31	3.34
$\langle \rho^2 \rangle$	9.304	9.214	9.474	8.60	8.74
$\langle z^2 \rangle$	2.439	3.286	3.124	2.35	2.38
D_o	-0.377	-0.211	-0.256	-0.356	-0.358
D_2	-	0.192	-0.165	+0.095	+0.098

TABLE 5.9(c)

Binding Energies of Triaxial ^{32}S

Total	238.93	256.64	266.59	242.2	186.
Proton	96.71	107.05	112.41	-	-
Neutron	142.23	149.55	154.19	-	-
BE/A	7.467	8.020	8.33	7.57	5.82

TABLE 5.9(d)

Single Particle Levels of Triaxial ^{32}S

Protons

π	Mindet	HFC	V-LA	Lineg	Bl
+	43.71 (0)	33.63 (0)	42.41 (0)	38.1 (0)	52.7 (0)
-	33.71 (1)	28.46 (1)	33.75 (1)	27. (1)	34. (1)
-	33.26 (1)	23.78 (1)	29.93 (1)	25. (1)	30. (1)
-	26.33 (0)	21.22 (0)	26.05 (0)	21. (0)	24.5 (0)
+	21.60 (1)	16.35 (2)	19.15 (2)	14. (2)	14.3 (2)
+	20.97 (2)	15.91 (1,2)	18.00 (1,2)	13. (2)	13.0 (2)
+	17.38 (2)	11.93 (1)	14.47 (0,2)	11. (0)	11.5 (0)
+	15.20 (0)	11.56 (1,2)	13.58 (0,1)	10.5 (1)	11.0 (1)
+	-	5.29 (0)	7.41 (1)	5.5 (1)	-0.5 (1)
GAP	-	6.37	6.17	5.0	11.5

Neutrons

+	50.02 (0)	39.08 (0)	47.92 (0)	-	-
-	39.42 (1)	33.85 (1)	39.15 (1)	-	-
-	39.01 (1)	29.21 (1)	35.35 (1)	-	-
-	32.15 (0)	26.58 (0)	31.46 (0)	-	-
+	27.09 (1)	21.78 (2)	24.41 (2)	-	-
+	26.47 (2)	21.26 (1)	23.21 (1,2)	-	-
+	22.87 (2)	17.28 (1)	19.64 (0,2)	-	-
+	20.63 (0)	17.02 (1,2)	18.84 (0,1)	-	-
+	-	10.94 (0)	12.92 (1)	-	-
GAP	-	6.08	5.92	5.10	11.17

It must be realized that the HFC configuration may be forced by the tendency of this program with this force, to remove density from the central region to the prolate zones.

This nucleus gives us an opportunity to study the single particle levels and other properties for various configurations of an A particle system. For the HFC, ^{32}S nucleus, all three configurations are basically a ring of four alpha particles above and below the x-y plane. The differing distances between the alpha particles creates the differences in the radii, energies and single particle levels. (Table 5.10). The triaxial configuration is the ground state. Single particle energies are lowest for protons and neutrons as well. Consistent with this the gap is larger, indicating more stability. However the prolate radius is smallest, closer to the experimental value of 3.24±0.2 fm. The characteristic proton single particle energy levels are seen in Fig. 5.32.

For triaxial ^{32}S, the gaps have a similar pattern to previous observations. The V-LA calculation used λ=0.01. The neutron and proton levels were separated by about 5.5 MeV.

Zofka and Ripka stated that ^{32}S may become spherical with the addition of a spin orbit term in the Hamiltonian. This was not the case. The true ground state of ^{32}S may be a linear combination of several configurations, some already mentioned above, or perhaps some without good parity (Kelson 1971); pear shaped states requiring excitations from the s-d to the p-f shell.

Figure 5.31

Proton Single Particle Energy Levels of Triaxial ^{32}S

(a) Mindet Calculations

(b) HFC Calculations

(c) V-LA Calculations

(d) Lineg Calculations

(e) Bl Calculations

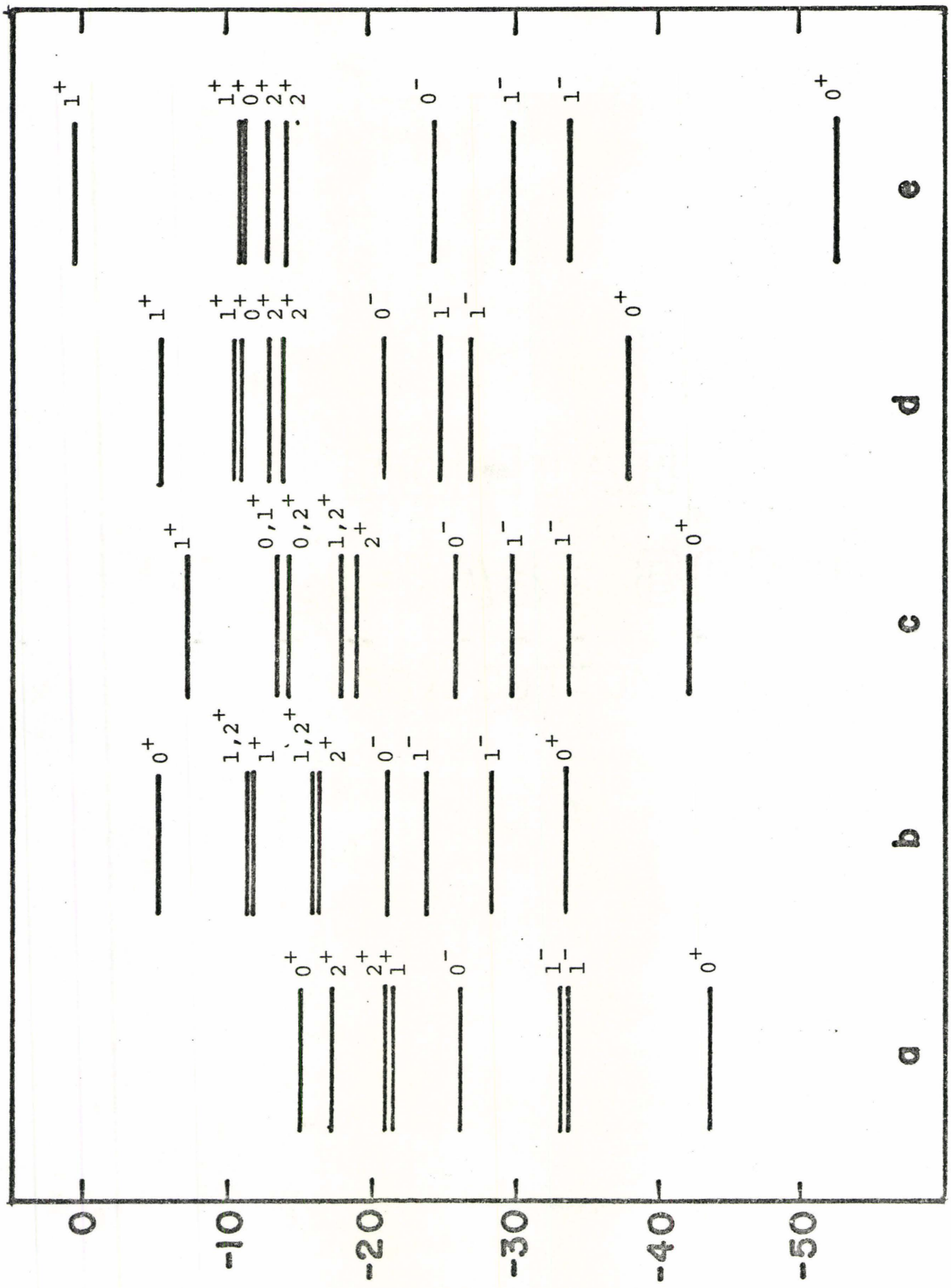

Figure 5.31

TABLE 5.10

Properties of Various Configurations of ^{32}S

a. Radii	Prolate	Oblate	Triaxial
Mass	3.482	3.557	3.536
Proton	3.494	3.567	3.546
Neutron	3.471	3.547	3.525
Charge	(3.56)	(3.64)	(3.62)
b. Shape Parameters			
$\langle r^2 \rangle^{1/2}$	3.482	3.557	3.536
$\langle \rho^2 \rangle$	6.973	9.569	9.214
$\langle z^2 \rangle$	5.153	3.082	3.286
D_o	0.275	-0.269	-0.211
D_2	0.0	0.001	-0.192
c. Binding Energies			
Total	254.60	255.96	256.64
Proton	105.80	106.87	107.05
Neutron	148.80	149.10	149.55
BE/A	7.956	7.999	8.020

d. Proton Binding Energies

π	ε	(m_ℓ)	k	ε	(m_ℓ)	k	ε	(m_ℓ)
+	33.57	(0)	1/2	33.01	(0)	1/2	33.63	(0)
-	27.67	(0)	1/2	27.19	(1)	3/2	28.46	(1)
-	23.89	(1)	3/2	25.58	(1)	1/2	23.78	(1)
-	21.40	(1)	1/2	20.14	(0)	1/2	21.22	(0)
+	16.00	(1)	3/2	16.93	(2)	5/2	16.35	(2)
+	15.80	(0,1)	1/2	15.64	(1,2)	3/2	15.91	(1,2)
+	11.11	(1,0)	1/2	12.94	(1)	1/2	11.93	(1)
+	10.98	(2)	5/2	11.54	(2,1)	3/2	11.66	(1,2)
+	6.60	(2)	3/2	5.56	(0)	1/2	5.29	(0)
GAP	4.38			5.98			6.37	

Figure 5.32

Proton Single Particle Energy Levels of ^{32}S

(a) Prolate

(b) Oblate

(c) Triaxial

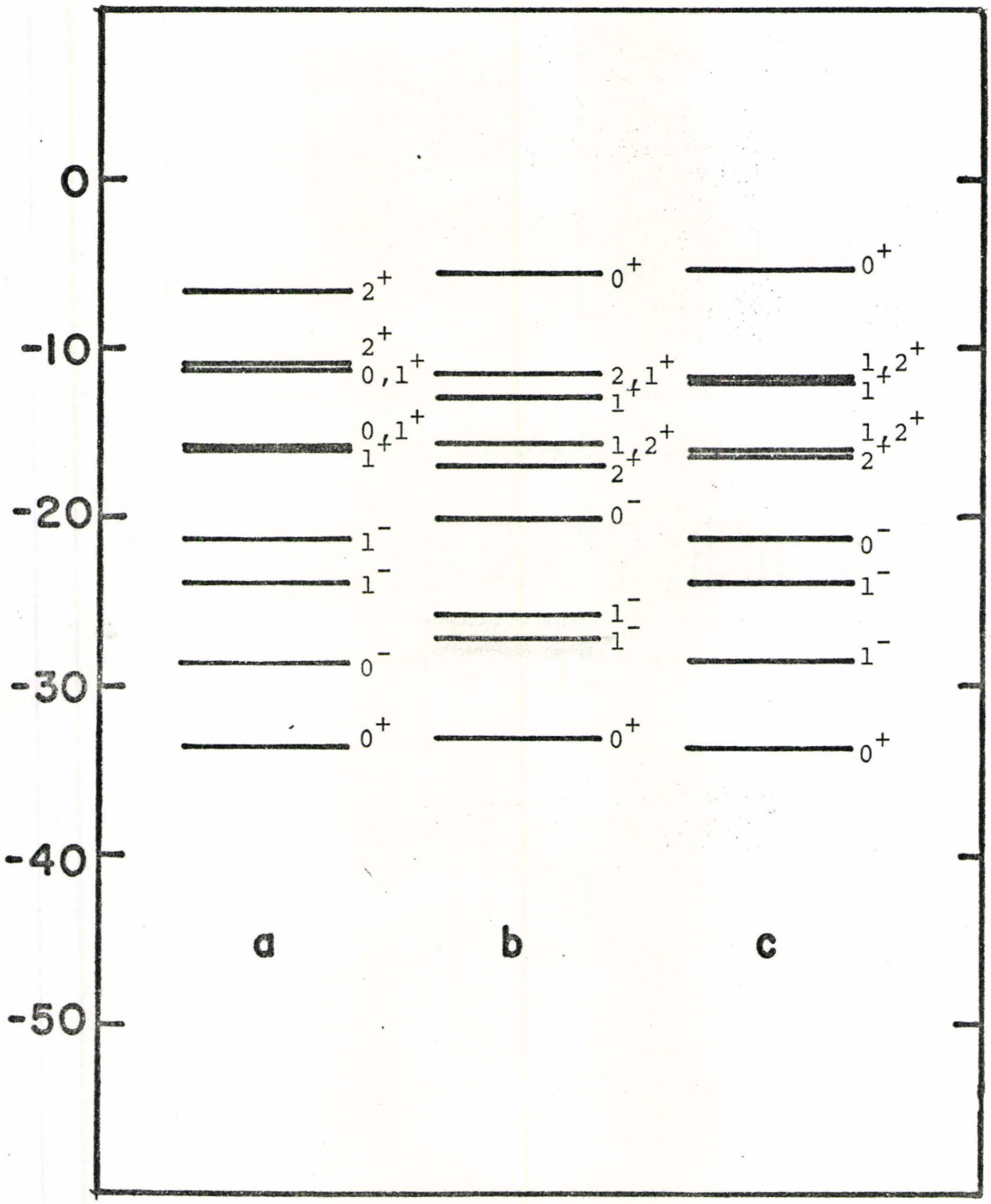

Figure 5.32

5.4.5 Argon 36

Argon is almost spherical with a very small negative quadrupole moment. At first glance one cannot miss the wide, and very deep depression in the density in the interior of ^{36}Ar. (Fig. 5.33). The outer contours are very similar to those of ^{40}Ca, with something removed from the centre.

This appears to be a bubble nucleus. X. Campi in a parallel calculation obtained a similar ground state bubble shape for ^{36}Ar assuming it to be spherical. In a recent paper by C.Y. Wong et al (1972) it was suggested that the bubble was somewhat deeper than would be obtained from simple removal of the 2s state from ^{40}Ca. We also checked this with the HFC ^{40}Ca, but the density dropped only 20%. The central density of Calcium was found to be

40% due to ϕ_{000}

20% " ϕ_{002}

40% " ϕ_{100}

The best explanation of the depression is obtained by subtracting the ^{4}He density profile from the ^{40}Ca profile. As one can see, (Fig. 5.34) this density difference is parallel to the ^{36}Ar density profile. It would appear that ^{40}Ca is composed of a central alpha particle with the other nine arranged around it in the form of a "shell". ^{36}Ar is just the shell after the central ^{4}He "yolk" has been removed. The removal of this inner density causes the shell density to relax inward

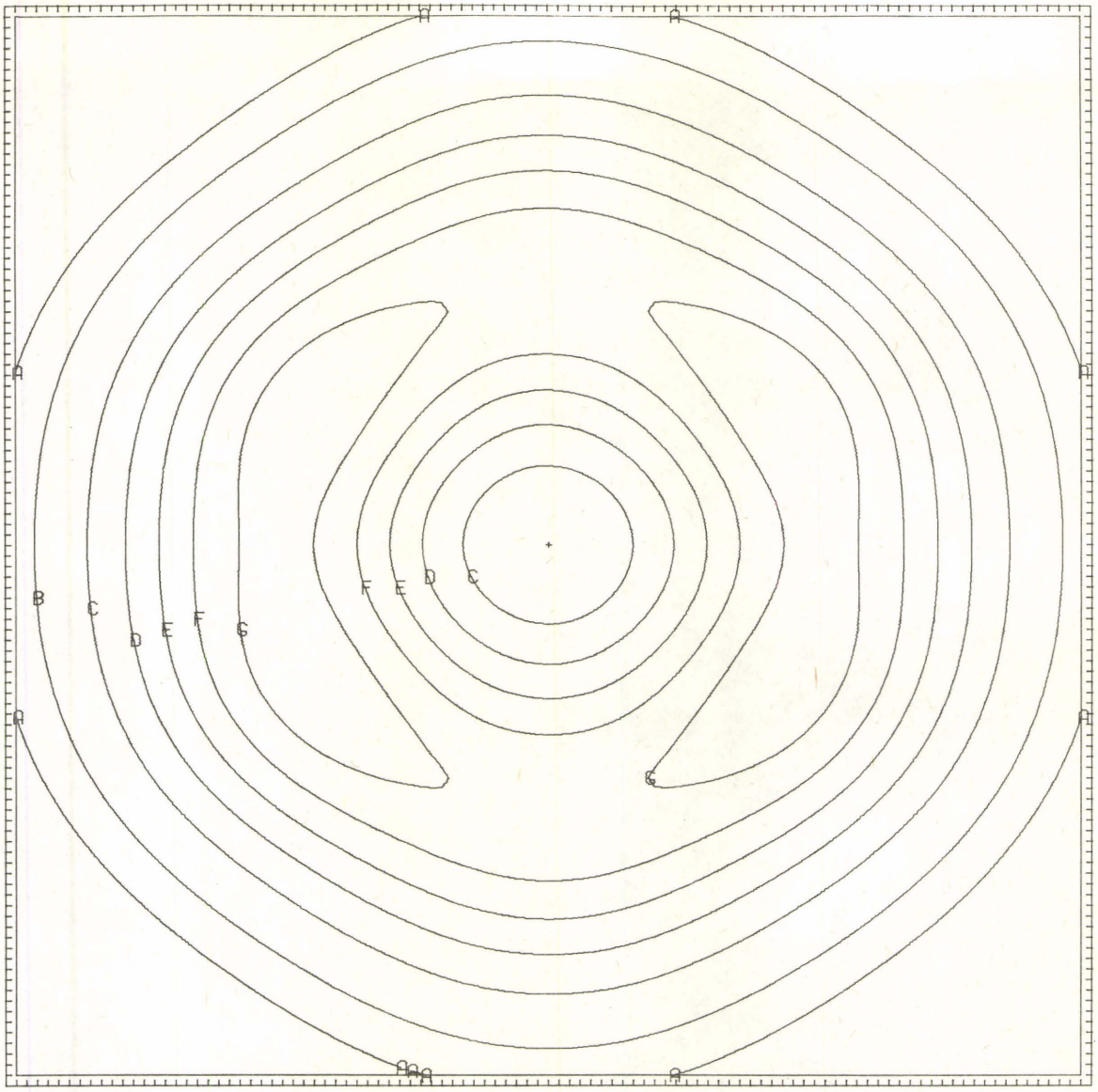

Figure 5.33

Density distribution of ^{36}Ar

Figure 5.34

Density Profile of ^{36}Ar

(a) Broken and Dotted Line - ^{40}Ca density

(b) Solid Line - ^{36}Ar density

(c) Broken Line - (^{40}Ca - ^{4}He) density

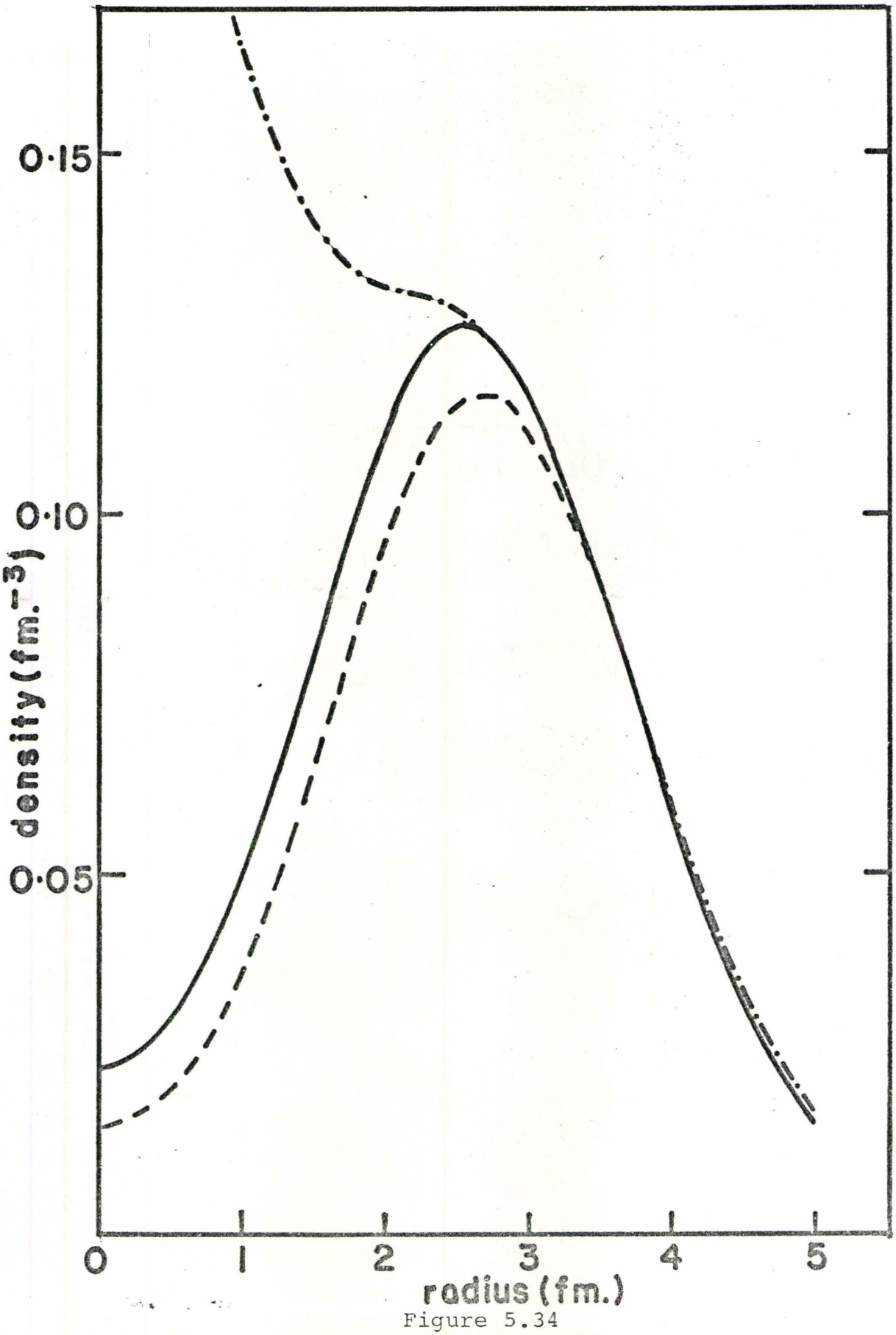

Figure 5.34

Figure 5.35

Proton Single Particle Energy Levels of ^{36}Ar and ^{40}Ca

(a) HFC levels of Oblate ^{36}Ar

(b) HFC levels of Oblate ^{40}Ca

(c) HFC levels of Prolate ^{36}Ar

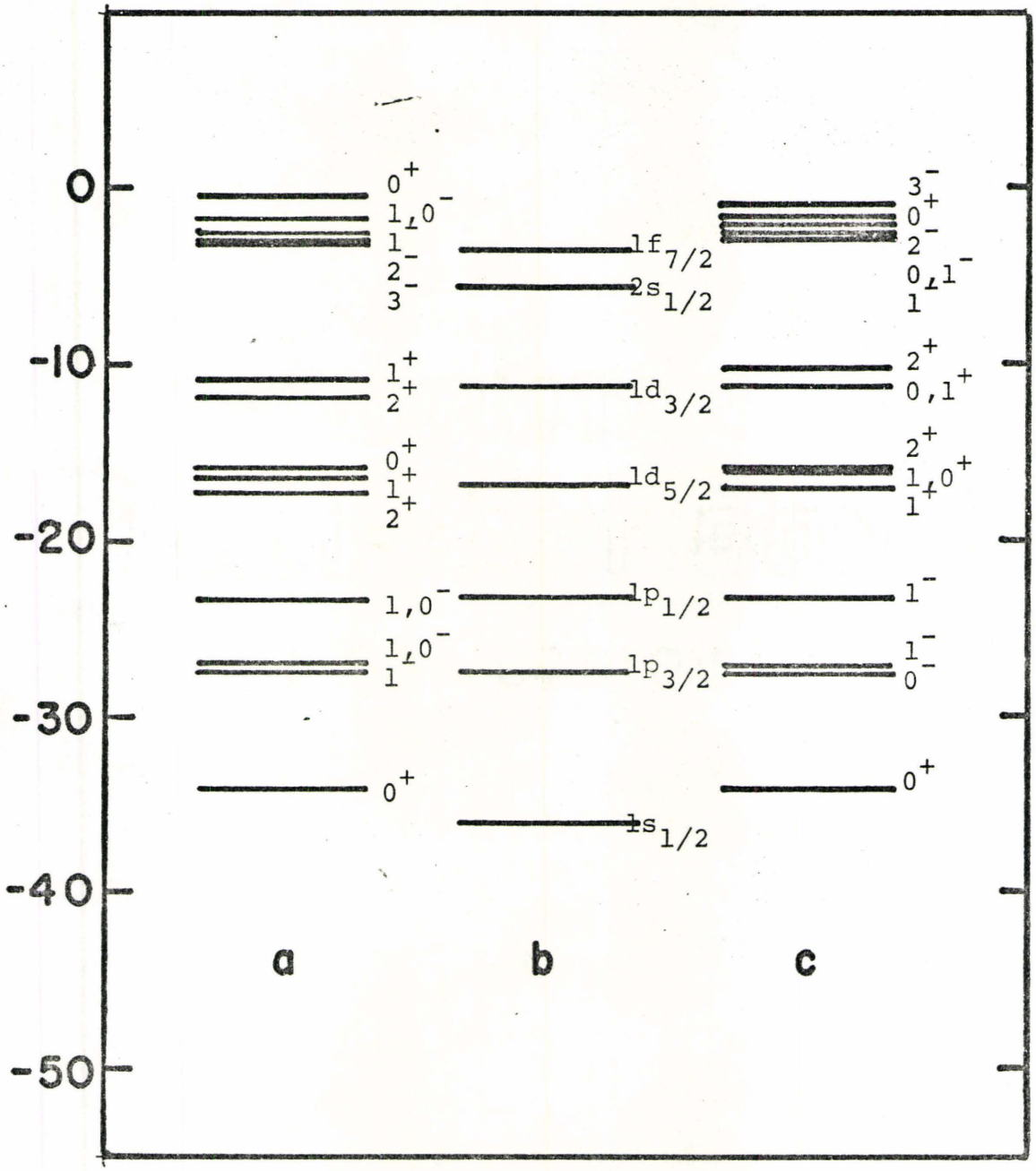
0
-10
-20
-30
-40
-50
0+
1,0−
1−
2−
3−
1+
2+
0+
1+
2+
1,0−
1,0−
1
0+
1f7/2
2s1/2
1d3/2
1d5/2
1p1/2
1p3/2
1s1/2
3−
0+
2−
0,1−
1
2+
0,1+
2+
1,0+
1+
1−
1−
0−
0+
a
b
c

Figure 5.35

Figure 5.36

Density Profile of ^{36}Ar

(a) X. Campi's Calculation

(b) Oblate Calculation

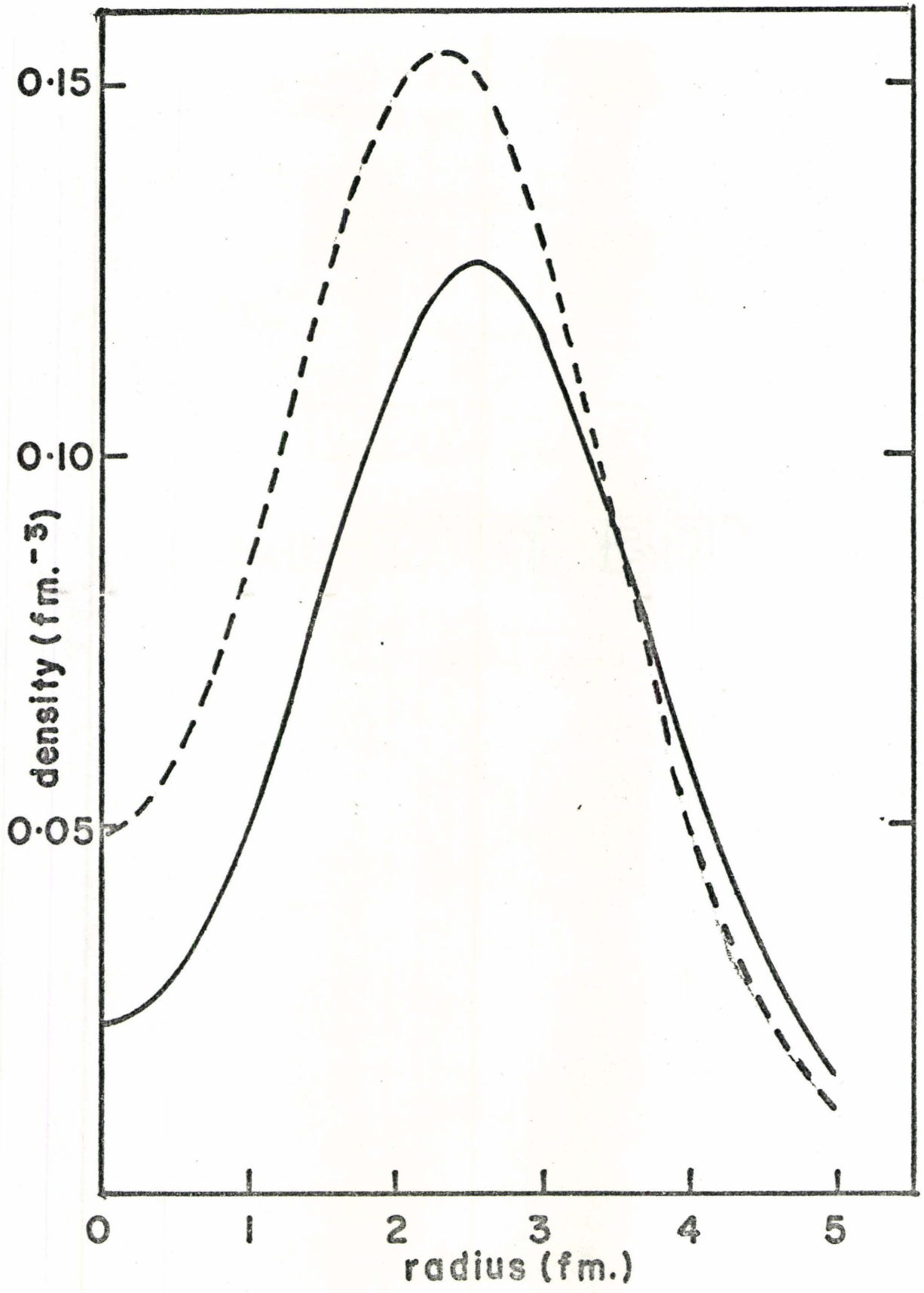

Figure 5.36

slightly. This would seem to indicate an overwhelming tendency for nuclei to maintain a structure as close to the closed shell nuclei as possible, even if the structure is something as improbable as a bubble.

X. Campi found the HFC solution for ^{36}Ar with a uniform (non bubble) shape lay about 3 MeV above the bubble state. Lassey (1972) found that some forces produced a central maximum. However V-LA gave a minimum. An attempt to obtain a central maximum with HFC failed. The state was slightly prolate, with not quite as deep a hole, a slightly smaller radius, total energy about 2.7 MeV above the ground state and single particle levels almost identical to the oblate, except for labelling and a slightly lower unoccupied 0+ state (Fig. 5.35).

It is interesting to compare the ^{36}Ar single particle levels with those of ^{40}Ca. The levels are remarkably similar. One can see the spin orbit splitting is similar in each. One also sees the splitting of levels by deformation, and the relative ordering of the prolate or oblate single particle levels. Finally one can observe the dramatic drop of the occupied $2s_{1/2}$ level. However, even this is not a large enough drop (Sect 5.3.2). The hole in ^{36}A is so deep that the 0+ level has moved above some of the negative parity $f_{7/2}$ states. Clearly both resemble the ^{40}Ca nucleus except for the 0+ level due to the empty central region.

As one would expect the radii were considerably larger using our approach. The X. Campi calculation had a central

density at 0.048 fm^{-3} a peak of 0.155 fm^{-3} at 2.35 fm and dropped below the HFC density at 3.5 fm. The HFC nucleus had a central density of 0.023 fm^{-3} and a peak of 0.126 fm^{-3} at 2.6 fm. (See Fig. 5.36). Clearly the density approximation has removed density from the central region to the surface. The depression is intensified, however the bubble is clearly due to the force G-0.

Not only is X. Campi's radius smaller than HFC and V-LA, so are those of Zofka and Ripka. V-LA still produces slightly larger radii than HFC. (Table 5.11).

The shape parameters indicate no asymmetry D_2. However the quadrupole moment D_o, although always negative varies considerably. X. Campi's of course is 0.0. The HFC value is the next largest, with V-LA being a factor of two larger, then Lineg and B1 another factor of two larger. It would appear that the quadrupole moment is very sensitive either to the force or the method of calculation. The latter is at least partly suggested by the results, since HFC and V-LA are both small relative to Lineg and B1. However Lassey, using the same program found D_o to vary by as much as a factor of two using various forces.

The energies are best for HFC and V-LA with V-LA still slightly more bound. The X. Campi and Lineg energies are very similar, continuing the pattern observed for spherical nuclei. B1 is far too low. (Table 5.11).

TABLE 5.11

Properties of ^{36}Ar

a.	Radii	Mindet	HFC	X. Campi	V-LA	Lineg	Bl
	Mass	3.461	3.590	3.330	3.614	3.35	3.37
	Proton	-	3.600	3.348	3.622	3.40	3.41
	Neutron	-	3.580	3.311	3.606	3.30	3.33
	Charge	-	(3.67)	3.417	3.695	3.46	3.48
b.	Shape Parameters						
	$\langle r^2 \rangle^{1/2}$	3.461	3.590	3.330	3.614	3.35	3.37
	$\langle \rho^2 \rangle$	9.044	8.905	9.392	9.322	8.428	8.59
	$\langle z^2 \rangle$	2.937	3.985	3.696	3.739	2.795	2.76
	D_o	-0.265	-0.073	+0.0	-0.141	-0.253	-0.27
	D_2	0.00	0.00	0.00	0.00	0.00	0.00
c.	Binding Energies						
	Total	275.58	296.49	280.76	309.57	282.16	218.2
	Proton	109.37	121.55	-	128.56	-	-
	Neutron	166.22	174.94	-	181.00	-	-
	BE/A	7.655	8.236	7.799	8.599	7.85	6.0
	Experimental	306.71					

TABLE 5.11(d)

Single Particle Levels

(i) McMaster Approach

Protons

m_ℓ	π	Mindet	k	m_ℓ	π	HFC	V-LA
0	+	45.04	1/2	0	+	34.14	43.52
1	-	35.14	3/2	1	-	27.53	34.22
1	-		1/2	1,0	-	26.93	33.56
0	-	31.06	1/2	0,1	-	23.40	29.15
2	+	22.36	5/2	2	+	17.34	20.42
2	+		3/2	1,2	+	16.54	19.31
1	+	20.27	1/2	0,1	+	15.87	18.46
1	+		3/2	2,1	+	11.89	14.54
0	+	17.34	1/2	1,0	+	10.99	13.25
		-	1/2	0	+	0.37	6.73
		-	7/2	3	-	3.20	4.48
GAP		-				7.79	6.52
0	+	52.08	1/2	0	+	40.22	49.61
1	-	41.56	3/2	1	-	33.58	40.22
1	-		1/2	1,0	-	32.98	39.61
0	-	37.55	1/2	0,1	-	29.36	35.12
2	+	28.54	5/2	2	+	23.34	26.22
2	+		3/2	1,2	+	22.55	25.13
1	+	26.42	1/2	0,1	+	21.81	24.31
1	+		3/2	2,1	+	27.89	20.36
0	+	23.48	1/2	1,0	+	16.94	19.12
		-	1/2	0	+	7.18	13.26
		-	7/2	3	-	8.87	10.08
GAP		-				8.07	5.84

Table 5.11(d) Continued

(ii) X. Campi

$n\ell_J$	π	Protons	Neutrons
$1s_{1/2}$	+	38.795	45.275
$1p_{3/2}$	-	27.860	34.160
$1p_{1/2}$	-	25.965	32.294
$1d_{5/2}$	+	15.518	21.646
$2s_{1/2}$	+	5.544	11.599
$1d_{3/2}$	+	9.624	15.667
GAP		4.080	4.068

(iii) Zofka and Ripka Protons

m_ℓ	π	Lineg	Bl
0	+	39.	56.
1	-	27.	34.5
0	-	23	29.5
2	+	14	15.5
0	+	12.5	12.5
1	+	11.5	11.5
0	+	5.0	-1.
Neutron Gap		6.21	12.17
Proton Gap		6.5	12.5

Figure 5.37

Proton Single Particle Energy Levels of ^{36}Ar

(a) Mindet Calculation

(b) HFC Calculation

(c) X. Campi Calculation

(d) V-LA Calculation

(e) Lineg Calculation

(f) Bl Calculation

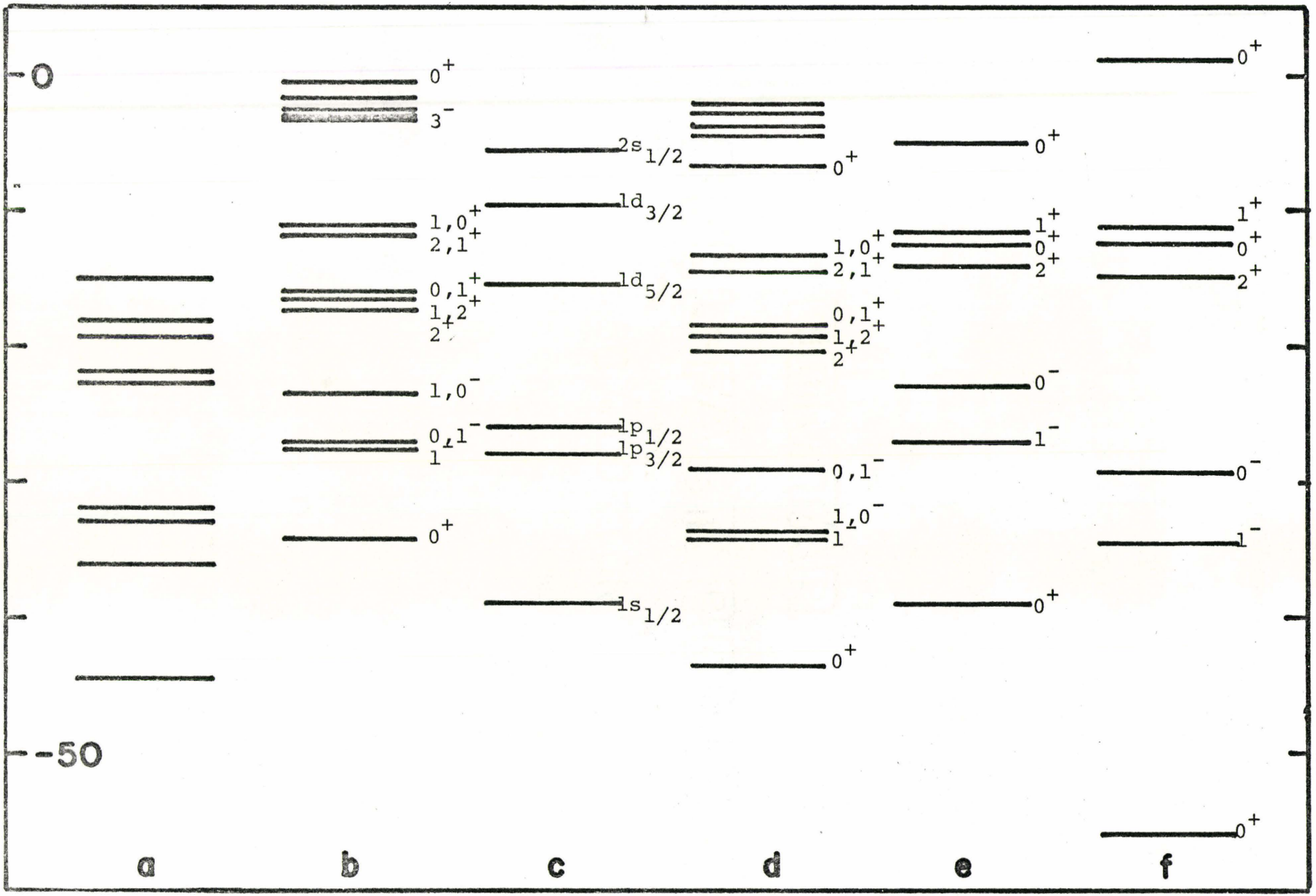
0
-50
a
b
c
d
e
f
0+
3−
1,0+
2,1+
0,1+
1,2+
2+
1,0−
0,1−
1
0+
2s1/2
1d3/2
1d5/2
1p1/2
1p3/2
1s1/2
0+
1,0+
2,1+
0,1+
1,2+
2+
1,0−
0,1−
1,0−
1
0+
0+
1+
0+
2+
0−
1−
0+
0+
1+
0+
2+
0−
1−
0+

Figure 5.37

The single particle levels are each individually similar to their corresponding ^{40}Ca single particle spectrum with the exception of deformation splitting, and the elevated 0+ levels. The spectra of the various calculations have similar patterns. All have an unoccupied 0+ level and a fairly large gap. This may indicate that each of the calculations we have compared is a bubble nucleus. (Fig. 5.37).

5.5 Conclusions

5.5.1 Systematics

In contrast to Mindet and Lineg the binding energy per nucleon for HFC rises rather smoothly with A to a maximum for ^{36}Ar. The anomalous drop for ^{40}Ca is believed to be a consequence of a limited basis. In general the HFC BE/A is 0.4-0.5 MeV higher than Lineg, both of which increase with A. However, HFC is about 0.5 MeV below experiment. (Fig. 5.38).

The mass radius of HFC is consistently about 0.2 fm higher than Lineq or experiment. A similar pattern would exist for charge radius, except the curves would be a little higher. This curve, like the BE/A curve also has very small curvature. (Fig. 5.39).

The only pattern rigorously followed by the quadrupole moment D_o is that doubly magic nuclei have a value 0.0, being oblate for smaller A and prolate for slightly larger A. In the region halfway between one may have Hartree Fock solutions with two or more competitive forms.

Figure 5.38

Binding Energy Versus Atomic Number

(a) Circles - Experimental Values

(b) Solid Line with circles - HFC Calculations

(c) Solid Line With triangles - Mindet Calculations

(d) Broken Line With Circles - Lineg Calculations

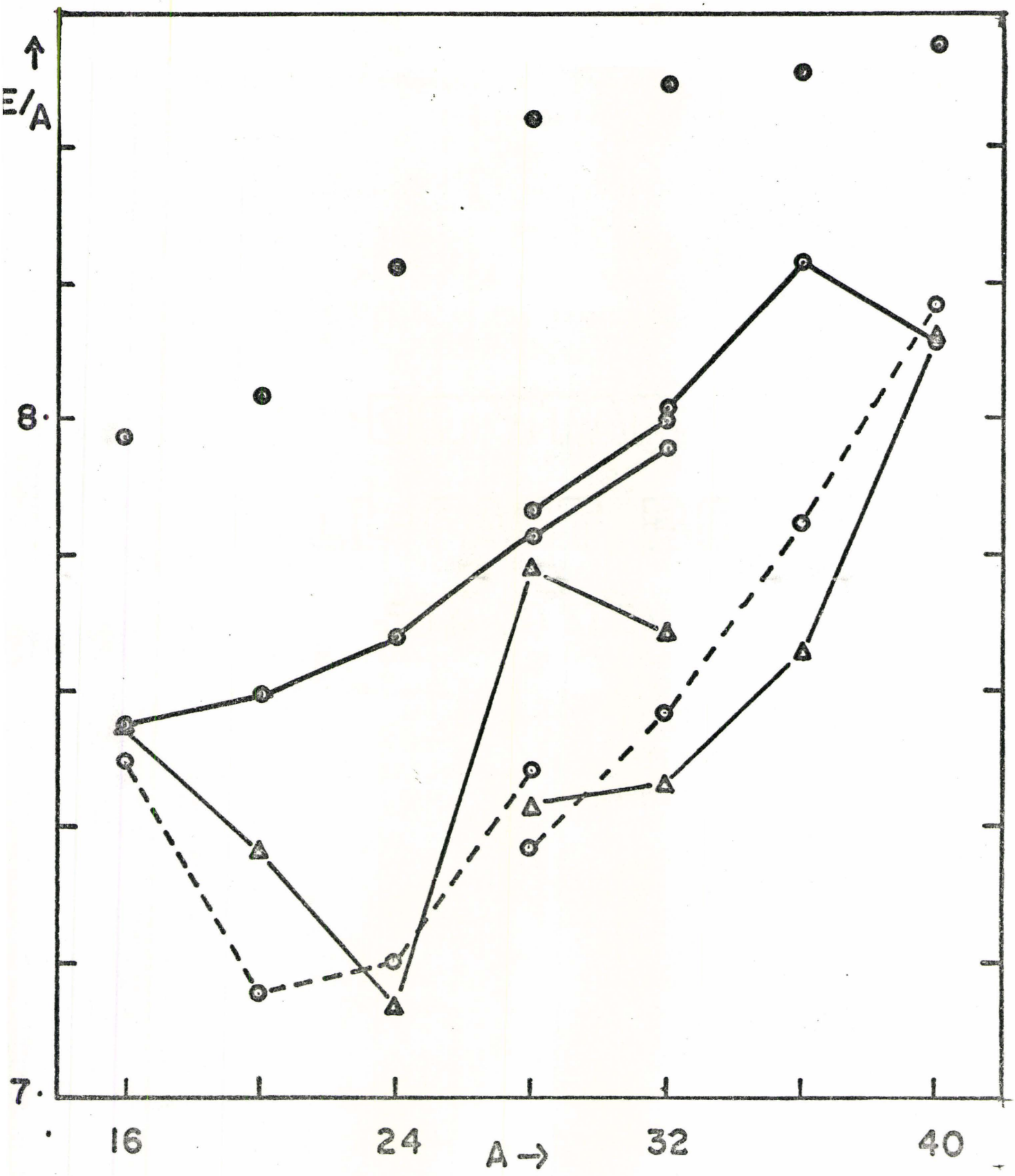

Figure 5.38

Figure 5.39

Mass Radius in Fermis Versus Atomic Number

(a) Solid Line - HFC Calculations

(b) Broken Line - Lineg Calculations

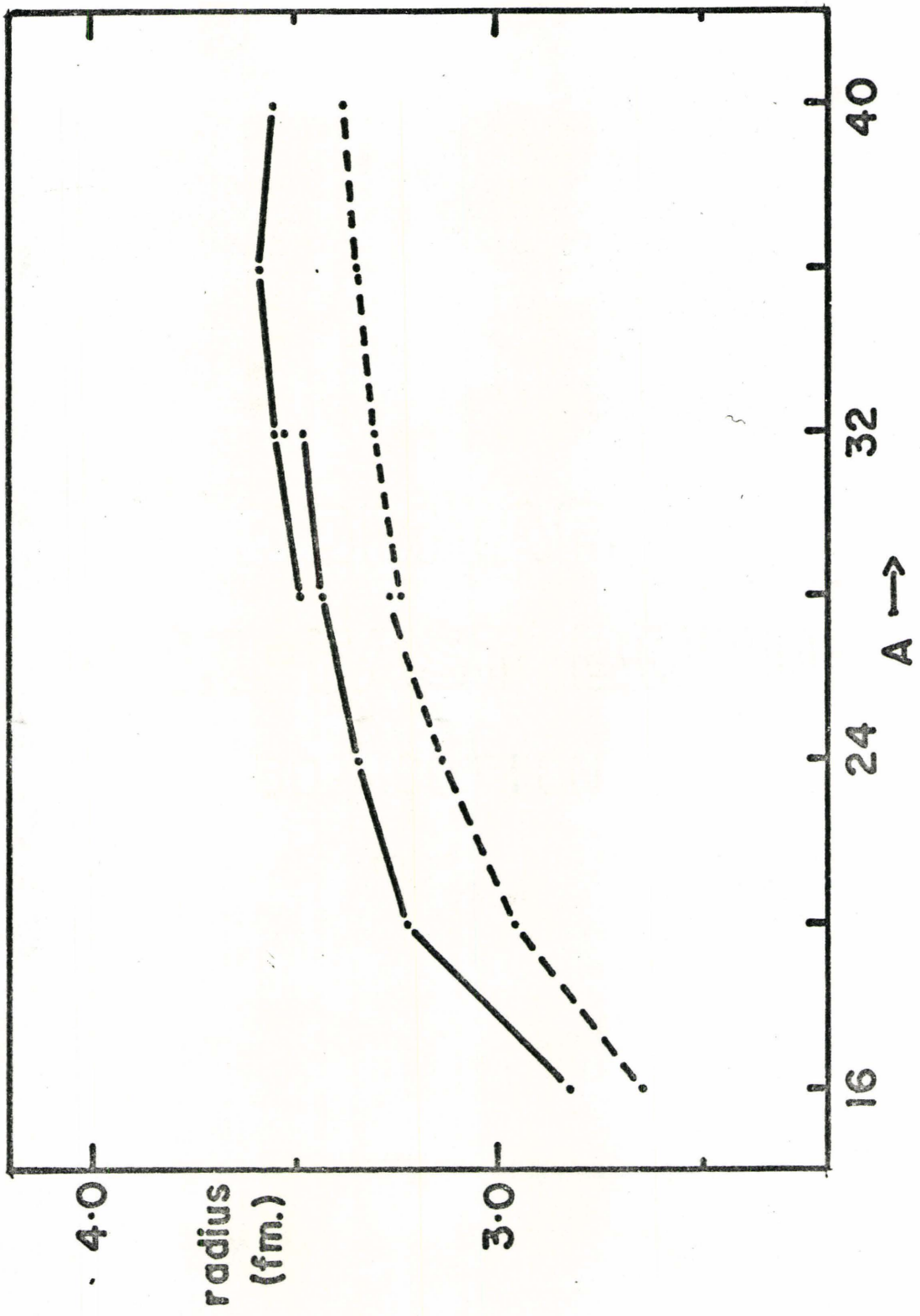

Figure 5.39

Figure 5.40

HFC Single Particle Energy Levels Versus Atomic Number

(a) Left-hand side prolate nuclei

(b) triaxial ^{32}S

(c) Right-hand side oblate nuclei

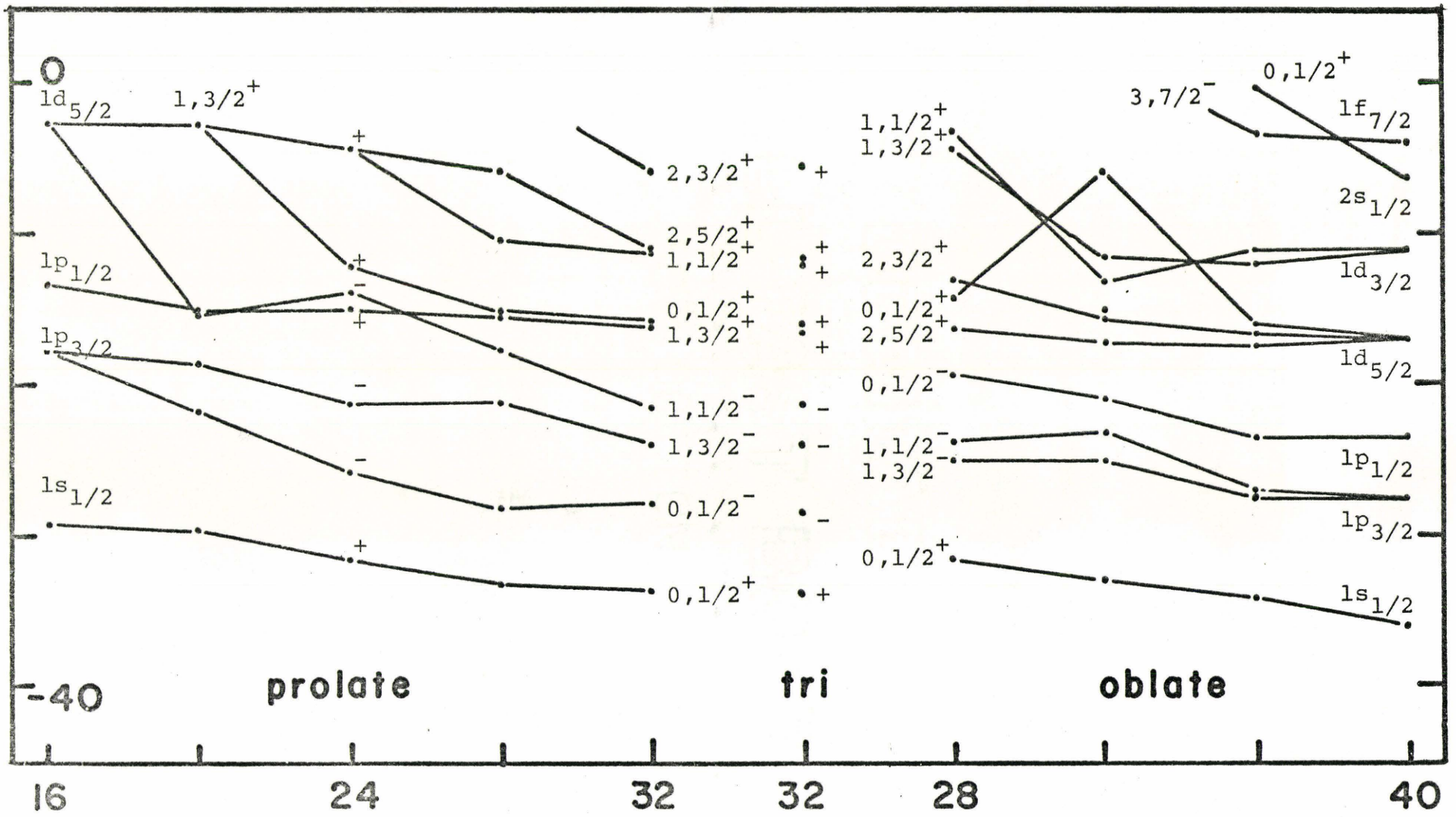
0
-40
$1d_{5/2}$
$1,3/2^+$
$1p_{1/2}$
$1p_{3/2}$
$1s_{1/2}$
$2,3/2^+$
$2,5/2^+$
$1,1/2^+$
$0,1/2^+$
$1,3/2^+$
$1,1/2^-$
$1,3/2^-$
$0,1/2^-$
$0,1/2^+$
$1,1/2^+$
$1,3/2^+$
$2,3/2^+$
$0,1/2^+$
$2,5/2^+$
$0,1/2^-$
$1,1/2^-$
$1,3/2^-$
$0,1/2^+$
$3,7/2^-$
$0,1/2^+$
$1f_{7/2}$
$2s_{1/2}$
$1d_{3/2}$
$1d_{5/2}$
$1p_{1/2}$
$1p_{3/2}$
$1s_{1/2}$
prolate
tri
oblate
16
24
32
32
28
40

Figure 5.40

TABLE 5.12

Radii of Nuclei	^{4}He	^{16}O	^{20}Ne	^{24}Mg	$^{28}Si^{P}$	$^{28}S^{o}$	$^{32}S^{P}$	$^{32}S^{o}$	$^{32}S^{T}$	^{36}Ar	^{40}Ca
Mass	1.853	2.827	3.234	3.35	3.440	3.496	3.482	3.557	3.535	3.590	3.561
Proton	1.856	2.838	3.245	3.36	3.452	3.507	3.494	3.567	3.546	3.600	3.570
Neutron	1.851	2.815	3.222	3.34	3.428	3.485	3.471	3.547	3.525	3.580	3.551
Shape Parameters of Nuclei											
$r^{2\ 1/2}$	1.853	2.827	3.234	3.35	3.440	3.496	3.482	3.557	3.535	3.590	3.561
^{2}	2.289	5.326	4.909	5.440	5.640	9.520	6.973	9.569	9.214	8.904	8.453
z^{2}	1.145	2.663	5.546	5.799	6.236	2.703	5.153	3.082	3.286	3.985	4.226
D_{o}	0.0	0.0	0.592	0.548	0.581	-0.337	0.275	-0.269	-0.211	-0.73	0.0
D_{2}	0.0	0.0	0.0	-0.164	0.0	0.0	0.0	0.0	0.192	0.0	0.0
Binding Energies of Nuclei											
Total	29.746	120.785	151.911	184.239	219.080	220.236	254.600	255.965	256.638	296.494	324.175
Proton	14.534	54.597	67.407	80.003	92.877	93.921	105.797	106.868	107.052	121.551	128.373
Neutron	15.212	66.188	84.503	104.236	126.203	126.315	148.804	149.097	149.549	174.942	195.802
Experiment	28.295	127.617	160.642	198.251	236.532	236.532	271.773	271.773	271.773	306.708	342.360
BE/A	7.43	7.54	7.59	7.677	7.824	7.865	7.956	7.999	8.020	8.236	8.104
BE/A(Exp)	7.074	7.976	8.032	8.260	8.448	8.448	8.493	8.493	8.493	8.520	8.559

Single Particle Levels

	^{4}He	^{16}O	^{20}Ne	^{24}Mg	$^{28}Si^{P}$	$^{28}Si^{o}$	$^{32}S^{P}$	$^{32}S^{o}$	$^{32}S^{T}$	^{36}Ar	^{40}Ca
Protons											
	18.87	29.17	29.63	31.64	33.12	31.56	33.57	33.01	33.64	34.42	36.03
		17.98	21.85	25.78	28.06	24.97	27.67	27.19	28.46	27.53	27.39
			18.55	21.46	21.09	23.56	23.89	25.59	23.78	26.93	
		13.32	15.07	15.00	17.44	19.13	21.40	20.15	21.22	23.40	23.23
			14.98	13.92	15.35	15.84	16.00	16.93	16.35	17.34	
				12.29	15.24	14.00	15.80	15.65	15.91	16.54	16.90
					10.43	12.99	11.11	12.94	11.93	15.87	
							10.98	11.54	11.66	11.89	11.22
										10.99	
											5.68
noccupied	-0.51	2.53	2.80	4.33	5.59	4.30	6.60	5.56	5.29	3.20	3.55
GAP	19.38	10.79	12.18	7.96	4.84	8.69	4.38	5.98	6.37	7.79	2.13
Neutrons											
	19.59	32.25	33.25	35.85	38.05	36.36	39.13	38.52	39.08	40.22	43.09
		21.05	25.31	29.92	32.89	29.70	33.15	32.60	33.85	33.58	34.25
			22.21	25.31	26.00	28.27	29.37	30.96	29.21	32.99	
		16.32	18.57	18.97	22.26	23.93	26.89	25.46	26.58	29.36	29.94
			18.45	18.45	20.16	20.50	21.43	22.30	21.79	23.34	

Table 5.12 Continued

	^{4}He	^{16}O	^{20}Ne	^{24}Mg	$^{28}Si^{P}$	$^{28}Si^{o}$	$^{32}S^{P}$	$^{32}S^{o}$	$^{32}S^{T}$	^{36}Ar	^{40}Ca
				16.37	20.12	18.68	21.25	20.97	21.26	22.55	23.58
					15.30	17.64	16.57	18.24	17.29	21.81	
							16.41	16.89	17.02	17.89	17.90
										16.94	
											13.05
noccupied	0.58	5.66	6.63	8.98	10.65	9.26	12.41	11.25	10.94	8.87	9.94
GAP	19.01	10.66	11.82	7.39	4.65	8.38	4.00	5.64	6.08	8.07	2.11

Asymmetry follows from the filling of only one of the $m_\ell = \pm m$ wavefunctions, where m = 1,2,...

The entire panorama of HFC observations for each nucleus is tabulated in table 5.12.

The proton single particle levels are reasonably flat indicating good saturation properties. There is a smooth flow of levels from one nucleus to another without wild jumps in values, except for the empty 0 1/2+ level of oblate and triaxial ^{32}S. (Fig. 5.40). The s.p. levels are compressed owing to the strong density dependence and the $s_{1/2}$ or 0 1/2+ levels are high owing to the density approximation.

5.5.2 Clustering

Clustering has been discussed previously, (Section 5.4.1) and by Lassey (1972). However some observations are worthwhile.

First, alpha particle clustering is clearly observable. Particles find it energetically favourable to be in groups of four - two protons and two neutrons. This should not come as a great surprise however. ^4He as a free nucleus is incredibly stable. An addition of one neutron to ^3He causes a gain in energy of 20.58 MeV while the addition of another neutron to ^4He is impossible. A similar gain is made by adding a proton to ^3H. It should not be surprising if this stability were not at least partly preserved in the nucleus. Indeed, Day has shown that some four body clustering is present in nuclear matter, con-

TABLE 5.13

Nucleus	A	BINDING ENERGY (MeV)	ΔB.E. (MeV)	B.E. Per Nucleon (MeV)
Helium	3	7.72		2.57
			20.58	
	4	28.30		7.08
			-0.96	
	5	27.34		5.47
Carbon	11	73.44		6.68
			18.72	
	12	92.16		7.68
			4.95	
	13	97.11		7.47
Oxygen	15	111.95		7.46
			15.67	
	16	127.62		7.98
			4.14	
	17	131.76		7.75
Neon	19	143.77		7.57
			16.87	
	20	160.64		8.03
			6.76	
	21	167.40		7.97
Calcium	39	326.32		8.37
			15.73	
	40	342.05		8.55
			8.36	
	41	350.41		8.54

Figure 5.41

Neutron absorption cross section (in barns)
vs neutron number

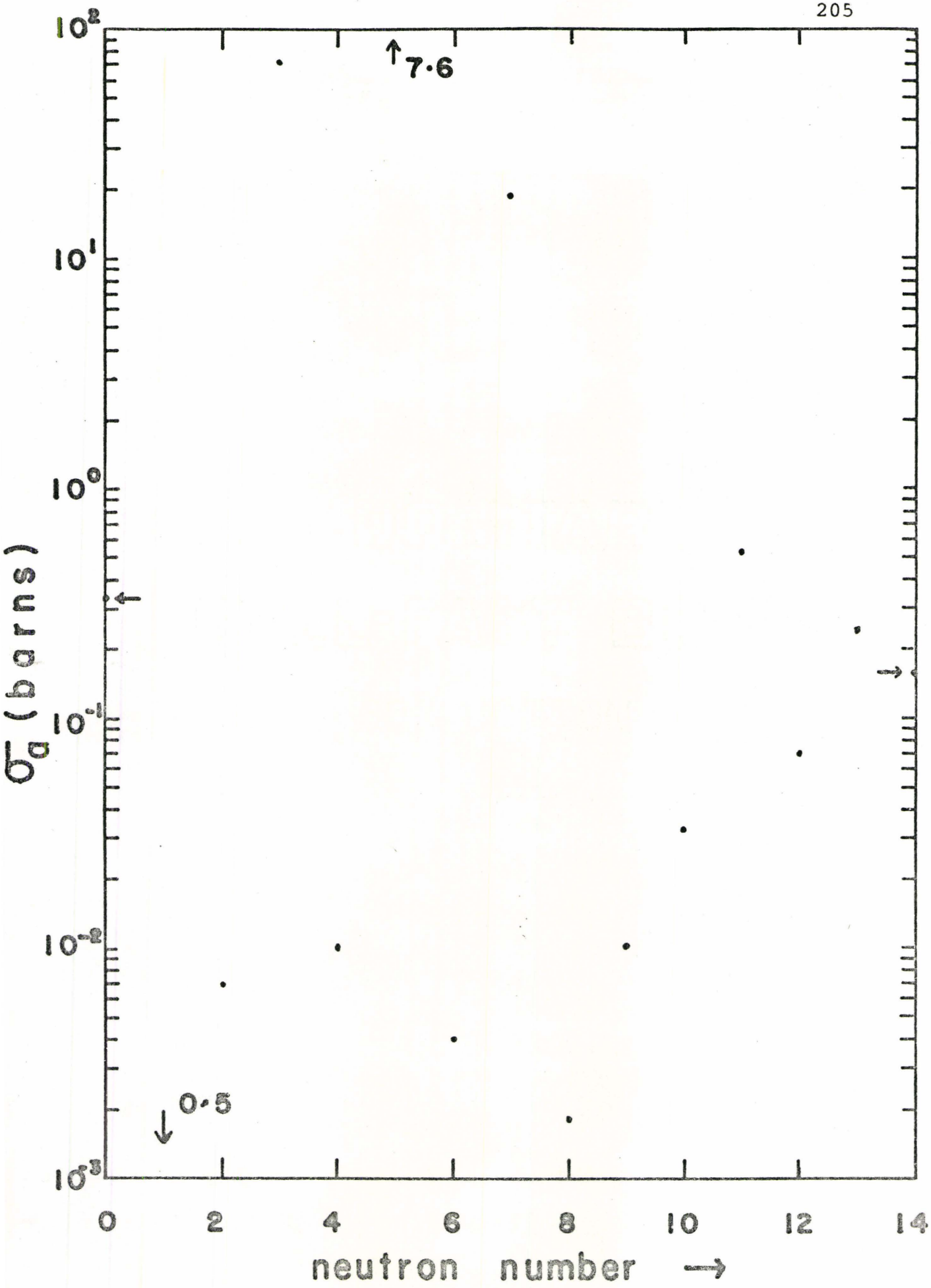
10^2
10^1
10^0
10^{-1}
10^{-2}
10^{-3}
σ_a (barns)
7·6
0·5
0
2
4
6
8
10
12
14
neutron number →

Figure 5.41

Figure 5.42

Neutron scattering cross section in barns vs neutron number

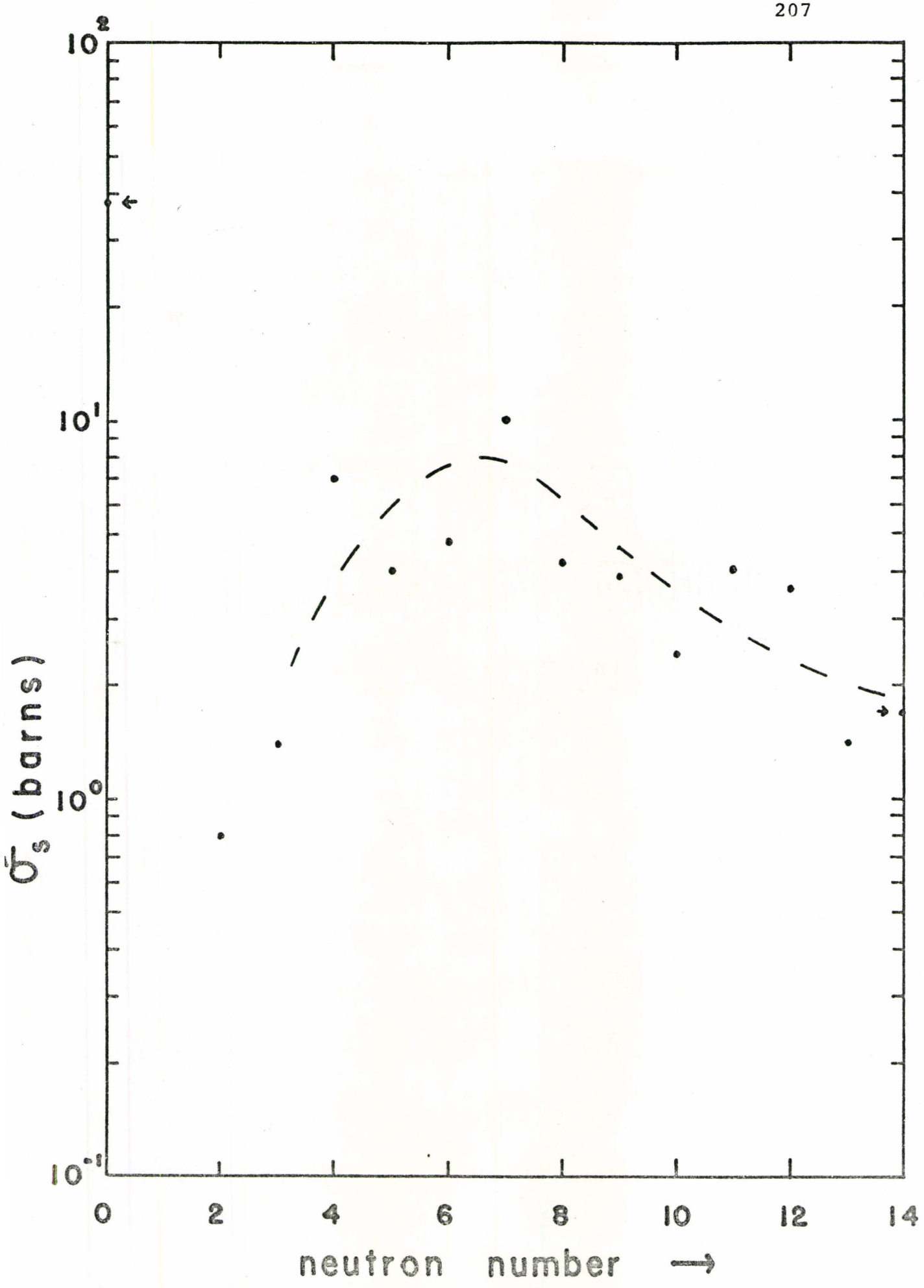
10^2
10^1
10^0
10^{-1}
$\bar{\sigma}_s$ (barns)
0
2
4
6
8
10
12
14
neutron number →

Figure 5.42

tributing about one MeV per particle of binding energy.

As can be seen in Table 5.13, many 4A nuclei are extremely stable. Not only can this be seen in terms of energy differences, but also in terms of cross-section. From Figure 5.41 we see that the neutron absorption cross section is very low for even numbers of neutrons, and high for odd. From Fig. 5.42 the scattering cross section is highest for ^{12}C and ^{16}O. The optimization of these stability properties, coupled with low mass is of course desirable for nuclear reactor moderators. Thus we see that these important nuclear properties, as some properties in Chemistry, are dependent on the geometry of the nucleus.

To further illustrate what I mean, ^{4}He is not the only clustering noticable in the density maps. The ^{12}C ring is observable in ^{20}Ne, and prolate ^{28}S. The ^{16}O tetrahedron in ^{20}Ne, ^{24}Mg, and prolate ^{28}S. The planar, four hole-four particle excited ^{16}O is seen in ^{32}S. Both ^{40}Ca in a positive form and ^{4}He in a negative form are present in ^{36}Ar. Thus clustering is not confined to only Helium. These of course correspond to the broader gaps in the shell model spectrum, not just the doubly magic nuclei.

Another interesting analysis is done by considering the geometry illustrated by the density maps to be merely ^{4}He nuclei separated by some bond distance, and calculate the bond energy. This is done using experimental binding energies, and

the HFC geometry. The bond energy Q is calculated as follows:

$Q = \{B.E.(^{A}_{Z}) - \frac{A}{4} \times (28.295)\} \div N_B = \Delta E/N_B$

where N_B is the number of bonds counted between ^{4}He clusters. For example ^{12}C would have $N_B=3$, ^{16}O would have $N_B = 6$ etc. The remarkable thing is that this Q is almost a constant (See Table 5.14 and Fig. 5.43). Further evidence for the alpha particle, observed years ago, is that ΔE is linear with A.(Fig. 5.44).

A further indication of this alpha structure is alpha decay of 4A nuclei. Curiously, the energy required to trigger alpha decay is the same order of magnitude as the bond energy times the number of bonds broken.

Nuclei	α Energy	n	Q	nxQ
^{12}C	7.66	2	2.425	4.85
^{16}O	9.6	3	2.432	7.27
^{20}Ne	7.49	3	2.132	6.396
	9.50	4	2.132	8.528
^{24}Mg	11.22	3	2.589	7.77
		5	2.589	12.70
^{28}Si	-	- too many bonds		
^{32}S	very high - too many bonds			

In the above table n is the number of bonds broken, Q the bond energy and nQ the total energy lost.

In each case above more energy is needed than just the energy of the n bonds. Some energy is distributed to the rest

TABLE 5.14

Bond Energies

Nuclei	BE($^{A}_{Z}$)	$\frac{A}{4}$x28.295	ΔE	N_B	Q
^{12}C	92.160	84.885	7.275	3	2.425
^{16}O	127.617	113.180	14.537	6	2.423
^{20}Ne	160.647	141.475	19.187	9	2.132
^{24}Mg	198.251	167.770	28.481	11	2.589
$^{28}Si(o)$	236.532	198.065	38.467	16	2.404
$^{32}S(t)$	271.773	226.360	45.413	∿16-18	2.523
$^{32}S(p)$	271.773	226.360	45.413	∿18-20	2.523
^{36}Ar	306.708	254.655	52.153	21	2.483
^{40}Ca	342.048	282.950	59.098	∿27-30	2.189

Figure 5.43

Bonding Energy Versus Atomic Number

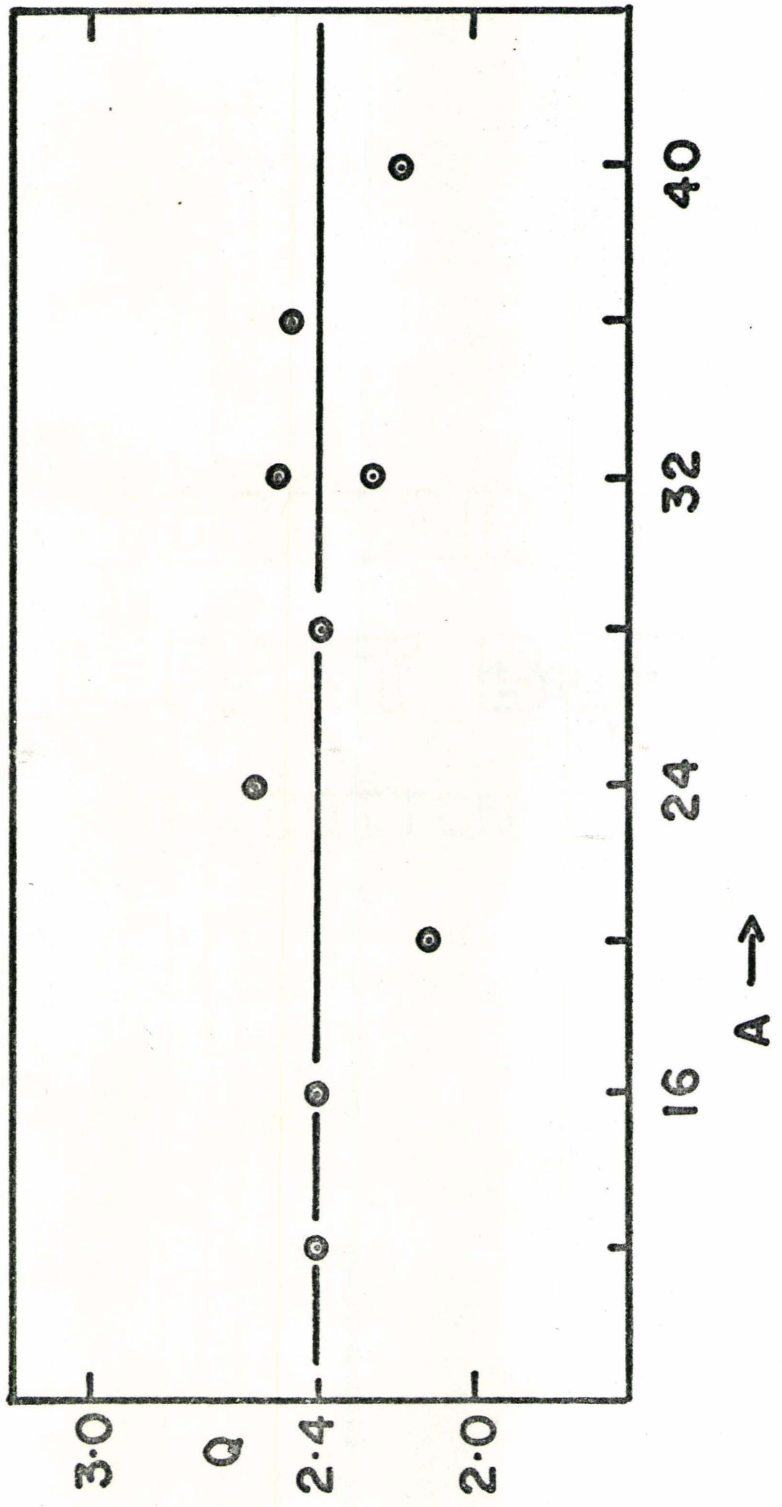

Figure 5.43

Figure 5.44

Alpha Cluster Energy Difference Versus Atomic Number

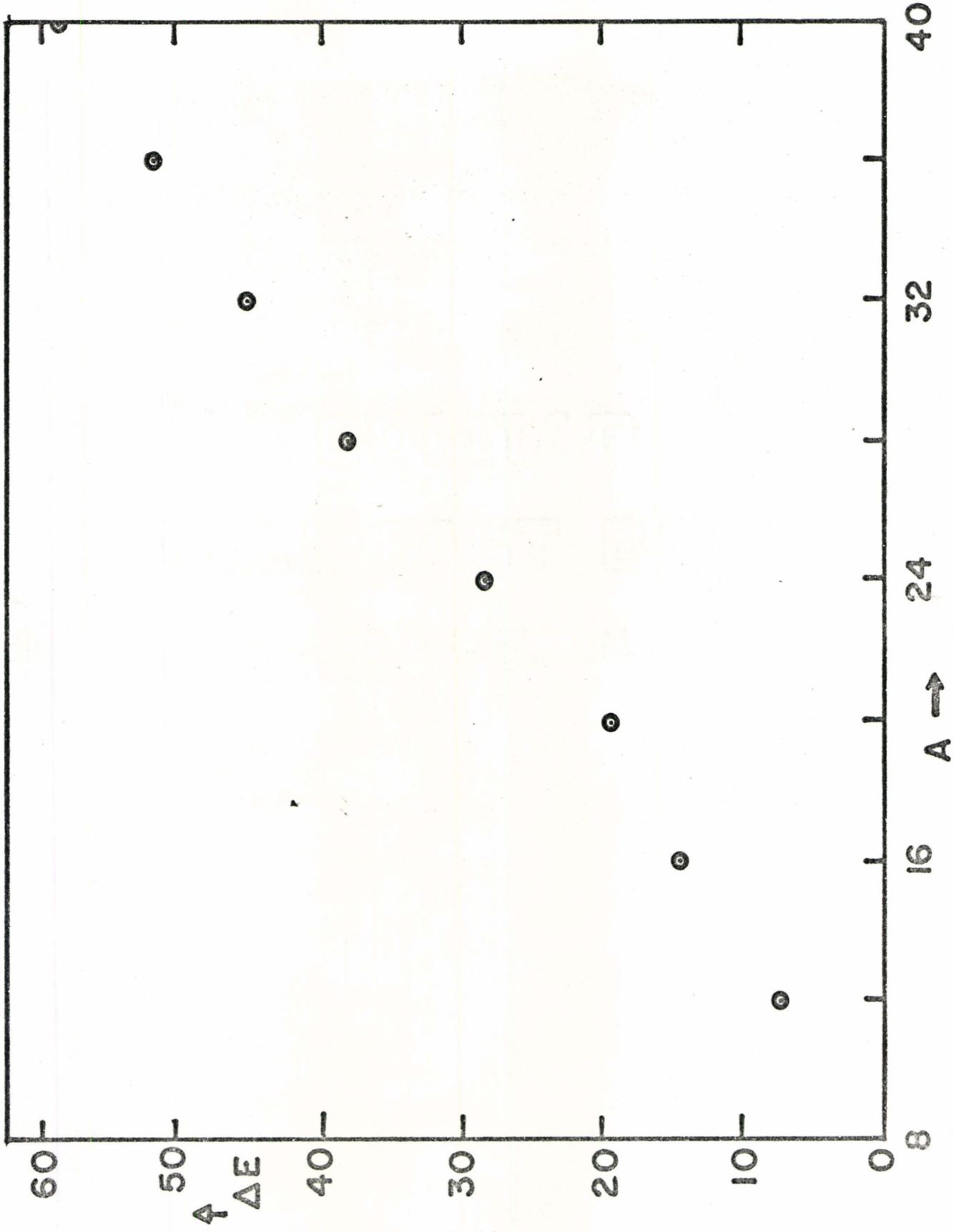

Figure 5.44

of the nucleus, perhaps in a vibration or rotation mode. ^{20}Ne has different decay channels depending on which alpha is ejected.For ^{24}Mg only the outer prolate alphas are removed. For heavier nuclei the energy for alpha decay is either very high or not indicated at all. This is because there are too many bonds to be broken.

It is conceivable, that as we study the structure of nuclei, more of their properties may be understood in terms of their geometry. Such things as radii and shape are obvious. Single particle levels can partly be explained this way. Going backwards, using the clustering and bonding concepts one can obtain total energy. Separating the procedure for protons and neutrons will give two different bonding energies. The procedure may be made more sophistocated by considering bonding of more complex clusters than ^{4}He. Even saturation becomes understood in terms of very stable clusters.

The alpha particle approach has been tried by Brink et. al. (1970) using force B1. He obtained solutions which were more bound for ^{12}C, ^{16}O and ^{20}Ne. However his heavier nuclei were not as bound as the more conventional Hartree Fock. In addition they obtained quite different configurations for both ^{24}Mg and ^{28}S. The ^{24}Mg nucleus was oblate, having a ring of four alphas surrounding two central alphas on the z axis. The oblate ^{28}Si resembled a flattened prolate configuration, two carbon rings above and below a central alpha.

Clearly this is too simple a model.

5.5.3 Discussion of Zofka and Ripka's Paper

In the paper by Zofka and Ripka there are several misconceptions.

It is suggested that ^{28}Si and ^{32}S are spherical nuclei owing to the electromagnetic properties of their neighbouring odd A nuclei. This is not supported by recent experiment using the reorientation effect. ^{28}Si is oblate and ^{32}S is prolate.

It is suggested that the addition of a spin orbit interaction could cause ^{12}C, ^{28}Si and ^{32}S to become spherical. This we did not observe. It is suggested that these nuclei have the right number of nuclei to form closed shells. However these moderate gaps in the shell model spectrum do not necessitate spherical nuclei. Spin orbit may take a $d_{3/2}$ level above the $2s_{1/2}$, but it also forces down the $d_{5/2}$ level and too much spin orbit could bring an $f_{7/2}$ below the $2s_{1/2}$ level.

It is suggested that the energy gap is a measure of stability of a HF solution and hence B1 is more stable since the neutron energy gaps are consistently larger. Aside from the fact that no spin orbit was included, which would have reduced the gaps, the spread in levels in largely due to the strength of the density dependence and the subsequent rearrangement term. In addition the separation energy is not

necessarily equal to the single particle energy especially for density dependent forces. Thus one cannot equate the gap with stability.

In view of their small gaps with density dependence it was wondered whether the energy gain due to deformation would be overcome by the spin orbit interaction thus favouring a spherical nucleus. This was not so.

They also seem to suggest that their structures for the heavier nuclei are not alpha type because they are different than the configurations of Brink et. al. This is not true. They are different, but they are merely different configurations of alpha particles.

It has been suggested that for the Lineg force the repulsive rearrangement term is of the form $\rho^2(\partial V/\partial \rho)$, where V is the effective interaction which acts mainly on the high density central region to raise preferentially the lower orbits. However the lower levels are raised owing to the rearrangement term which forces a smaller average single particle level of 24 MeV rather than an average of 32 MeV for no density dependence. In addition, even though the form of the rearrangement term would appear to be that of a surface potential, Campi has found that it spread rather evenly over the entire nucleus. In addition the central density is not always high. If the central density is very low, the 0+ levels will be quite high.

As Ripka and Zofka found for Lineg, the Sprung G-0 force gives good results when renormalized. We have obtained reasonable

single particle energies, density distributions, radii and binding energies.

5.5.4 Suggestions

It has been shown that the results depend to a significant degree on the method of calculation. Very different forces, Lineg and B1 or HFC and V-LA gave similar results. On the other hand different programs, HFC and X. Campi, obtained differing results. The fault is clearly on the part of HFC and V-LA. The density must not be replaced by a single gaussian but by a double (or more) guassian approximation. At the same time, the Slater exchange function can be approximated by a gaussian instead of a constant λ.

One would like to be able to calculate four hole-four particle $^{16}O^*$, ^{12}C and ^{8}Be.

It would be impractical to increase the basis until larger faster and cheaper computers are available. Before that day arrives more sophist cated techniques may well be evolved.

It will be interesting to calculate the $4A\pm1$ nuclei. I believe the 4A structure will be maintained, with the extra particle, or hole density spread and over the entire nucleus.

Finally, it might also be interesting to calculate some excited states or alternative configurations of various nuclei.

5.5.5 Epilogue

Having compared the structure of ^{20}Ne to the 15000 year old Venus of Willendorf, I have concluded that the Ontario Government has spent two dollars for every one of those years to prove there is nothing new in Physics.

Appendix 1

Cylindrical Harmonic Oscillator Wave Functions

This appendix is a review of the paper by Copley and Volkov (1965). The basis functions are eigenfunctions of the wave equation

$$\frac{\hbar^2}{2M}\left[-\nabla^2 + \alpha^2\rho^2 + \beta^2 z^2\right]\psi_{n,m,n_z}(\rho,z,\phi)$$

$$= E_{n,m,n_z}\,\psi_{n,m,n_z}(\rho,z,\phi)$$

The energy eigenvalue is

$$E_{n,m,n_z} = (2n + |m| + 1)\,\frac{\hbar^2\alpha}{2M}$$

$$+ (n_z + \frac{1}{2})\,\frac{\hbar^2\beta}{2M}$$

The eigenfunctions are of the form

$$\psi_{n,m,n_z}(\rho,z,\phi) = P_n^{\,m}(\sqrt{\alpha}\rho)\,Z_{n_z}(\sqrt{\beta}z)\,\Phi_m(\phi)$$

where

$$P_n^{\,m}(\sqrt{\alpha}\rho) = \left(\frac{2\alpha n!}{(n+|m|)!}\right)^{1/2}(\alpha^{1/2}\rho)^{|m|}\,L_n^{|m|}(\alpha\rho^2)e^{-1/2\alpha\rho^2}$$

$L_n^{|m|}(\alpha\rho^2)$ is the associated Laguerre polynomial

$$Z(\sqrt{\beta}z) = \left(\frac{\beta^{1/2}}{\pi^{1/2}2^{n_z}n_z!}\right)^{1/2} H_{n_z}(\sqrt{\beta}z)e^{-1/2\beta z^2}$$

$Hn_z(x)$ is the Hermite polynomial

$$\phi_m(\phi) = \frac{1}{(2\pi)^{1/2}}\,e^{im\phi}$$

The quantum numbers satisfy the following equation

$$N = 2n + |m| + n_z$$

where N = 0, 1, 2 ...

The oscillator lengths α and β are chosen to ensure the orthogonality of the basis states. (Lassey(1972) and Manning (1967)). See Table A.1.

In order that orthogonality hold one must adhere to the following conditions.

Either $\alpha_4 = \alpha_1$ or $\beta_6 = \beta_1$

" $\alpha_7 = \alpha_2$ or $\beta_8 = \beta_2$

" $\alpha_8 = \alpha_3$ or $\beta_{10} = \beta_3$

TABLE A.1

Number	n	m	n_z	parity	Oscillator	Parameters
1	0	0	0	+	α_1	β_1
2	0	0	1	-	α_2	β_2
3	0	+1	0	-	α_3	β_3
4	0	-1	0	-	α_3	β_3
5	0	0	2	+	α_4	β_1
6	0	+1	1	+	α_5	β_4
7	0	-1	1	+	α_5	β_4
8	0	+1	0	+	α_6	β_5
9	0	-2	0	+	α_6	β_5
10	1	0	0	+	α_1	β_6
11	0	0	3	-	α_7	β_2
12	0	+1	2	-	α_8	β_3
13	0	-1	2	-	α_8	β_3
14	0	+2	1	-	α_9	β_7
15	0	-2	1	-	α_9	β_7
16	1	0	1	-	α_2	β_8
17	0	+3	0	-	α_{10}	β_9
18	0	33	0	-	α_{10}	β_9
19	1	+1	0	-	α_3	β_{10}
20	1	1	0	-	α_3	β_{10}

BIBLIOGRAPHY

P.K. Banerjee and D.W.L. Sprung. Can. J. Phys. 49 (1971) 1899.

R. Becker. Bull. Am. Phys. Soc. BJ1, April 1973.

R.K. Bhaduri and C.S. Warke. Phys. Rev. Lett. 20 (1968) 1379.

R.K. Bhaduri, Y. Nogami, and C.K. Ross, Phys. Rev. C. 2 (1970) 2082.

R.J. Blin-Stoyle. Phil. Mag. 46 (1955) 973.

B.H. Brandow in Proc. Int. Summer School of Physics Enrico Fermi, course XXXVI (Academic Press, New York, 1966).

D.M. Brink and E. Boeker. Nucl. Phys. A91 (1967) 1.

D.M. Brink, H. Friedrich, A. Wieguny and C. Wong. Phys. Lett. 33B (1970) 143.

K.A. Bruechner, J.L. Gammel and H. Weitzner, Phys. Rev. 110 (1958) 431.

X. Campi and D.W.L. Sprung. Nucl. Phys. A194 (1972) 401.

X. Campi. Ph.D. Thesis, Orsay, (1973).

L.A. Copley and A.B. Volkov. Nucl. Phys. 84 (1966) 417.

B. Day. Rev. Mod. Phys. 39, (1967) 719.

B. Day. Phys. Rev. 187 (1969) 1269.

I.J. Donnelly. Nucl. Phys. A111 (1968) 201.

F. Everling, L.A. Konig, J.H.E. Mattauch and A.H. Wapstra. Nucl. Phys. 18 (1960) 529.

V. Fock. Zeits. f. Physik 61, (1930) 126.

T. Hamada and I.D. Johnson. Nucl. Phys. 34 (1962) 383.

D.R. Hartree. Proc. Comb. Phil. Soc. 24 (1928) 111.

D.J. Hughes. Ph.D. Thesis, McMaster (1970).

I. Kelson. Phys. Rev. Lett. 26 (1971) 1386.

K.R. Lassey and A.B. Volkov. Phys. Lett. 36B (1971) 4.

K.R. Lassey. Ph.D. Thesis, McMaster University (1972).

B.A. Loiseau, Y. Nogami and C.K. Ross, Nucl. Phys. A165 (1971) 601.

M.R.P. Manning. Ph.D. Thesis, McMaster (1967) unpublished.

M.R.P. Manning and A.B. Volkov. Phys. Lett. 26B (1967) 60.

K. Nakai, J.L. Quebert, F.S. Stephens and R.M. Diamond. Phys. Rev. Lett. 24 (1970) 903.

K. Nakai, F.S. Stephens and R.M. Diamond. Phys. Lett. 34B (1971) 389.

J.W. Negele. Phys. Rev. C1 (1970) 1260.

R.V. Reid. Ann. Phys. 50 (1968) 411.

G. Ripka. Nuclear Models with Density Dependent Effective Interactions. Lecture given at the 14th International Meeting of Physicists at Duilovo Yugoslovia, September, 1969.

P. Siemens. Nucl. Phys. A141 (1970) 225.

J.C. Slater. Phys. Rev. 32 (1928) 339.

J.C. Slater. Phys. Rev. 35 (1930) 210.

D.W.L. Sprung and P.K. Banerjee. Nucl. Phys. A168 (1971) 273.

D.W.L. Sprung. Nucl. Phys. A182 (1972) 97.

D.W.L. Sprung. "Advances in Nuclear Physics" Vol. 5. E. Vogt and M. Baranger, Editors. Plenum Press, N.Y. (1972).

D.G. Vautherin and M. Veneroni. Phys. Lett. 25B (1967) 125.

A.B. Volkov. Phys. Lett. 12 (1964) 118.

A.B. Volkov. Nucl. Phys. 74 (1965) 33.

A.B. Volkov. Nucl. Phys. A141 (1970) 337.

C.Y. Wong. Phys. Lett. 41B (1972) 455.

J. Zofka and G. Ripka. Phys. Lett. 34B (1971) 10.

J. Zofka and G. Ripka. Nucl. Phys. A168 (1971) 65.